NAVAL POSTGRADUATE SCHOOL

MONTEREY, CALIFORNIA

THESIS

OPTIMAL DATA TRANSMISSION ON MIMO OFDM CHANNELS

by

Luís Miguel Mendes Simões

December 2008

Thesis Advisor:	Roberto Cristi
Second Reader:	Frank Kragh

Approved for public release; distribution is unlimited

THIS PAGE INTENTIONALLY LEFT BLANK

REPORT DOCUMENTATION PAGE			Form Approved OMB No. 0704-0188
Public reporting burden for this collection of information is estimated to average 1 hour per response, including the time for reviewing instruction, searching existing data sources, gathering and maintaining the data needed, and completing and reviewing the collection of information. Send comments regarding this burden estimate or any other aspect of this collection of information, including suggestions for reducing this burden, to Washington headquarters Services, Directorate for Information Operations and Reports, 1215 Jefferson Davis Highway, Suite 1204, Arlington, VA 22202-4302, and to the Office of Management and Budget, Paperwork Reduction Project (0704-0188) Washington DC 20503.			
1. AGENCY USE ONLY ***(Leave blank)***	**2. REPORT DATE** December 2008	**3. REPORT TYPE AND DATES COVERED** Master's Thesis	
4. TITLE AND SUBTITLE Optimal Data Transmission on MIMO OFDM Channels			**5. FUNDING NUMBERS**
6. AUTHOR(S) Luís Miguel Mendes Simões			
7. PERFORMING ORGANIZATION NAME(S) AND ADDRESS(ES) Naval Postgraduate School Monterey, CA 93943-5000			**8. PERFORMING ORGANIZATION REPORT NUMBER**
9. SPONSORING /MONITORING AGENCY NAME(S) AND ADDRESS(ES) N/A			**10. SPONSORING/MONITORING AGENCY REPORT NUMBER**
11. SUPPLEMENTARY NOTES The views expressed in this thesis are those of the author and do not reflect the official policy or position of the Department of Defense or the U.S. Government.			
12a. DISTRIBUTION / AVAILABILITY STATEMENT Approved for public release; distribution is unlimited			**12b. DISTRIBUTION CODE**

13. ABSTRACT (maximum 200 words)

This thesis investigates the Physical Layer performance of single-input single-output (SISO) wireless communications systems, as well as multi antenna techniques such as multiple-input single-output (MISO) and multiple-input multiple-output (MIMO) systems, the last two utilizing the Alamouti-based space-time block coding (STBC) technique. All cases are based on the IEEE 802.16-2004 standard with OFDM using different values of coding rates. International Telecommunications Union (ITU) channel models are selected for the wireless channel in the simulation process. The particular setting we are interested in is the case where partial Channel State Information (CSI) is fed back to the transmitter for optimal control on the transmission rate. The performance results of the simulated SISO, MISO and MIMO systems are compared among themselves.

14. SUBJECT TERMS SISO, MISO, MIMO, STBC, OFDM, IEEE 802.16-2004, ITU channel models, CSI.			**15. NUMBER OF PAGES** 105
			16. PRICE CODE
17. SECURITY CLASSIFICATION OF REPORT Unclassified	**18. SECURITY CLASSIFICATION OF THIS PAGE** Unclassified	**19. SECURITY CLASSIFICATION OF ABSTRACT** Unclassified	**20. LIMITATION OF ABSTRACT** UU

NSN 7540-01-280-5500 Standard Form 298 (Rev. 2-89)
Prescribed by ANSI Std. 239-18

THIS PAGE INTENTIONALLY LEFT BLANK

Approved for public release; distribution is unlimited

OPTIMAL DATA TRANSMISSION ON MIMO OFDM CHANNELS

Luís Miguel Mendes Simões
Lieutenant, Portuguese Navy
B.S., Portuguese Naval Academy, 1996

Submitted in partial fulfillment of the
requirements for the degree of

MASTER OF SCIENCE IN ELECTRICAL ENGINEERING

from the

NAVAL POSTGRADUATE SCHOOL
December 2008

Author: Luís Miguel Mendes Simões

Approved by: Roberto Cristi
Thesis Advisor

Frank Kragh
Second Reader

Jeffrey Knorr
Chairman, Department of Electrical and Computer Engineering

THIS PAGE INTENTIONALLY LEFT BLANK

ABSTRACT

This thesis investigates the Physical Layer performance of single-input single-output (SISO) wireless communications systems, as well as multi antenna techniques such as multiple-input single-output (MISO) and multiple-input multiple-output (MIMO) systems, the last two utilizing the Alamouti-based space-time block coding (STBC) technique. All cases are based on the IEEE 802.16-2004 standard with OFDM using different values of coding rates. International Telecommunications Union (ITU) channel models are selected for the wireless channel in the simulation process. The particular setting we are interested in is the case where partial Channel State Information (CSI) is fed back to the transmitter for optimal control on the transmission rate. The performance results of the simulated SISO, MISO and MIMO systems are compared among themselves.

THIS PAGE INTENTIONALLY LEFT BLANK

TABLE OF CONTENTS

LIST OF FIGURES

LIST OF TABLES

THIS PAGE INTENTIONALLY LEFT BLANK

LIST OF ACRONYMS AND ABBREVIATIONS

AWGN	Additive White Gaussian Noise
BER	Bit Error Rate
BPSK	Binary Phase Sift Keying
CDMA	Code Division Multiple Access
CSI	Channel State Information
dB	decibel
DFT	Discrete Fourier Transform
DWTS	Digital Wideband Transmission System
ETSI	European Telecommunications Standards Institute
FDM	Frequency Division Multiplexing
FFT	Fast Fourier Transform
ICI	Inter-Carrier Interference
IDFT	Inverse Discrete Fourier Transform
IFFT	Inverse Fast Fourier Transform
ISI	Inter-Symbol Interference
ITU	International Telecommunications Union
LOS	Line of Sight
MIMO	Multiple Input Multiple Output
MISO	Multiple Input Single Output
MRRC	Maximal-Ratio Receiver Combining
OFDM	Orthogonal Frequency Division Multiplexing
PSK	Phase Shift Keying
QAM	Quadrature Amplitude Modulation
QPSK	Quadrature Phase Shift Keying
RF	Radio-frequency
RMS	Root Mean Square
SIMO	Single Input Multiple Output
SISO	Single Input Single Output

SNR	Signal to Noise Ratio
STBC	Space Time Block Code
TDD	Time Division Duplexing
UHF	Ultra High Frequency
VHF	Very High Frequency

EXECUTIVE SUMMARY

To achieve effective use of bandwidth in mobile wireless communications, broadband techniques like Orthogonal Frequency Division Multiplexing (OFDM) have been developed in the last decades. Features of OFDM which make it attractive are its capabilities of easily adapting to all sorts of adverse conditions caused by multipath, interference and low Signal to Noise Ratio. Because of its advantages, OFDM is widely used in several standards adopted worldwide. IEEE® 802.11, IEEE® 802.16 and HiperMAN are some examples. These standards are also known by their commercial designations: Wi-Fi, WiMAX, and HiperMAN, respectively.

The performance of OFDM can be further improved by data rate adaptation. In such techniques, the signal-to-noise ratio (SNR) at each subcarrier is measured and the information is fed back to the transmitter. This is normally designated as channel state information (CSI) feedback. By this technique we can also improve robustness against narrowband interference, since in this case only some of the subcarriers are affected.

Other techniques used currently to improve the performance in wireless communications systems are based on multiple antennas on the transmitter and/or on the receiver. These schemes increase the capacity of a wireless link leading to higher data rates. In particular by single-input multiple-output (SIMO) configurations we obtain receiver diversity while transmit diversity is achieved in the multiple-input single-output (MISO) case. They enhance performance by space time coding (with MISO) or they mitigate fading (by SIMO). Furthermore, the utilization of multiple antennas permits the focus of the transmitted energy in specific directions by beam-forming, accomplishing spatial multiplexing of multiple users. The overall effects of multiple-input multiple-output (MIMO) can be summarized in terms of reduction of the bit error rate (BER), increase of system capacity and a more efficient use of the transmitted power. Furthermore the combination of OFDM with MIMO techniques turns out to be very attractive in terms of improved performance.

The goal of this thesis was to investigate the performance of MIMO OFDM communication systems with CSI feedback, in particular using the IEEE® 802.16-2004 standard. Several steps were performed on the path to obtain this objective. Three systems were used to obtain the results presented in this thesis: SISO, 2x1 MISO and 2x2 MIMO. All systems have the CSI feedback feature. The SISO system served as the baseline comparison for the remaining systems as those had additional features to achieve higher performances. Both the MISO and MIMO systems were implemented using the transmit diversity technique known as Alamouti's scheme.

In the simulations performed during this thesis work the International Telecommunications Union (ITU) channel models were selected, since they are the most frequently used power-delay profiles in simulation environments for modeling purposes. These models have three types of users: Indoor, Pedestrian and Vehicular. For each one of these types of users the ITU specifies two profiles of multipath: Profile A, with shorter time spread, replicates rural macro-cellular surroundings, while profile B reproduces an urban macro-cellular environment. For scenarios of micro-cells with radius less than 500m, profile A is also suggested.

The simulations were performed using SIMULINK® R2008a from MathWorks™. The results obtained in this thesis are presented in terms of BER curves and it was performed in several phases. First, the systems were developed and their performance was measured for each of the ITU user-channels profiles. From the results obtained several SNR thresholds vectors were defined to enable the systems' utilization of the partial CSI feedback feature. This was named *auto rate control mode*. Under this configuration all systems were tested for ITU user-channels profiles of interest, in particular the indoor and pedestrian categories. A last phase of tests was conducted when shadowing effects on the channels were simulated to observe all systems' response and performance.

As expected, the simulations show that an increase in the number of antennas used in a wireless communications system enhances its performance and capacity. In particular the 2x1 MISO system outperformed the SISO system and was outperformed by the 2x2 MIMO system. The improvements in terms of SNR vary among the user-

channels profiles used in the simulations. In general, the MISO system presented a 2dB to 3dB average performance improvement compared to SISO system. The MIMO system also showed a performance improvement of the same magnitude when compared to the MISO system. In some cases the MIMO system reached peak performance improvements of 18dB when compared to the SISO system. As a result, the MIMO system capacity is higher than that of the MISO system and the capacity of this is higher than the SISO system.

THIS PAGE INTENTIONALLY LEFT BLANK

ACKNOWLEDGMENTS

Quero agradecer aos meus pais pelas condições de vida que me facultaram durante a minha infância e juventude, que em conjunto com seu permanente apoio e amor me permitiram sonhar e voar tão alto. Agradeço também à minha família, Carla, a minha esposa, e os meus dois preciosos tesouros: Francisco e Henrique. Particularmente nesta fase trabalhosa da minha vida, agradeço à Carla pela sua compreensão, presença, companheirismo e amor. Aos meus filhos agradeço a sua existência, presença, inocência e amor constantes. Todos foram os meus mais fortes factores motivantes nos momentos mais difíceis. Estendo também uma palavra de apreço ao meu tutor o CFR EMA Cancela Roque pela sua disponibilidade, sinceridade e simplicidade. Igualmente, à hierarquia da Marinha de Guerra Portuguesa devo o facto de me ter facultado a possibilidade de enriquecer o meu conhecimento académico.

Quando il mio maestro e mentore di tesi Roberto Cristi la ringrazio per la sua disponibilità, incoraggiamento e la libertà che mi ha permesso di attraversare la linea di meta con la mia *Ferrari* senza incidente. Grazie mille!

An enormous word of sincere appreciation goes to my very good friend Stanley Florkowski (Stash), Captain USA. I thank him for his friendship and prompt availability and also his wife Jeong and son Danny. All three have been great friends to me, my wife and my boys. Also, worthy of mention is Stash's patience in reading this document and giving me his words of advice.

Finally, I would like to thank all of my professors at NPS for having the patience of teaching me so much great knowledge. All, with their own particular style, were capable of transmitting clear and error free messages. "Bravo Zulu!"

THIS PAGE INTENTIONALLY LEFT BLANK

I. INTRODUCTION

A. BACKGROUND

Eagerness to achieve higher goals has led mankind to an unprecedented technological level. Globalization may have started in the fifteenth century with the Europeans expanding their empires throughout the globe. Today, however, today we live the true meaning of globalization, particularly on information sharing in real time. Behind this high-performance global information distribution system lies the work of scholars, engineers and technicians, all fairly unknown to the common user. This global development in wireless communications has pushed to the limits of available resources such as bandwidth and capacity. The need for accommodating growing demands requires higher technical sophistication in wireless communications due to the environment in which they are employed. However, mankind wants more and more.

Today's wireless communications goals are narrower bandwidth, lower power consumption, higher data rates, and error-free data links. The physical world in which we live imposes some bounds to all these variables. In both civilian and military wireless communication applications, reliable data links are highly desirable. The need to operate such systems reliably in adverse conditions such as in dense urban environments or in hostile jamming scenarios led to the development of a number of advanced techniques at each layer of a communication system. In this thesis, we will focus particularly on the physical layer.

Currently, the two big families of transmitted broadband signals through out the world are code division multiple access (CDMA) and orthogonal frequency division multiplexing (OFDM). The latter, in particular, is widely used in several standards adopted worldwide. IEEE® 802.11, IEEE 802.16® and HiperMAN (high-performance metropolitan area network) by the European Telecommunications Standards Institute (ETSI) are by far the most popular examples [1]. Often, these standards are known by their commercial designations: Wi-Fi, WiMAX and HiperMAN, respectively. The main reason for selecting OFDM in all the referenced standards is its capability of obtaining

better performance in multipath channel environments [2]. These circumstances are permanently found mostly in metropolitan and sub-urban areas, where the demand for broadband wireless communications is extremely high due to large population density. The performance of OFDM can be significantly improved by subcarrier data rate adaptation on the basis of the signal-to-noise ratio (SNR) at each subcarrier. In turn, this would improve robustness against narrowband interference, affecting only part of the subcarriers. Furthermore, OFDM allows effective implementation of single-frequency networks, which is particularly attractive for broadcasting purposes [2].

Conversely, the present-day use of multiple antennas on the transmitter and/or on the receiver has become a viable technique to increase the capacity of a wireless link [3]. OFDM systems obtain frequency diversity by using multicarrier modulation [1]. Systems with multiple antennas, in contrast, can create a number of independent channels leading to spatial diversity [1]. The main advantage of spatial diversity over time and frequency diversity is that it does not require additional resources of time and bandwidth [1], [3]. In addition, using multiple antennas we can focus the transmitted energy in specific directions by beam-forming, so that we can obtain spatial multiplexing of multiple users [1]. Particular configurations of interest are receiving diversity for the case of single-input multiple-output (SIMO) and transmit diversity for the case of multiple-input single-output (MISO). These configurations and the basic single-input single-output (SISO) do not allow spatial multiplexing. They enhance performance by space time diversity (with MISO) or they attenuate fading (by SIMO). In short, the advantages of multiple antennas systems can be listed as reducing the bit error rate (BER), increasing the system capacity, while enlarging the area of coverage and reducing the transmitted power [1]. By combining OFDM and multiple-input multiple-output MIMO schemes the overall wireless communication system performance is greatly enhanced.

B. OBJECTIVES

The goal of this thesis was to investigate the performance of MIMO OFDM communication systems with channel state information (CSI) feedback, in particular using the IEEE® 802.16-2004 standard. Several steps were performed on the path to

obtain this objective. Initially, a supplied SIMULINK® R2008a SISO OFDM model, from MathWorks™, was benchmarked. On the basis of this a SIMULINK® R2008a MISO OFDM model, MathWorks™, was modified and its performance measured. Finally, the MISO OFDM model has been extended to MIMO OFDM, and its performance measured. In all these models, a feature of partial CSI is fed back to the transmitter for optimal control on the transmission rate. The performance results of the simulated SISO, MISO and MIMO OFDM systems are compared among themselves. International Telecommunications Union (ITU) channel models were selected for the wireless channel in the simulation process, since they are the most frequently used power-delay profiles in simulation environments for modeling purposes [1].

C. RELATED WORK

SIMO, MISO and in particular MIMO systems have been an exciting, active area of research in the past fifteen years because of their capability of increasing wireless communication capacity. It all started in 1994 when Paulraj and Kailath patented the "Increasing capacity in wireless broadcast systems using distributed transmission/directional reception [3],[4]." Telatar showed in [5] the benefits of using MIMO systems on additive Gaussian channel with and without fading. In the following year, Foschini introduced a "Layered space-time architecture for wireless communication in fading environments when using multiple antennas" in [6]. Later, together with Gans they presented some results in [7], on the limits of wireless communication in a fading environment using MIMO systems. In 1998 Tarokh et al. presented the performance criterion and construction of space-time block codes (STBC) in [8], pointing to high data rate wireless communications systems with multiple transmitting antennas. In that same year, Alamouti proposed a transmit diversity technique for MISO systems that provided the same diversity order as the maximal-ratio receiver combining (MRRC) of a $1\text{x}2$ SIMO system [9]. He also showed the possibility of implementing such a scheme for a $2\text{x}2$ MIMO system and pointed to a generalization of $2\text{x}M$ MIMO systems, where M is the number of receiving antennas. This scheme does not require any CSI feedback to the transmitter. His proposal became very popular due to its simple implementation and

the performance enhancements obtained. This scheme was eventually adopted by the IEEE 802.16 Broadband Wireless Access Working Group as part of this standard and it is an option of implementation to improve the IEEE 802.16-2004 based communication systems [10]. Nowadays, MIMO OFDM is still a very active research area. Some studies are pointing to more elaborate techniques where CSI feedback is considered to further improve broadband wireless communication links. Linear pre-coding using CSI feedback, and per-antenna power and rate feedback to reach MIMO OFDM theoretical capacity were recently proposed in [11] and [12], respectively.

D. THESIS ORGANIZATION

This thesis is organized into five chapters. The present chapter is the thesis introduction. Chapter II provides discussion related to OFDM, multipath channels, multiple input and output channels, and Alamouti's transmit diversity scheme. Chapter III offers a description on the several models used to obtain the results presented in this thesis, which are explained and interpreted in Chapter IV. Finally, Chapter V presents a summary of the conducted work, the conclusions and suggestions for further research.

II. MULTIPLE INPUT MULTIPLE OUTPUT ORTHOGONAL FREQUENCY DIVISION MULTIPLEXING

A. INTRODUCTION

In this chapter, we will introduce the theoretical basis behind OFDM and channel models. The concepts of path loss, shadowing, multipath, and MIMO will be introduced. In particular, the MIMO approach will be derived from the basic SISO configuration. Furthermore, a description of the space-time coding known as Alamouti's scheme will be presented. The necessary relations to its implementation in the transmitter and receiver for the 2x1 MISO and 2x2 MIMO configurations will also be established.

B. ORTHOGONAL FREQUENCY DIVISION MULTIPLEXING

1. Frequency Division Multiplexing

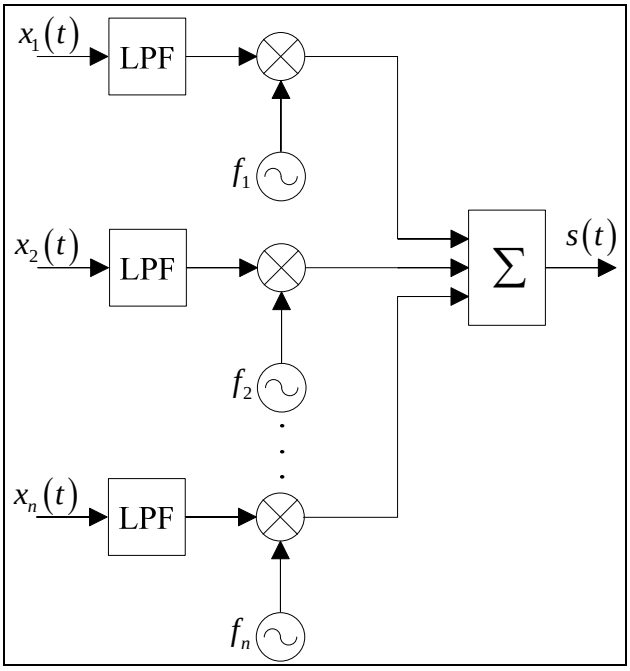

Figure 1. FDM Transmitter, after [13].

OFDM is one of the methods employed for efficient transmission of data blocks. Its concept is a refinement of frequency division multiplexing (FDM), where each carrier frequency is modulated with a separate information symbol, carrying one or more bits. A simplified representation of FDM transmitter is shown in Figure 1. The complex baseband representation of a particular time varying signal corresponding to the *n*th subcarrier with frequency f_n can be written as

$$s_n(t) = x_n(t)e^{j2\pi f_n t}. \tag{2.1}$$

Summing all the signals we obtain an expression for the output of the FDM transmitter as

$$s(t) = \sum_{n=1}^{N} x_n(t)e^{j2\pi f_n t}. \tag{2.2}$$

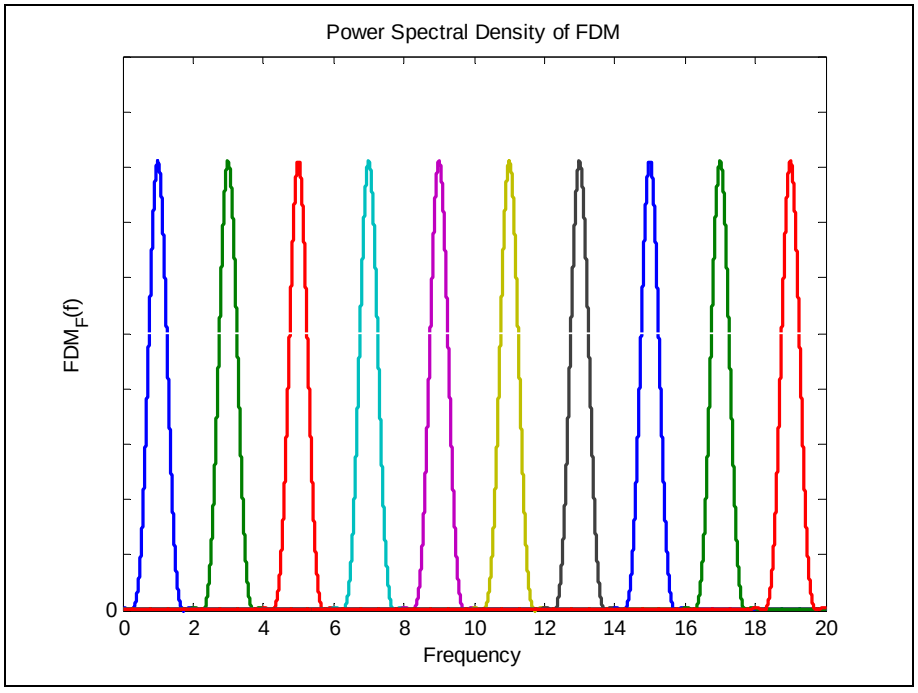

Figure 2. FDM Spectrum, after [2].

As depicted in Figure 2, in standard FDM a guard band between channels exists to avoid inter-carrier interference (ICI). It becomes clear that such a solution demands a great amount of bandwidth. To solve this particular disadvantage of FDM, in the 1960s

the concept of OFDM was proposed [2]. The original proposals pointed to the transmission of parallel data streams using FDM in which the channels no longer had a guard band in-between, but actually had an overlap. Figure 3 presents this concept. It is visible in comparing these two plots that a bandwidth gain of almost 50% is achievable. In creating an overlapping FDM, technique the problem of crosstalk between channels (sub-carriers) arises.

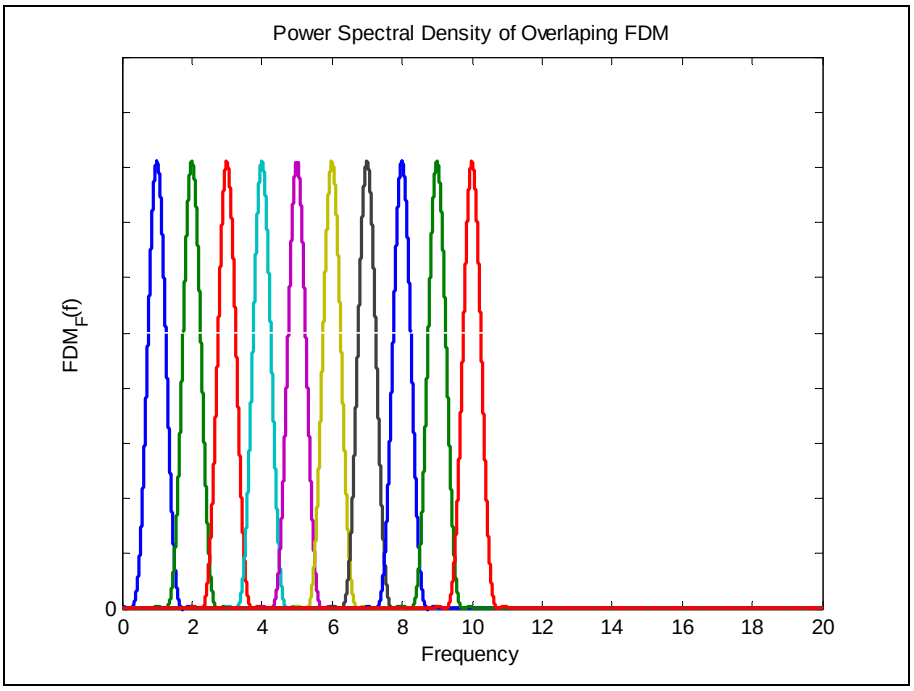

Figure 3. Overlapping FDM Spectrum, after [2].

2. Orthogonal Frequency Division Multiplexing

To eliminate the drawback of crosstalk in an overlapped FDM spectrum, the subcarriers must be *orthogonal* to each other in the sense of a standard inner product.

A baseband complex representation of the basic circuit for the OFDM transmitter with N subcarriers is shown in Figure 4. The complex baseband representation of a M-QAM signal corresponding to the nth subcarrier with frequency f_n can be written as [14]

$$s_n(t) = b_n e^{j2\pi f_n t}, 0 \le t \le T \tag{2.3}$$

where each symbol b_n takes values from an M-QAM alphabet in the time interval T, which represents a symbol period. Then, the normalized output signal of the OFDM transmitter becomes the superposition of all subcarriers as

$$s(t) = \frac{1}{N}\sum_{n=0}^{N-1} s_n(t) = \frac{1}{N}\sum_{n=0}^{N-1} b_n e^{j2\pi f_n t}, 0 \le t \le T . \tag{2.4}$$

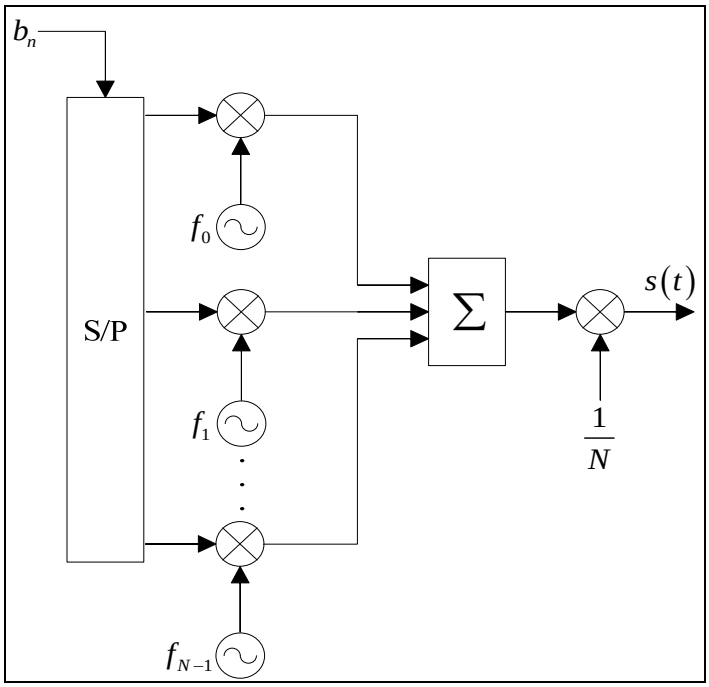

Figure 4. Oscillator Based OFDM Transmitter, after [1].

If this signal is sampled periodically with sampling interval $T_s = T/N$ and the spacing between subcarrier frequencies is established as $1/T$ (i.e. $f_n = n/T$), then the normalized output signal of the OFDM transmitter calculated at samples $t = kT_s$ can be expressed as

$$s(kT_s) = \frac{1}{N}\sum_{n=0}^{N-1} b_k e^{j2\pi \frac{kn}{N}} \tag{2.5}$$

which by definition is the Inverse Discrete Fourier Transform (IDFT).

It is difficult to assemble an OFDM transmitter with several modulators, one for each subcarrier, each containing its own oscillator, where the spacing between frequencies is critical to obtain the desired orthogonality. By reaching the result expressed in equation (2.5), it is clear that instead of constructing a traditional multi-oscillator based transmitter, it is far simpler to build such a system using an IDFT chip, generate the overall OFDM signal in baseband and digital format, and finally convert it to analog and translate it to radio-frequency (RF) before transmitting it to a channel. This conceptual OFDM transmitter is depicted in Figure 5.

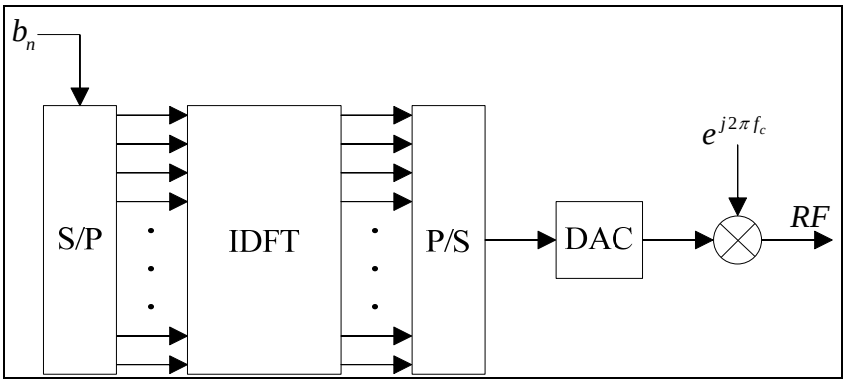

Figure 5. IDFT Based OFDM Transmitter, after [1].

In Figure 6 we present the general spectrum of a single subcarrier of an OFDM signal, considering the use of squared pulses in the modulation process. Its magnitude spectrum is then of the form $\text{sinc}\left[T\left(f - f_{sc}\right)\right]$. As depicted in Figure 7, the spectrum of each subcarrier will have zero crossings at frequencies $f_{sc} = n/T$ with integers $n = 1, 2, ..., N-1$, and the peak frequency at $n = 0$. By forcing the subcarrier frequencies to be multiples of the symbol period, they will be orthogonal in this interval. It is visible that, by establishing the previous relations, at the maximum of each subcarrier all other subcarriers are zero. Such a relation will allow a demodulation process free of interference from all other subcarriers present in the OFDM signal. This is called ICI avoidance [2]. The OFDM demodulation process uses the Discrete Fourier Transform (DFT). A simplified block diagram is presented in Figure 8.

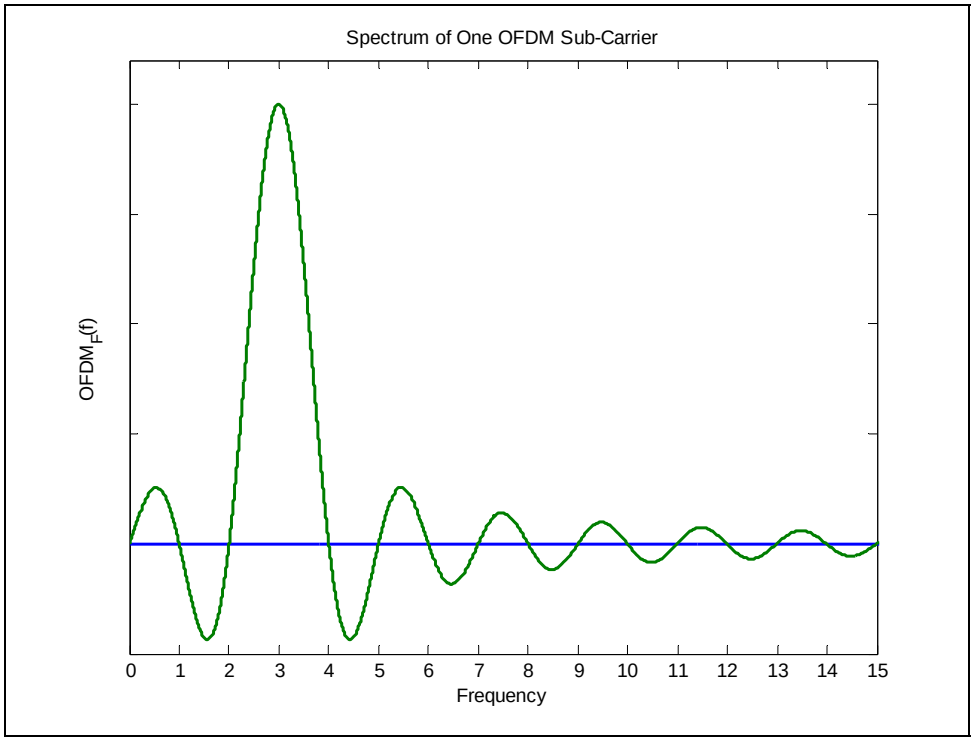

Figure 6. Sub-Carrier OFDM Spectrum, after [2].

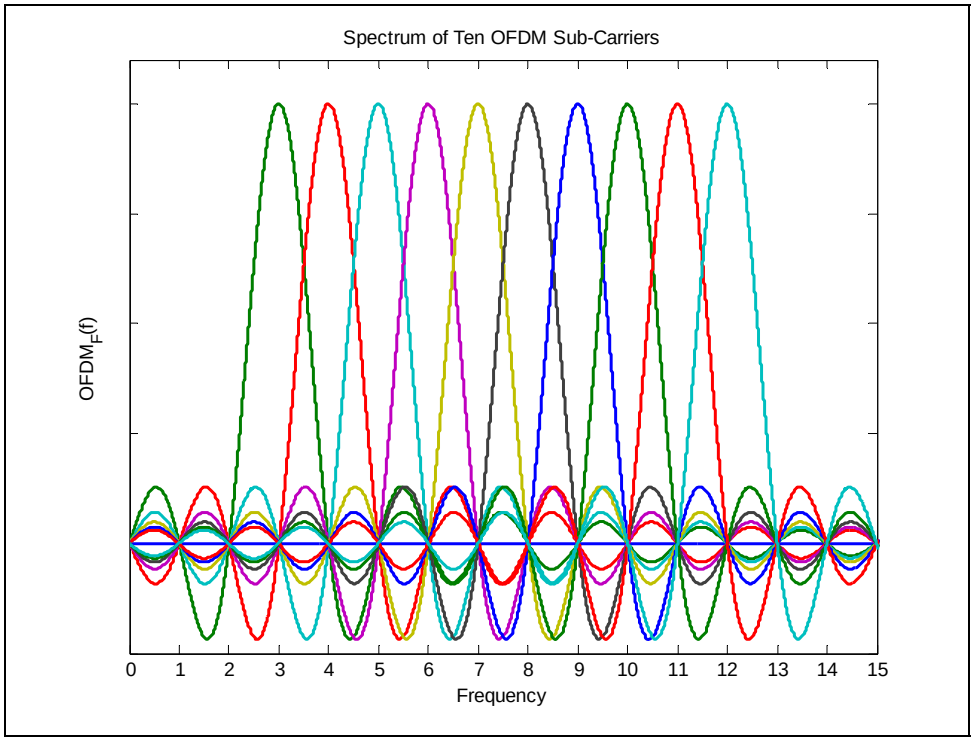

Figure 7. OFDM Signal Spectrum with Ten Sub-Carriers, after [2].

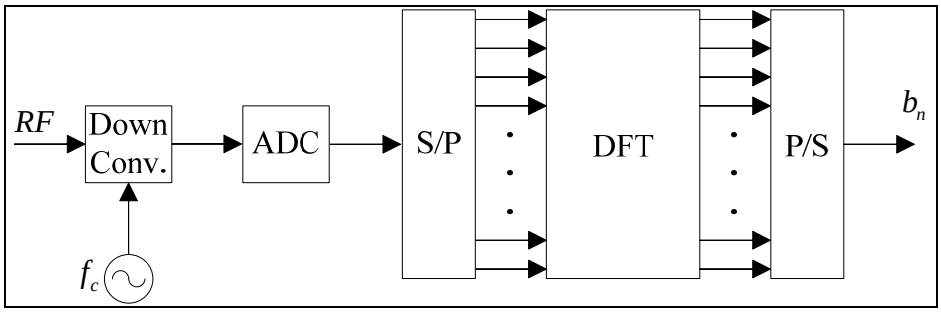

Figure 8. DFT Based OFDM Receiver, after [15].

C. CHANNELS

1. Additive White Gaussian Noise Channel

The simplest wireless communication channel model is the additive white Gaussian noise (AWGN) channel. As depicted in Figure 9, the output of the channel $r(t)$ is simply the sum of the input signal $s(t)$ and the noise source $n(t)$.

$$r(t) = s(t) + n(t). \tag{2.6}$$

The noise source has its main origin on the electronics of the receiver, but also from space noise. The basic thermal noise model assumes a power spectral density that is flat for all frequencies [16]

$$G_n(f) = \frac{N_0}{2} \text{ W/Hz}. \tag{2.7}$$

Because of its uniform power spectral density noise power is designated as white noise. Its autocorrelation function is the inverse Fourier transform of the noise power spectral density, which is a delta function scaled by $N_0/2$ [16]

$$R_n(\tau) = \mathcal{F}^{-1}\{G_n(f)\} = \frac{N_0}{2}\delta(\tau). \tag{2.8}$$

The power spectral density and its autocorrelation function are shown in Figure 10 and Figure 11, respectively. This model is described statistically as a Gaussian process, for this reason it takes the name of additive white Gaussian noise.

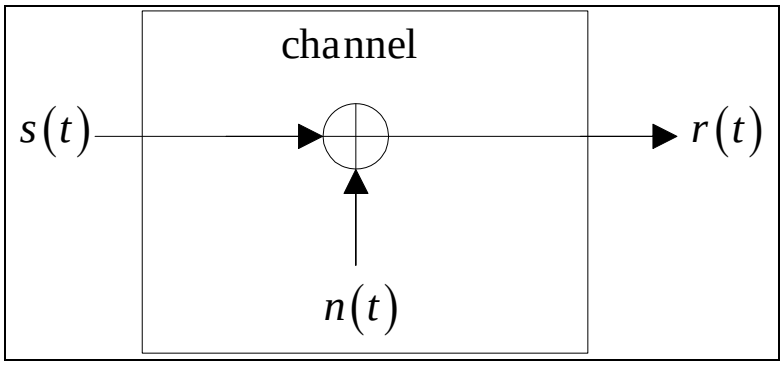

Figure 9. Additive White Gaussian Noise Channel, after [15].

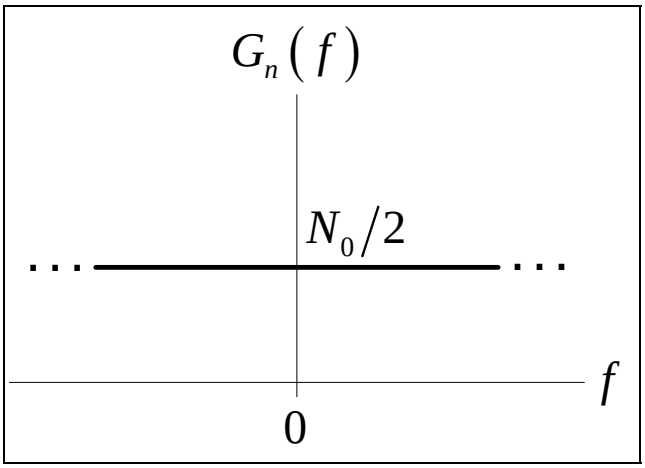

Figure 10. White Noise Power Spectral Density, from [16].

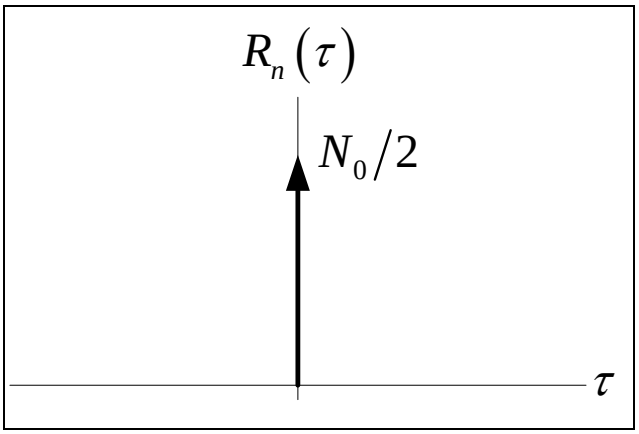

Figure 11. White Noise Autocorrelation Function, from [16].

2. Linear Time Varying Channel

The linear time varying channel model is an evolved AWGN channel, which includes physical characteristics such as multipath propagation. Starting with equation (2.6), the channel output $s(t)$ becomes the convolution of the input with the time varying channel impulse response, plus the AWGN [15]

$$r(t) = s(t) * h(\tau, t) + n(t) = \int_{-\infty}^{+\infty} h(\tau, t)\, s(t-\tau)\, d\tau + n(t) \tag{2.9}$$

where $h(\tau, t)$ is the channel response at time t in reaction to an impulse applied at time $t - \tau$. The linear time-variant channel with AWGN model is presented in Figure 12.

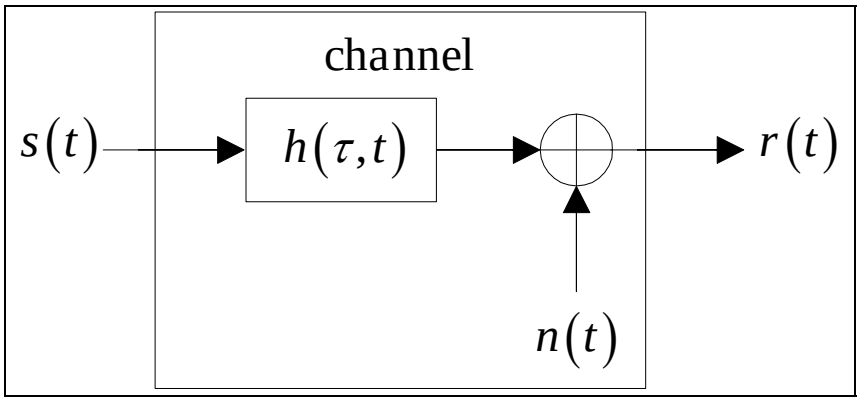

Figure 12. Linear Time Varying Channel with AWGN Model, after [15].

3. Large-Scale and Small-Scale Fading

Some authors [16], [17] divide the wireless channel effects in two types of fading effects: large-scale and small-scale fading. Specifically, the effects that cause the received power to vary are caused by long, medium and short distance phenomenons. These are path loss, shadowing and fading, respectively [1]. The first two are considered large-scale fading and the last small-scale fading.

a. Path Loss

The power obtained at a receiver antenna, placed at distance d from the transmitter, is obtained by application of Friis' free space loss equation [17]

$$\mathrm{P_r}(d) = \frac{G_t G_r \lambda^2}{(4\pi d)^2} P_t \tag{2.10}$$

where P_t is the transmitted power, G_t is the transmitter antenna gain, G_r is the receiver antenna gain, and λ is the wavelength. From equation (2.10) the path loss in dB can defined as

$$PL(d) = 10\log\left(\frac{P_t}{\mathrm{P_r}}\right) = -10\log\left(\frac{G_t G_r \lambda^2}{(4\pi d)^2}\right). \tag{2.11}$$

In order to accommodate a number of environments causing propagation losses we consider the general model [1]

$$\mathrm{P_r}(d) = P_t PL(d_0)\left(\frac{d_0}{d}\right)^{\gamma} \tag{2.12}$$

where $\mathrm{P_r}(d)$ is the received power at the receiver placed at a distance d from the transmitter, $PL(d_0)$ is the measured path loss at a reference distance d_0, and γ is the path loss exponential. Values for this parameter are presented in Table 1 and are dependent on the propagation environment. From equation (2.12) the empirical path loss in dB can be expressed as

$$PL_{emp}(d) = 10\log\left(\frac{P_t}{\mathrm{P_r}}\right) = \left[PL(d_0)\right] + 10\gamma\log\left(\frac{d}{d_0}\right). \tag{2.13}$$

Table 1. Path Loss Exponent vs. Environment, from [17].

Environment	Path Loss Exponent, γ
Free space	2
Urban area cellular radio	2.7 to 3.5
Shadowed urban cellular radio	3 to 5
In building line-of-sight	1.6 to 1.8
Obstructed building	4 to 6
Obstructed in factories	2 to 3

b. Shadowing

A further factor to consider on the received power at the receiver is the loss caused by random obstructions. These are normally caused by buildings, trees or vehicles that can appear between a transmitter and a mobile receiver radio-wave propagation path. Such effect is called shadowing [1]. From equation (2.12) we can incorporate the shadowing effect as a random variable

$$\mathrm{P_r}(d) = P_t PL(d_0)\chi\left(\frac{d_0}{d}\right)^{\gamma} \tag{2.14}$$

where χ is a sample of the shadowing random process. It is clear that the power at the receiver is now modeled in a way that original path loss is an expected received power value (or mean), and the shadowing is a random alteration around the expected value. Normally, the shadowing χ is modeled as a lognormal random variable as [1]

$$\chi = 10^{x/10}, \text{ where } \quad x \sim N\left(0, \sigma_s^2\right) \tag{2.15}$$

in which the shadowing standard deviation σ_s of the Gaussian distribution is expressed in dB. Typically this parameter is of the order of $6-12\text{dB}$ [1].

From equation (2.14) the empirical path loss plus shadowing in dB can be expressed as

$$PL_{emp}(dB) = 10\log\left(\frac{P_t}{P_r}\right) = \left[PL(d_0)\right] + 10\gamma\log\left(\frac{d}{d_0}\right) + [X] \qquad (2.16)$$

where $\left[PL(d_0)\right]$ is as defined before and $[X]$ is a zero mean Gaussian random variable with standard deviation σ_s expressed in dB.

c. Fading

Fading or specifically small-scale fading is influenced by a number of factors such as multipath propagation, speed of transmitter and/or receiver, speed of surrounding objects, and bandwidth of transmitted signal [17].

The relative transmitter or receiver velocities will introduce an apparent frequency change on the transmitted signal. This effect is designated as Doppler shift (or spread) and is expressed as [17]

$$f_d = \frac{v f_c \cos\theta}{c}, \qquad (2.17)$$

v is the relative speed between transmitter and receiver, f_c is the transmitted signal carrier frequency, θ is the angle between the direction of motion and propagation, and c is the speed of light. A parameter which can be defined from the Doppler shift is the coherence time and is expressed as [1]

$$T_c \approx \frac{1}{f_d}. \qquad (2.18)$$

From this relation it is understandable that if the Doppler shift is large the channel will change quicker than if the Doppler is small. This means that the Doppler plays an important role on the amount of time that we can consider the channel unaltered.

The multipath propagation is characterized as the sum of several received signals due to reflection on the propagation path. Some multipath channels will include a

line of sight (LOS) component and, in others, this component is negligible. In the literature statistical channel models for both cases (with and without LOS) are provided. These models are designated as Ricean fading channel and Rayleigh fading channel, respectively. Figure 13 presents the multipath channel with LOS. From this figure, it is clear that the received signal $r(t)$ will be composed of the original signal $s(t)$, plus delayed copies (two in this case) of the original signal

$$r(t) = a_1(t)s(t-\tau_1) + a_2(t)s(t-\tau_2) + a_3(t)s(t-\tau_3). \tag{2.19}$$

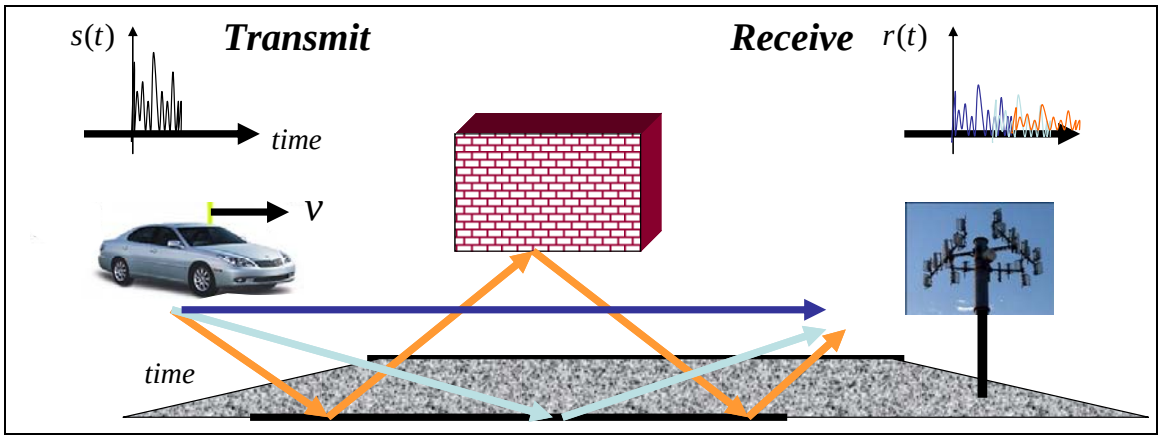

Figure 13. Multipath Channel with LOS, after [18].

In general the received signal can be considered a sum of attenuated, time delayed, phase shifted replicas of the original transmitted signal. The baseband impulse response of a multipath channel can be expressed as [17]

$$h_b(\tau,t) = \sum_{i=0}^{N-1} a_i(\tau,t) e^{\left[j\left(2\pi f_c \tau_i(t) + \varphi_i(\tau,t)\right)\right]} \delta\left(\tau - \tau_i(t)\right) \tag{2.20}$$

where we define excess delay as the delay between the first arriving multipath component $\tau_0 = 0$ and the *i*th multipath component. The propagation delay is neglected when plotting multipath channel impulse responses. $a_i(\tau,t)$ and $\tau_i(t)$ are the real amplitudes

and excess delays of the *i*th multipath component at time t, respectively. The term $2\pi f_c \tau_i(t) + \varphi_i(\tau, t)$ represents the phase shift due to propagation and also reflections or scattering in the path.

Based on the power spread $P(\tau)$ we can define the mean and the root mean square (RMS) value of the time delay as [17]

$$\bar{\tau} = \frac{\sum_i a_i^2 \tau_i}{\sum_i a_i^2} = \frac{\sum_i P(\tau_i)\tau_i}{\sum_i P(\tau_i)} \tag{2.21}$$

$$\tau_{RMS} = \sqrt{\overline{\tau^2} - \left(\bar{\tau}\right)^2} \tag{2.22}$$

where

$$\overline{\tau^2} = \frac{\sum_i a_i^2 \tau_i^2}{\sum_i a_i^2} = \frac{\sum_i P(\tau_i)\tau_i^2}{\sum_i P(\tau_i)}. \tag{2.23}$$

Now we can define the channel coherence bandwidth B_c as [1]

$$B_c \approx \frac{1}{5\tau_{RMS}} \approx \frac{1}{\tau_{\max}}. \tag{2.24}$$

The channel coherence bandwidth B_c gives an approximation on how wide is the distance between two frequencies that still have a correlated frequency response. That is, it defines the range of frequencies where a specific channel is regarded as having equal gain, thus the designation frequency flat.

Table 2. Broadband Fading Parameters vs. OFDM Design Impact, after [1].

Parameter	If "Large"?	If "Small"?	Design Impact
Delay spread, τ	If $\tau \gg T$, frequency selective	If $\tau \ll T$, frequency flat	The larger the τ to the T, the more severe the ISI
Coherence bandwidth, B_c	If $\frac{1}{B_c} \ll T$, frequency flat	If $\frac{1}{B_c} \gg T$, frequency selective	Guideline to subcarrier width $B_{sc} \approx B_c/10$ and number of subcarriers $L \geq 10B_w/B_c$
Doppler spread, $f_d = \frac{vf_c}{c}$	If $vf_c \gg c$, fast fading	If $vf_c \leq c$, slow fading	As f_d/B_{sc} becomes non-negligible, subcarrier orthogonality is compromised
Coherence time, T_c	If $T_c \gg T$, slow fading	If $T_c \leq T$, fast fading	T_c small necessitates frequent channel estimation and limits T but provides greater time diversity

All the parameters presented in this section are important when designing an OFDM system, since the channel characteristics will have an impact on the system performance. In Table 2 a summary of these parameters versus its design impact is presented. In this table, T is the symbol time and L is the number of subcarriers in an OFDM signal. Figure 14 shows the impact of both large-scale and small-scale fading on the received signal versus the transmitter to receiver distance.

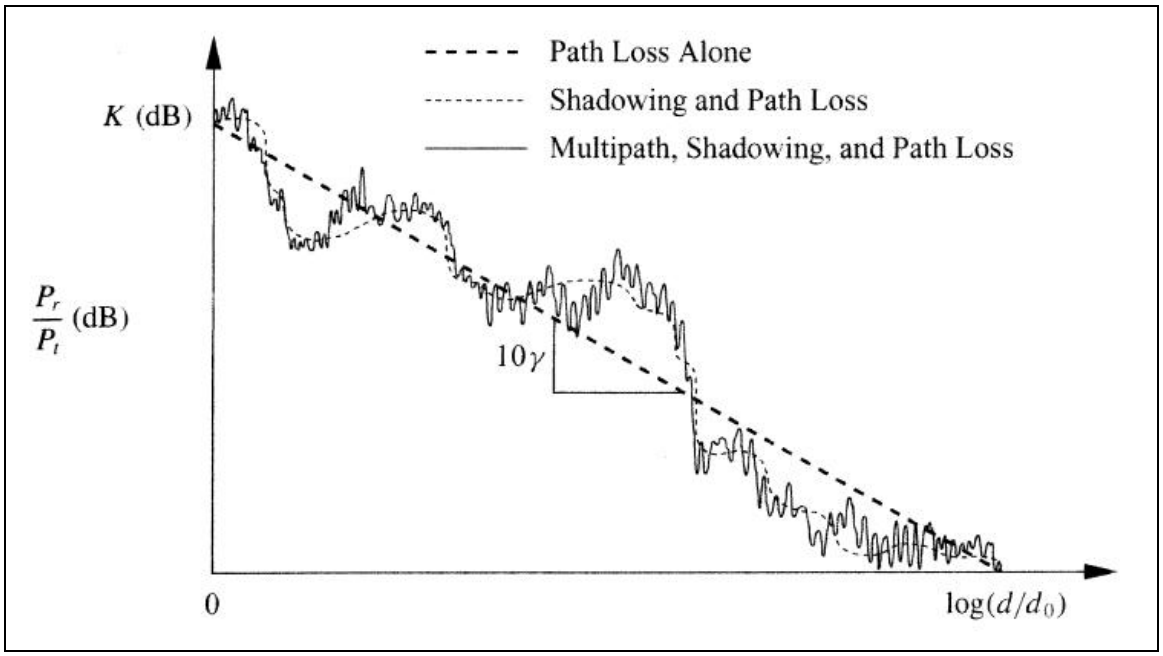

Figure 14. Combined Path Loss, Shadowing and Multipath Fading, from [19].

4. Single Input Single Output Channel

The SISO channel model, depicted in Figure 15, is the classical communication link between a single transmitting and single receiving antenna. As a starting point, let us consider equation (2.9) that was the mathematical representation of a received signal that had travel through a time varying channel with AWGN. From that starting point, for simplification purposes, we neglect the AWGN and consider that the channel is casual and its impulse response is finite with duration τ_{total}. Then a SISO received signal becomes

$$r(t) = s(t) * h(\tau, t) = \int_0^{\tau_{total}} h(\tau, t) s(t-\tau) d\tau \,. \tag{2.25}$$

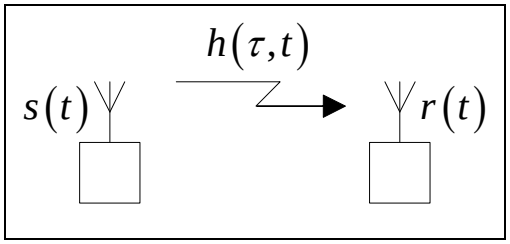

Figure 15. SISO Channel Model, after [1].

5. Single Input Multiple Output Channel

The SIMO channel model has a single transmitting antenna and several receiving antennas $i \in \{1,2,...,M_R\}$. The SIMO channel model is shown in Figure 16. In this case, each receiving antenna receives a signal that is the convolution between the transmitted signal and the *i*th channel impulse response $h_i(\tau,t)$

$$r_i(t) = s(t) * h_i(\tau,t), i = 1,2,...,M_R . \tag{2.26}$$

If we define both the received signal and the impulse responses as vectors of dimensions $M_R \times 1$ as follows

$$\mathbf{r}(t) = \left[r_1(t), r_2(t), \cdots r_{M_R}(t) \right]^T \tag{2.27}$$

$$\mathbf{h}(\tau,t) = \left[h_1(\tau,t), h_2(\tau,t), \cdots h_{M_R}(\tau,t) \right]^T \tag{2.28}$$

then equation (2.26) becomes

$$\mathbf{r}(t) = \mathbf{h}(\tau,t) * s(t). \tag{2.29}$$

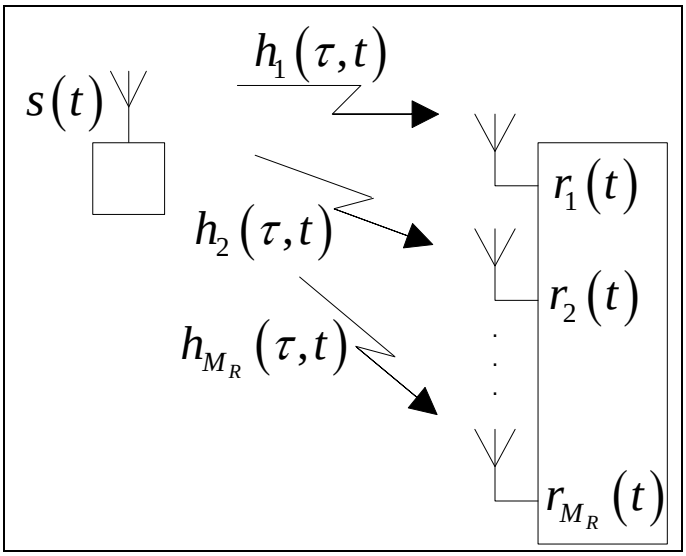

Figure 16. SIMO Channel Model, after [1].

6. Multiple Input Single Output Channel

The MISO channel is basically the opposite of the SIMO channel model. In this case we now have several transmitting antennas $j \in \{1,2,...,M_T\}$ and a single receiving antenna. Figure 17 represents such a model. In this case the received signal is the sum of each transmitted signal convolved with its respective path impulse response

$$r(t) = \sum_{j=1}^{M_T} s_j(t) * h_j(\tau,t). \tag{2.30}$$

Let us define the transmitted signals and the impulse responses as vectors of dimensions $M_T \times 1$ and $1 \times M_T$, respectively

$$\mathbf{s}(t) = \left[s_1(t),\, s_2(t), \cdots s_{M_T}(t) \right]^T \tag{2.31}$$

$$\mathbf{h}(\tau,t) = \left[h_1(\tau,t), h_2(\tau,t), \cdots h_{M_T}(\tau,t) \right] \tag{2.32}$$

then equation (2.30) can be expressed as

$$r(t) = \mathbf{h}(\tau,t) * \mathbf{s}(t). \tag{2.33}$$

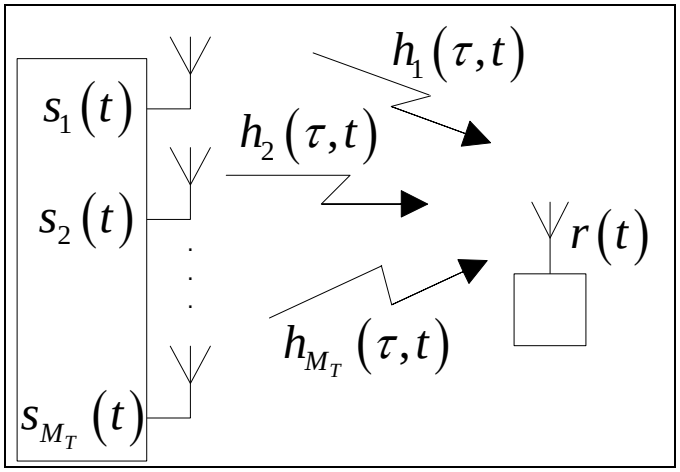

Figure 17. MISO Channel Model, after [1].

7. Multiple Input Multiple Output Channel

In the MIMO channel model, as depicted in Figure 18, we have several transmitting antennas $j \in \{1,2,...,M_T\}$ and several receiving antennas $i \in \{1,2,...,M_R\}$. In this case, the received signal $r_i(t)$ in the *i*th receiving antenna is the sum of all transmitted signals throughout all transmitting antennas M_T with all possible impulse responses $h_{i,j}(\tau,t)$

$$r_i(t) = \sum_{j=1}^{M_T} s_j(t) * h_{i,j}(\tau,t), i = 1,2,\cdots,M_R . \tag{2.34}$$

If we define all the possible channel impulse responses $h_{i,j}(\tau,t)$, between any *j*th transmitting antenna and any *i*th receiving antenna, in a matrix of dimensions $M_R \times M_T$ as

$$\mathbf{H}(\tau,t) = \begin{bmatrix} h_{1,1}(\tau,t) & h_{1,2}(\tau,t) & \cdots & h_{1,M_T}(\tau,t) \\ h_{2,1}(\tau,t) & h_{2,2}(\tau,t) & \cdots & h_{2,M_T}(\tau,t) \\ \vdots & \vdots & \ddots & \vdots \\ h_{M_R,1}(\tau,t) & h_{M_R,2}(\tau,t) & \cdots & h_{M_R,M_T}(\tau,t) \end{bmatrix} \tag{2.35}$$

and $\mathbf{s}(t)$ as defined in equation (2.31), then the output of the MIMO channel can be expressed as

$$\mathbf{r}(t) = \mathbf{H}(\tau,t) * \mathbf{s}(t) \tag{2.36}$$

where $\mathbf{r}(t)$ is as defined in equation (2.27).

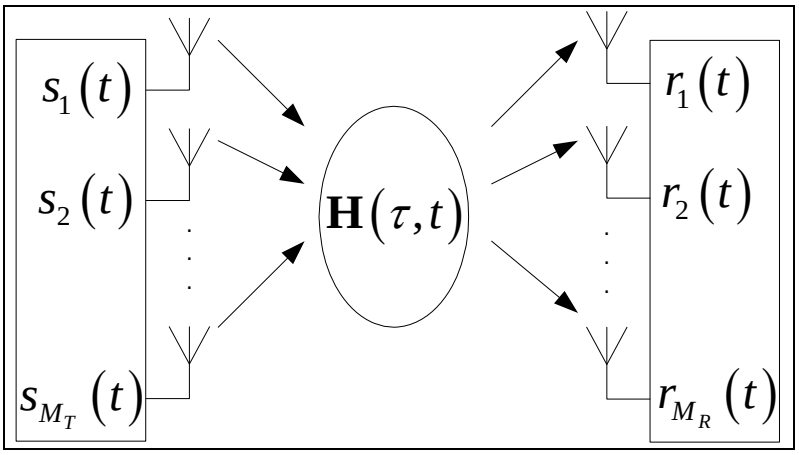

Figure 18. MIMO Channel Model, after [20].

8. Simulation of MISO, SIMO and MIMO Channels with Multipath

A multipath channel can be simulated as the sum of tapped delayed lines originated form a single input. Each line incorporates complex exponential time variant coefficients. This model is shown in Figure 19 and generically implements equation (2.20).

A MIMO 2x2 channel model with multipath, as depicted in Figure 20, can be expressed as [3]

$$\mathbf{H}(\tau,t)=\begin{bmatrix} e^{j\phi_1} & 0 \\ 0 & e^{j\phi_2} \end{bmatrix}\begin{bmatrix} 1 & \rho_R \\ \rho_R & 1 \end{bmatrix}\begin{bmatrix} h_1(\tau,t) & 0 \\ 0 & h_2(\tau,t) \end{bmatrix}\begin{bmatrix} 1 & \rho_T \\ \rho_T & 1 \end{bmatrix}\begin{bmatrix} e^{j\phi_3} & 0 \\ 0 & e^{j\phi_4} \end{bmatrix} \quad (2.37)$$

where $h_1(\tau,t)$ and $h_2(\tau,t)$ represent the multipath tapped delay line components and are written in the form

$$h_c(\tau,t)=h_c(0,t)\delta(\tau)+\sum_{i=1}^{N-1}h_c(i,t)\delta(\tau-\tau_i),\ for\ c=1,2\,. \quad (2.38)$$

The phases ϕ_i, with $i=1,2,3,4$, are chosen randomly and account for antenna position and the signal angle of arrival or angle of departure. The coefficients ρ_T and ρ_R account

for the level of correlation between the antennas at transmitter and receiver. The tapped delay line components $h_c(\tau,t)$ are independent complex Gaussian random variables with delay τ_i and phase shift φ_i.

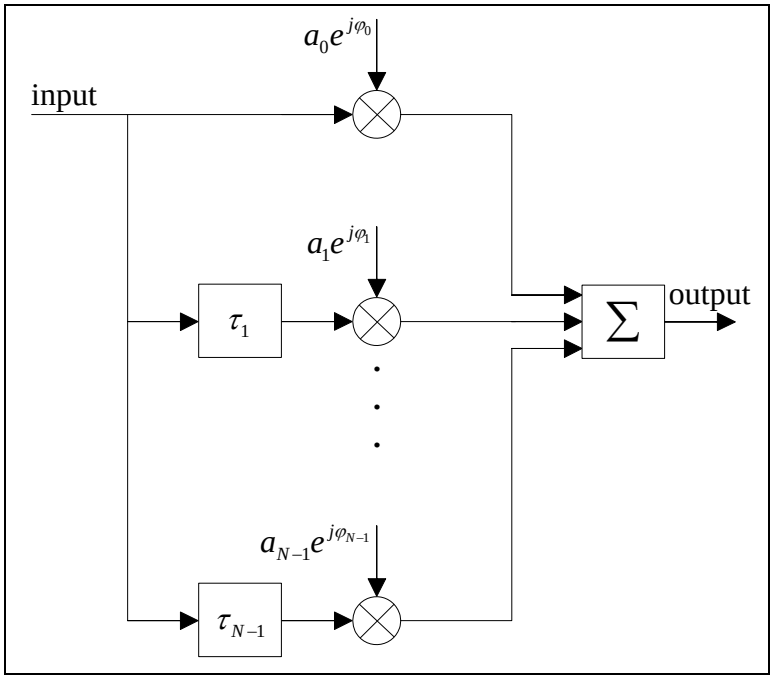

Figure 19. Multipath Channel Model, after [17].

The MISO and SIMO channel models can be constructed from a MIMO channel model by leaving a single output and a single input connected, respectively [3].

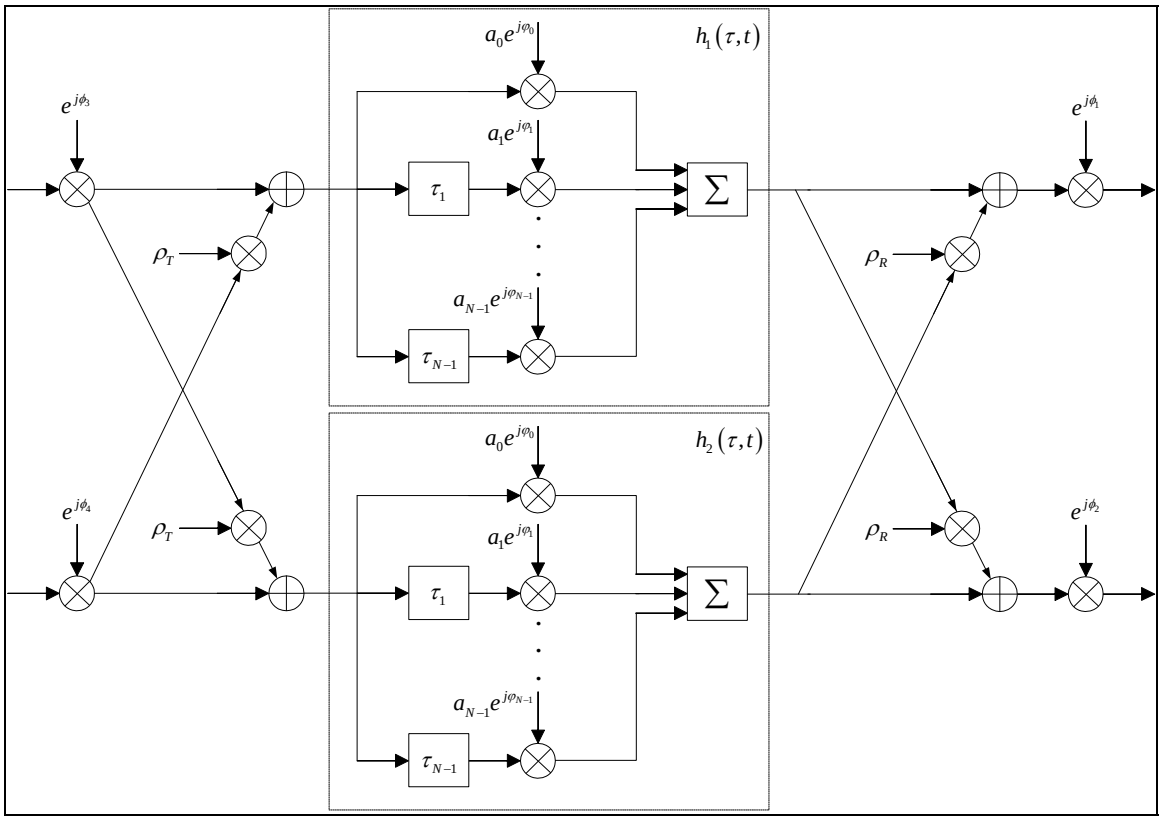

Figure 20. MIMO 2x2 Channel Model with Multipath, after [3].

D. ALAMOUTI'S SCHEME

1. Alamouti's Scheme in MISO 2x1 Configuration

Consider a MISO system with two transmitting antennas and one receiving antenna. Define the complex baseband signal from the first transmitting antenna (tx antenna 1) as s_1, and the signal from the second transmitting antenna (tx antenna 2) as s_2. In the following symbol period however, let antenna one transmit $-s_2^*$ and antenna two transmit s_1^*, where $*$ represents the complex conjugate of the symbol. The space-time encoding described is summarized in Table 3, where T is the symbol duration. The complete MISO 2x1 system using Alamouti's scheme is shown in Figure 21.

Table 3. Encoding and Transmission Sequence of Alamouti's Scheme, after [9].

	Antenna 1	**Antenna 2**
Time t	s_1	s_2
Time $t+T$	$-s_2^*$	s_1^*

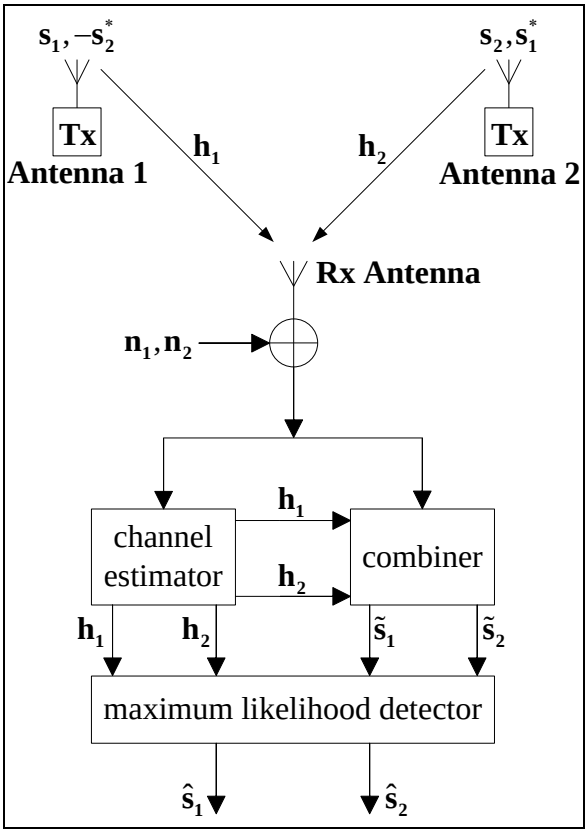

Figure 21. MISO 2x1 System using Alamouti's Scheme, after [9].

Now let us consider that the channels between the two transmitting antennas and the receiving antenna have flat fading behavior during two consecutive symbols, and that they can be modeled as complex exponentials. Then the channels can be expressed as [9]

$$\begin{aligned} h_1(t) &= h_1(t+T) = h_1 = \alpha_1 e^{j\theta_1} \\ h_2(t) &= h_2(t+T) = h_2 = \alpha_2 e^{j\theta_2} \end{aligned} \tag{2.39}$$

and the received signal at time t and $t+T$ can be written as [9]

$$\begin{aligned} r_1 &= r_1(t) = r(t) = h_1 s_1 + h_2 s_2 + n_1 \\ r_2 &= r_2(t) = r(t+T) = -h_1 s_2^* + h_2 s_1^* + n_2 \end{aligned} \tag{2.40}$$

where n_1 and n_2 are complex additive random variables that account for noise at the receiver.

The combiner receives the received signals and the channels estimates and constructs the following relations [9]

$$\begin{aligned} \tilde{s}_1 &= h_1^* r_1 + h_2 r_2^* \\ \tilde{s}_2 &= h_2^* r_1 - h_1 r_2^* \end{aligned} \tag{2.41}$$

which will be provided to the maximum likelihood detector. If we substitute equations (2.39) and (2.40) into the combiner equations (2.41), we can further expand these relations as [9]

$$\begin{aligned} \tilde{s}_1 &= \left(\alpha_1^2 + \alpha_2^2\right) s_1 + h_1^* n_1 + h_2 n_2^* \\ \tilde{s}_2 &= \left(\alpha_1^2 + \alpha_2^2\right) s_2 - h_1 n_2^* + h_2^* n_1 \end{aligned} . \tag{2.42}$$

Finally, the maximum likelihood detector will choose the symbol s_i, measuring the Euclidian distance between the received symbol and the symbols used in the constellation of the transmitted signal, and choosing the closest [9]

$$\left(\alpha_1^2 + \alpha_2^2 - 1\right)\left|s_i\right|^2 + d^2\left(\tilde{s}_1, s_i\right) \le \left(\alpha_1^2 + \alpha_2^2 - 1\right)\left|s_j\right|^2 + d^2\left(\tilde{s}_1, s_j\right), \forall i \ne j . \tag{2.43}$$

The outputs of the maximum likelihood detector $\hat{s}_1$ and $\hat{s}_2$ are the estimates of the transmitted symbols s_1 and s_2, respectively.

2. Alamouti's Scheme in MIMO 2x2 Configuration

The MIMO 2x2 Alamouti's scheme uses the same transmitting relations as the MISO 2x1 scheme. However, since we now have two antennas on the receiver, instead of one, the channel and the received signal will double when compared to the previous configuration. This system is depicted in Figure 22. The channels to antennas relations and received signals notation is presented in Table 4 and Table 5, respectively.

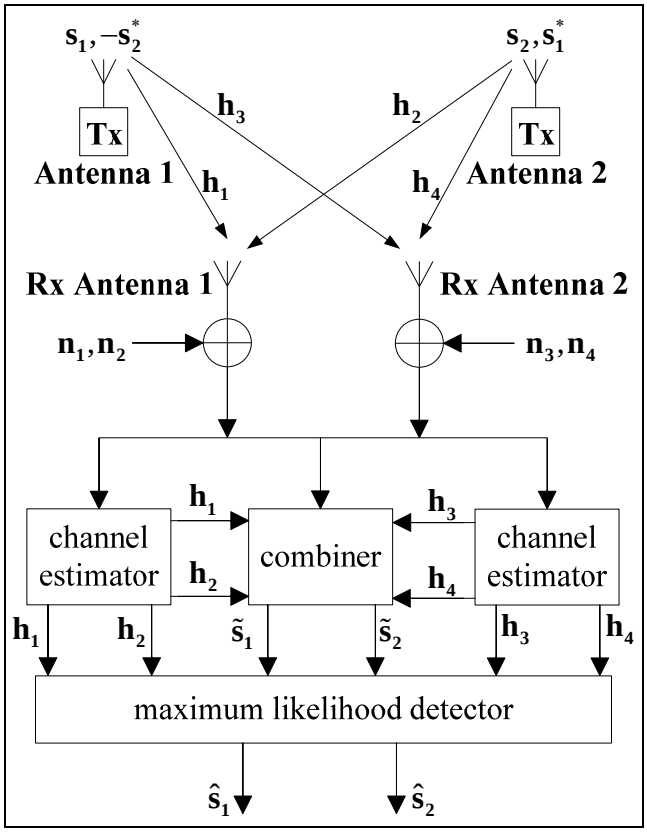

Figure 22. MIMO 2x2 System using Alamouti's Scheme, after [9].

Table 4. Channels to Antennas Relations of Alamouti's MIMO 2x2 Scheme, after [9].

	Rx Antenna 1	**Rx Antenna 2**
Tx Antenna 1	$h_1 = \alpha_1 e^{j\theta_1}$	$h_3 = \alpha_3 e^{j\theta_3}$
Tx Antenna 2	$h_2 = \alpha_2 e^{j\theta_2}$	$h_4 = \alpha_4 e^{j\theta_4}$

Table 5. Received Signals Notation of Alamouti's MIMO 2x2 Scheme, after [9].

	Rx Antenna 1	**Rx Antenna 2**
Time t	r_1	r_3
Time $t+T$	r_2	r_4

Now we can write the received signals presented in Table 5 as [9]

$$\begin{aligned} r_1 &= h_1 s_1 + h_2 s_2 + n_1 \\ r_2 &= -h_1 s_2^* + h_2 s_1^* + n_2 \\ r_3 &= h_3 s_1 + h_4 s_2 + n_3 \\ r_4 &= -h_3 s_2^* + h_4 s_1^* + n_4 \end{aligned} \tag{2.44}$$

where n_k with $k = 1,2,3,4$, are complex additive random variables that account for noise at the receiver. The combiner takes the received signals and the channel estimates and assembles the following relations [9]

$$\begin{aligned} \tilde{s}_1 &= h_1^* r_1 + h_2 r_2^* + h_3^* r_3 + h_4 r_4^* \\ \tilde{s}_2 &= h_2^* r_1 - h_1 r_2^* + h_4^* r_3 - h_3 r_4^* \end{aligned} \tag{2.45}$$

that can be further expanded, if we substitute in equations (2.44) and the relations expressed in Table 4, as [9]

$$\begin{aligned}\tilde{s}_1 &= \left(\alpha_1^2+\alpha_2^2+\alpha_3^2+\alpha_4^2\right)s_1 + h_1^* n_1 + h_2 n_2^* + h_3^* n_3 + h_4 n_4^* \\ \tilde{s}_2 &= \left(\alpha_1^2+\alpha_2^2+\alpha_3^2+\alpha_4^2\right)s_2 - h_1 n_2^* + h_2^* n_1 - h_3 n_4^* + h_4^* n_3\end{aligned}. \tag{2.46}$$

The maximum likelihood detector will then choose the symbol $\mathbf{s_1}$ and $\mathbf{s_2}$ using the following relations, respectively [9]

$$\begin{aligned}&\left(\alpha_1^2+\alpha_2^2+\alpha_3^2+\alpha_4^2-1\right)\left|s_i\right|^2 + d^2\left(\tilde{s}_1, s_i\right) \\ &\qquad \le \left(\alpha_1^2+\alpha_2^2+\alpha_3^2+\alpha_4^2-1\right)\left|s_j\right|^2 + d^2\left(\tilde{s}_1, s_j\right), \forall i \ne j, \text{for } s_1 \\ &\left(\alpha_1^2+\alpha_2^2+\alpha_3^2+\alpha_4^2-1\right)\left|s_i\right|^2 + d^2\left(\tilde{s}_2, s_i\right) \\ &\qquad \le \left(\alpha_1^2+\alpha_2^2+\alpha_3^2+\alpha_4^2-1\right)\left|s_j\right|^2 + d^2\left(\tilde{s}_2, s_j\right), \forall i \ne j, \text{for } s_2\end{aligned} \tag{2.47}$$

The outputs of the maximum likelihood detector $\hat{\mathbf{s}}_1$ and $\hat{\mathbf{s}}_2$ are the estimates of the transmitted symbols $\mathbf{s_1}$ and $\mathbf{s_2}$, respectively.

E. SUMMARY

In the present chapter, we have introduced OFDM modulation and channel characteristics important to OFDM systems design. Practical implementation of channel models was also introduced. Finally, Alamouti's scheme for MISO 2x1 and MIMO 2x2 systems was discussed. In the next chapter, we will describe the SISO, MISO and MIMO OFDM models used in simulations performed in this thesis to obtain the results presented in Chapter IV. Furthermore, a presentation on the ITU channel models will be provided.

III. MODELS DESCRIPTION

A. INTRODUCTION

In the previous chapter, the basic theory on channel models and OFDM modulation was presented. In this chapter, a description of the models used to obtain the results later presented in this thesis will be provided. The basis of the work conducted during the thesis is a model provided by the MathWorks™ in the MATLAB® & SIMULINK® R2008a software package. Specifically, the IEEE® 802.16-2004 OFDM PHY Link, Including Space-Time Block Coding model was used. This base model can be found under Demos-Blocksets-Application Specific Examples. The base model was modified and improved on several blocks and several settings were changed to meet the research and simulations requirements. As a result of the work presented in this thesis three models were developed as described in the following sections.

B. SISO OFDM MODEL

The SISO OFDM model is shown in Figure 23 and its blocks are presented in the following sections.

1. Forward Error Control and Modulator Bank

This bank comprises seven FEC and modulator lines, one for each of the seven modulation schemes and the overall coding rate used in the IEEE® 802.16 standard: BPSK $r = 1/2$; QPSK $r = 1/2$; QPSK $r = 3/4$; 16QAM $r = 1/2$; 16QAM $r = 3/4$; 64QAM $r = 2/3$; 64QAM $r = 3/4$.

a. BPSK r=1/2 FEC and Modulator

The stream of random bits generated by the Data Source block is provided in blocks of bits designated unconstructed blocks. Several data source blocks are collected to form the data blocks provided to the modulator .The sizes of these blocks are presented in Table 6. The last column of this table presents the final value of the blocks

of data bits after appending the tail byte of zero. The blocks of bits are encoded by a convolution encoder of rate $r = 1/2$ and generator polynomials $g_1 = 171_{oct}$ and $g_2 = 133_{oct}$. No puncturing is executed. The data is then interleaved and finally modulated with BPSK modulation.

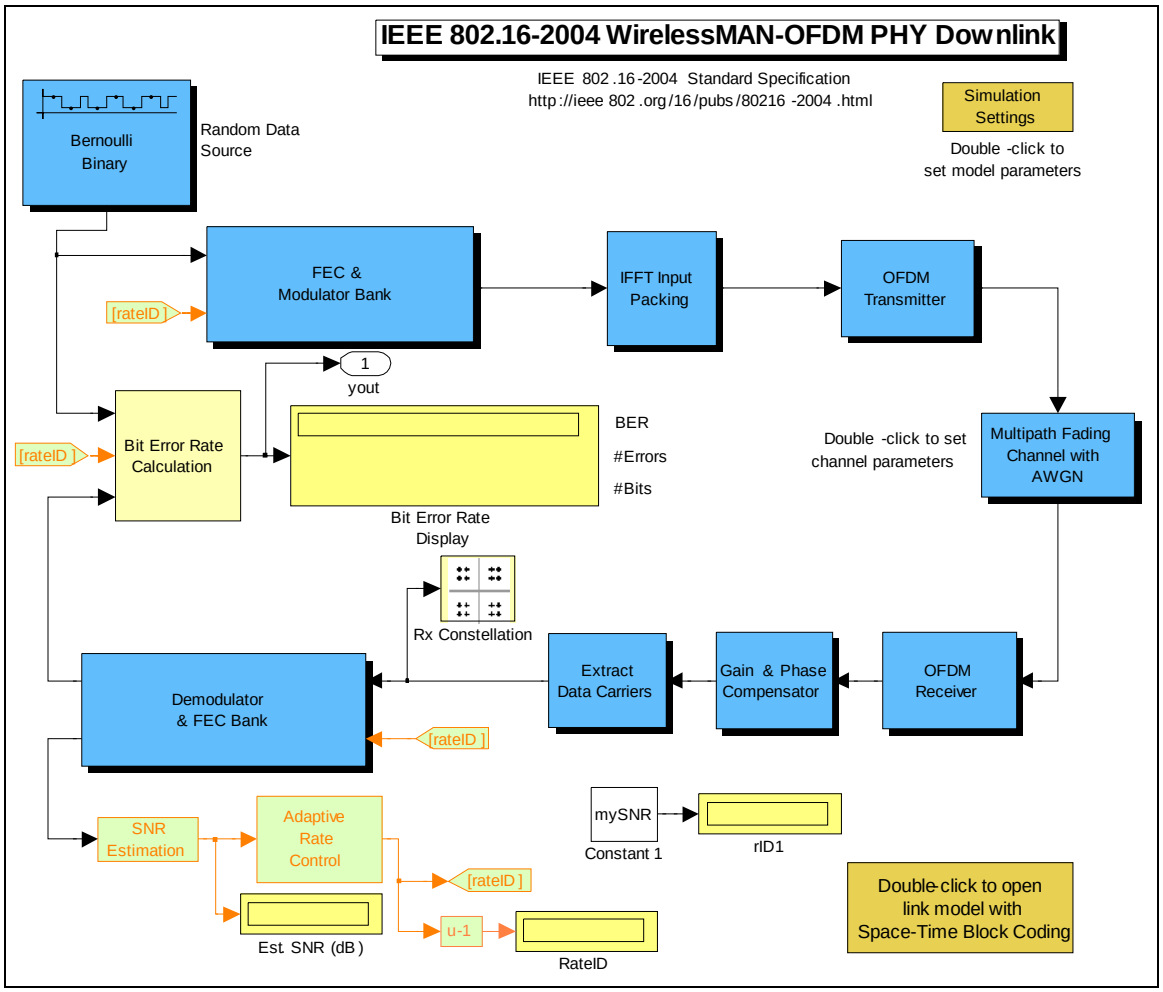

Figure 23. SISO OFDM Model.

Table 6. Data Block Size per Modulation Scheme.

Modulation scheme	Unconstructed block size	Block size before zero pad tail byte	Block size after zero pad tail byte
BPSK $r = 1/2$	12	88	96
QPSK $r = 1/2$	24	184	192
QPSK $r = 3/4$	36	280	288
16QAM $r = 1/2$	48	376	384
16QAM $r = 3/4$	72	568	576
64QAM $r = 2/3$	96	760	768
64QAM $r = 3/4$	108	856	864

b. Remaining FEC and Modulators

In the remaining six FEC and modulators lines the stream of random bits generated by the Data Source is grouped in blocks and padded as described in the previous section. The blocks of data are afterwards applied to a Reed-Solomon encoder with the specifications presented in Table 7. Following that operation the data is encoded by a convolutional encoder with generator polynomials presented in the previous section. This encoder also provides puncturing in order to obtain the overall coding rates previously stated. In Table 8, the convolution encoder puncturing configuration is presented and its conceptual implementation is depicted in Figure 24. The data is then interleaved and finally modulated with one of the modulation schemes presented in the first column of Table 7. Finally, the last block yields the respective modulation scheme block, i.e., the QPSK's lines have QPSK modulator blocks and the *M*-QAM lines have *M*-QAM modulator blocks.

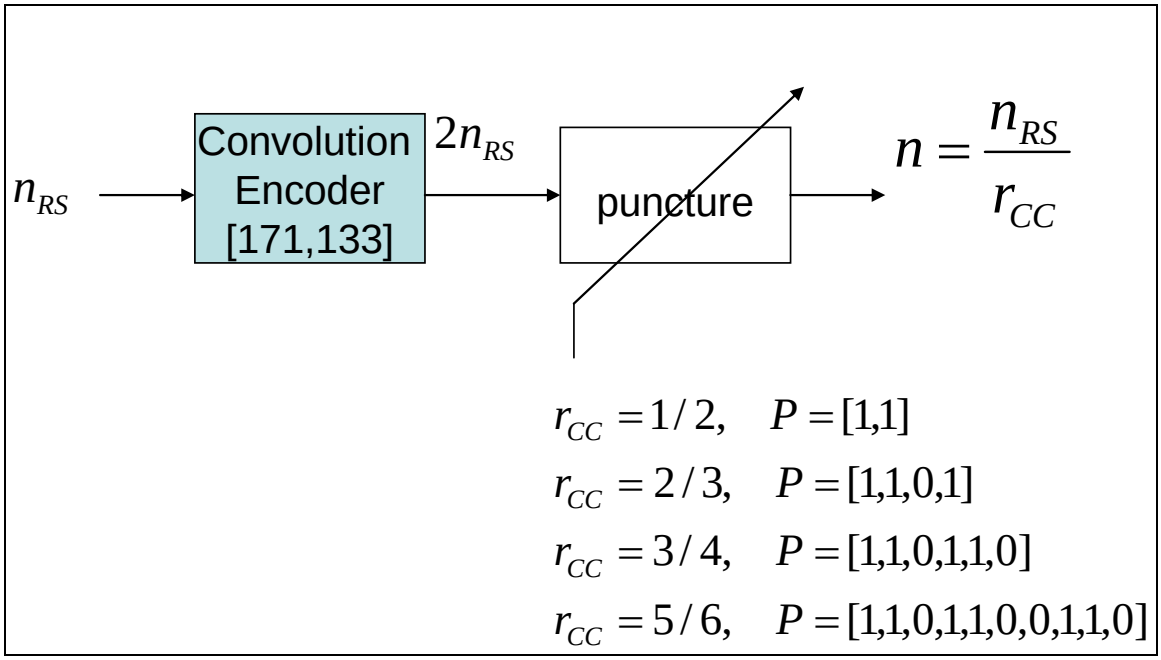

Figure 24. Convolution Encoder and Puncturing, after [18].

Table 7. Reed-Solomon Encoder Specifications, from [10].

Modulation scheme	**Overall coding rate**	**Reed-Solomon code**	**Convolution code rate**
QPSK $r = 1/2$	1/2	(32,24)	2/3
QPSK $r = 3/4$	3/4	(40,36)	5/6
16QAM $r = 1/2$	1/2	(64,48)	2/3
16QAM $r = 3/4$	3/4	(80,78)	5/6
64QAM $r = 2/3$	2/3	(108,96)	3/4
64QAM $r = 3/4$	3/4	(120,108)	5/6

Table 8. Convolution Encoder Puncturing Configuration, from [10].

	Code rates			
Rate	1/2	2/3	3/4	5/6
d_{free}	10	6	5	4
X	1	10	101	10101
Y	1	11	110	11010
XY	X_1Y_1	$X_1Y_1Y_2$	$X_1Y_1Y_2X_3$	$X_1Y_1Y_2X_3Y_4X_5$

2. OFDM Modulator

In the IFFT Input Packing block the data from the modulators is first transformed from serial to parallel and then distributed through the sub-channels. At this point the data corresponding to the DC carrier and the Pilot Carriers is generated. The DC index is simply set to zero in order to decouple the data from the carrier. The pilots are all produced using the same pseudo-random sequence, BPSK modulated as produced by the Pilot Generator. The indexing for the IFFT input is shown in Figure 25.

In the OFDM transmitter, first a short preamble is appended to the data provided by the IFFT Input Packing. The preamble, in all three models, is used for synchronization and to estimate the CSI. Then twenty-eight nulls in the lower indexes and twenty-seven nulls in the upper indexes are added to the original two-hundred-and-one indexes to provide frequency guard bands. The ordering of the data follows the modulo operation (256 carriers in this case) and it is shown in Figure 25.

A gain block is used to compensate for the number of sub-carriers and normalize the transmitted power. Its expression is given by

$$G = \sqrt{L_{FFT}} \cdot \sqrt{\frac{L_{FFT}}{L_{used}}} = \sqrt{256} \cdot \sqrt{\frac{256}{200}} \approx 18.1 . \qquad (3.1)$$

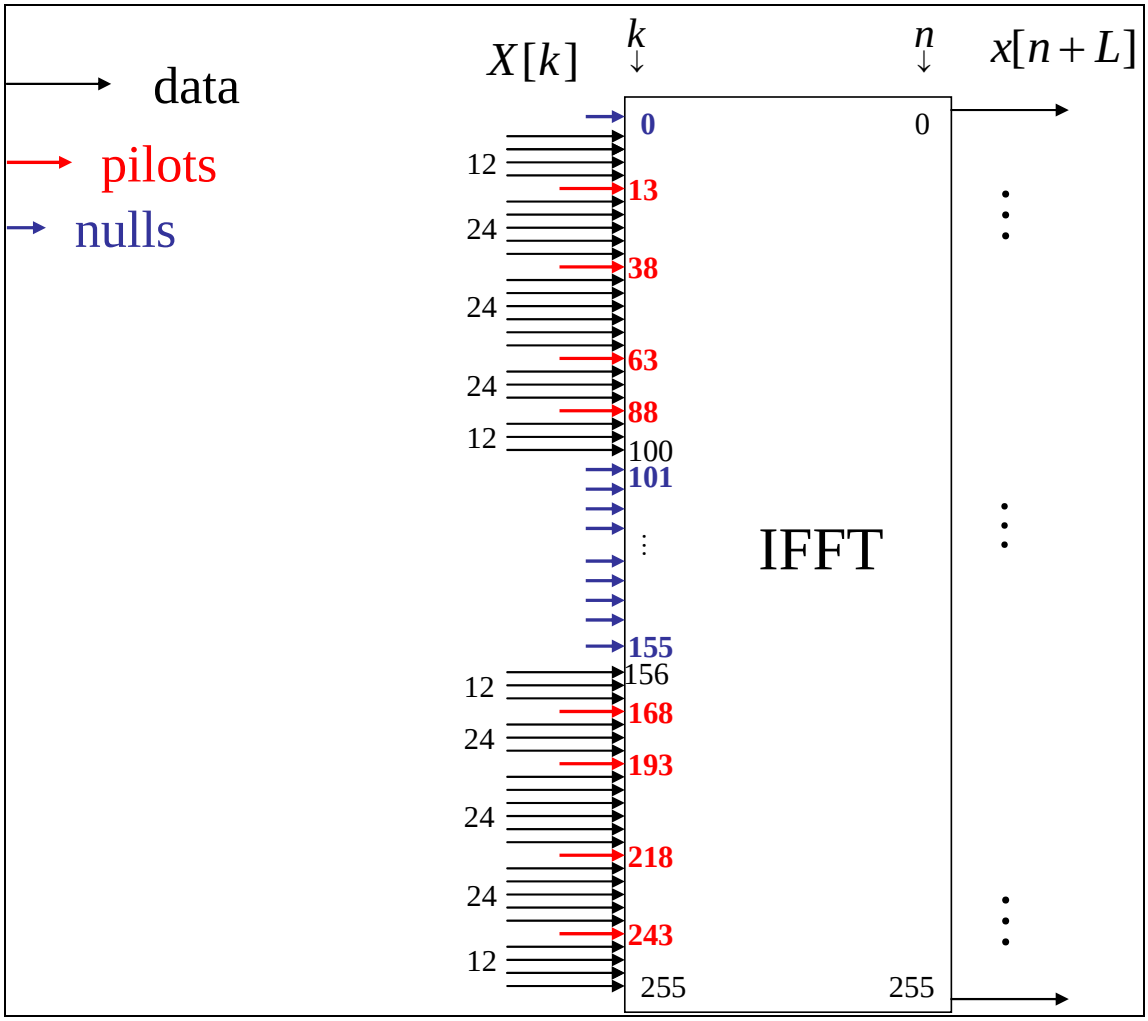

Figure 25. Inverse Fast Fourier Transform Input Packing, from [18].

3. Multipath Fading Channel with Additive White Gaussian Noise

This block can simulate three different channel configurations: AWGN channel only in which only noise is added to the signal; Frequency-flat fading with AWGN; Frequency-selective fading with AWGN. The simulations executed only the first and the last options, mainly. The fading mode and SNR in dB are defined by the user.

4. OFDM Receiver

In the OFDM receiver the data received from the channel is reshaped from serial to parallel, following the removal of the cyclic prefix. The data is then transformed through a FFT operation and then rescaled as in the OFDM transmitter to compensate for the number of sub-carriers used. This gain is given by equation (3.2). The data is then extracted after the FFT following an ordering analogous to Figure 25.

$$G = \frac{1}{\sqrt{L_{FFT}}} \cdot \sqrt{\frac{L_{FFT}}{L_{used}}} = \frac{1}{\sqrt{256}} \cdot \sqrt{\frac{256}{200}} \approx 0.07071. \qquad (3.2)$$

5. Gain and Phase Compensator

In this block the gain and phase of the received signal is corrected by comparing the original transmitted preamble with the received preamble. The calculated values of compensation are applied to the received signal after the DC component removal. The compensated signal is then sent to the data carriers' extraction block.

6. Data Carriers Extraction

In the data carriers' extraction block the pilot subcarriers are extracted and dumped. Recall that in this model the pilot subcarriers are not used for channel estimation, instead, the preamble is used for that effect. Finally, the data is converted from parallel to serial and sent to the demodulator and FEC bank and also to a constellation scope.

7. Demodulator and Forward Error Control Bank

As the FEC and modulator bank, this block is built with seven lines, one for each of the modulation schemes used.

a. BPSK r=1/2 Demodulator and FEC

In this line the data is demodulated, deinterleaved and decoded using a Viterbi decoder. Hard decision decoding is employed. The deinterleaver and Viterbi

decoder settings match those of the interleaver and convolution encoder used in the FEC and modulator bank, respectively. This block also modulates the demodulated data to be summed to the inverted received modulated data. This result is provided to the SNR estimation block for channel instantaneous SNR estimation.

b. Remaining Demodulators and FEC

The remaining six demodulators and FEC are implemented in the same form as the BPSK $r = 1/2$ demodulator and FEC, with the addition of the punctured Reed-Solomon decoder. Again, the hard decision decoding is used in the Viterbi decoder. Also, the deinterleaver, Viterbi decoder and punctured Reed-Solomon decoder settings match those of the interleaver, convolution encoder and Reed-Solomon encoder used in the FEC and modulator bank, respectively. The settings used are those presented in Table 7 and Table 8. For the remaining schemes, only the modulator and modulator blocks are replaced by other blocks with the respective modulation scheme.

8. SNR Estimation

In this block the instantaneous link SNR is calculated based on the estimated error between the transmitted and received symbols. This information will be used for adaptive rate control of the system. The root-mean-square of the column vectors of the signal is calculated and then the square of the matrix is computed. In the presence of complex elements the Hermitian transpose is performed. Finally, its reciprocal is calculated and the values obtained are translated to dB scale. The link overall estimated SNR in dB is then sent into the adaptive rate control block.

9. Adaptive Rate Control

In this block the instantaneous estimated channel SNR is compared with preloaded SNR values, which defines the limits of operation for each of the used seven modulation schemes. The circuit outputs an integer corresponding to the modulation scheme to be used by the transmitter and receiver units. The objective is to obtain an overall system with an error free data link. The output of this block is fed to the FEC and

Modulator bank and to the Demodulator and FEC bank to produce the adaptive rate control of the overall system. Also, its output is provided to the bit error rate block to correctly calculate the BER, since each modulation scheme has a different data block dimension. The values of the integer, designating rate ID, are presented in Table 9.

Table 9. Rate ID Encodings, from [10].

Rate ID	**Modulation scheme an overall rate**
0	BPSK $r = 1/2$
1	QPSK $r = 1/2$
2	QPSK $r = 3/4$
3	16QAM $r = 1/2$
4	16QAM $r = 3/4$
5	64QAM $r = 2/3$
6	64QAM $r = 3/4$

C. MISO OFDM MODEL

The MISO OFDM model is depicted in Figure 26. To avoid unnecessary description of blocks common to this model and the previous model, in the following section only the blocks that contain differences or are new in the MISO model will be described.

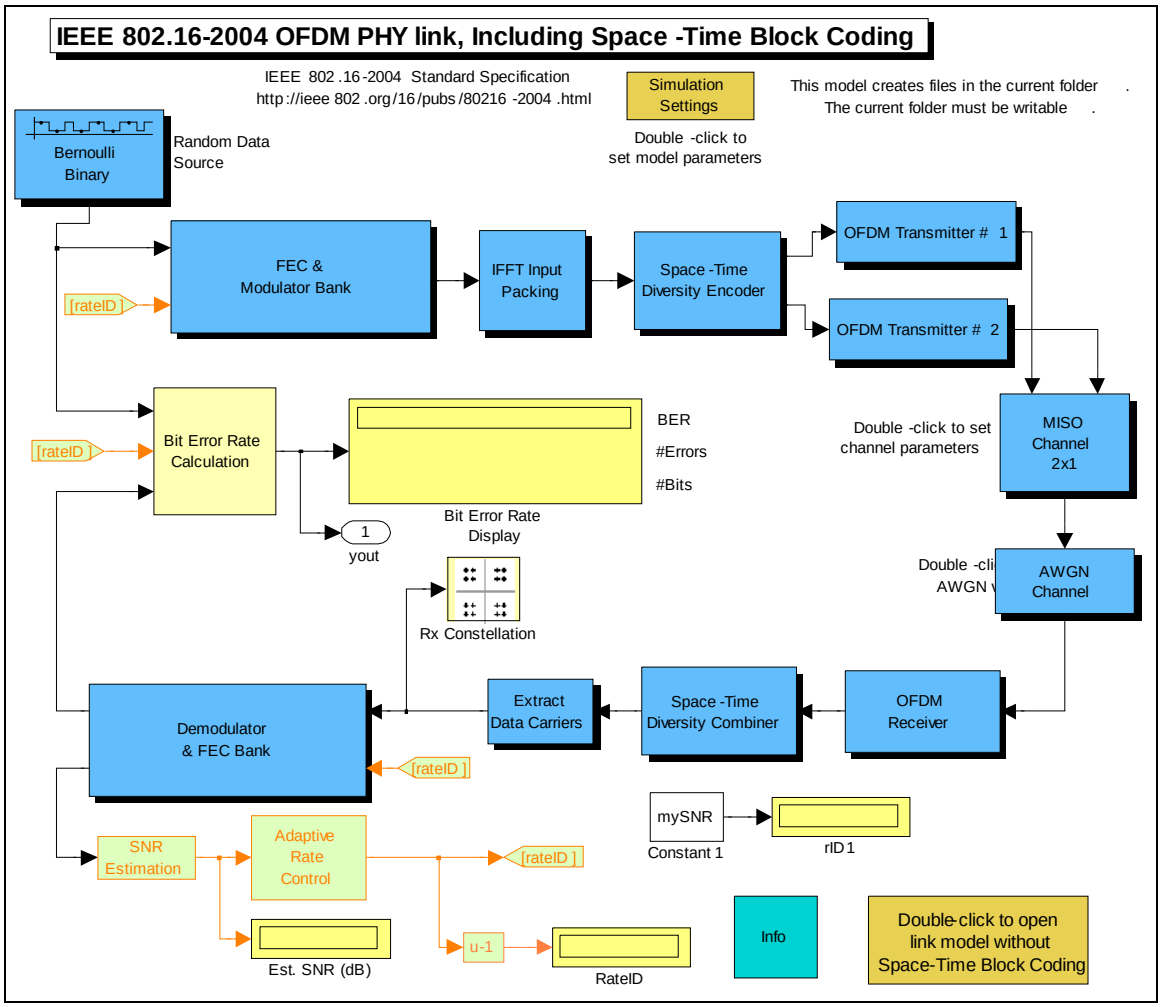

Figure 26. MISO OFDM Model.

1. Space-Time Diversity Encoder

The Space-Time Diversity Encoder is presented in Figure 27. This block receives the signal from the IFFT Input Packing block and produces two signals that are fed to the OFDM transmitters. The block itself is an embedded MATLAB® code S-function. It contains MATLAB® code that implements the Alamouti scheme described in Chapter II. The code is available in the Appendix.

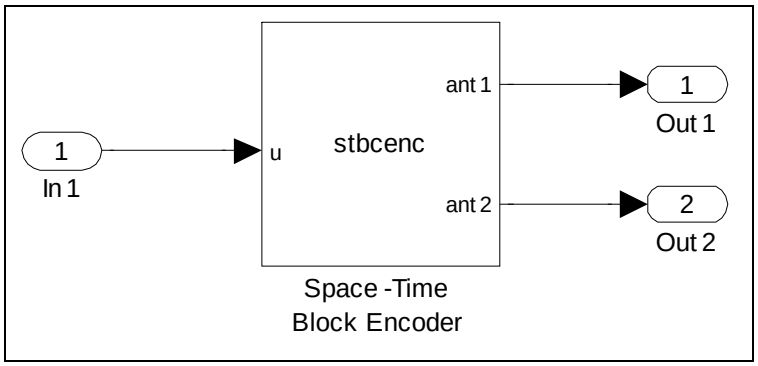

Figure 27. Space-Time Diversity Encoder.

2. OFDM Transmitters

Both OFDM transmitters have the same configuration as the SISO OFDM transmitter. However, in the MISO model the transmitters are supplied with two different preambles, in contrast to the SISO model where the transmitter was supplied with a single short preamble. The first transmitter is supplied with the even preamble and the second transmitter is supplied with the odd preamble.

3. MISO Fading Channel

This block, shown in Figure 28, simulates a MISO multipath fading channel with two inputs and one output. As discussed in the previous chapter it is a particular case of a MIMO channel obtained by simply disconnecting one of the outputs. The values for the phases were selected randomly. The correlation parameters simulated by the gain elements were selected to be 0.5 to simulate an intermediate level of correlation between the antenna elements. Considering the used carrier frequency $f_c = 2.3\text{GHz}$, the spacing d between antennas can be calculated using the relation [21]

$$\rho \approx J_0^2\left(\frac{2\pi d}{\lambda}\right), \tag{3.3}$$

where $J_0(x)$ is the Bessel function of the first kind of order zero and λ is the signal wavelength. Is this case the antennas spacing is $d \approx 0.18\lambda$.

The Rayleigh Fading elements simulate a multipath fading channel with parameters defined by the user.

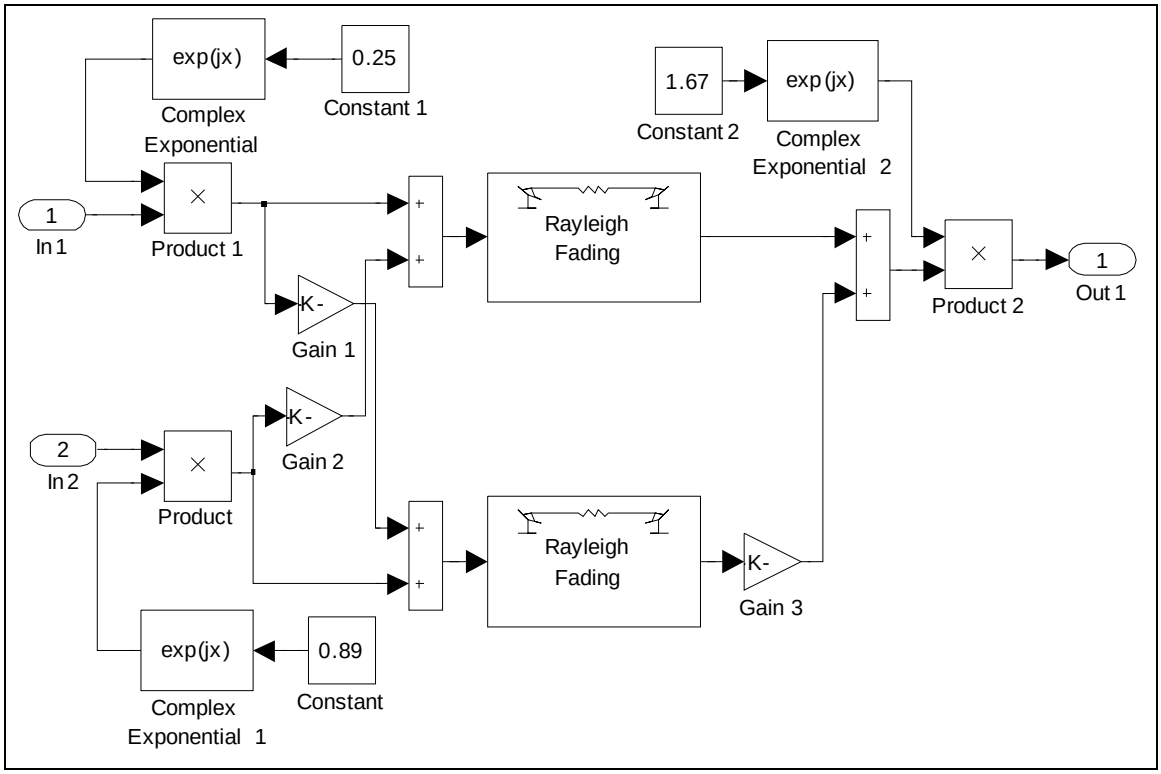

Figure 28. MISO Fading Channel.

4. Additive White Gaussian Noise Channel

The AWGN channel is a replica of the AWGN component used in the Multipath Fading Channel with AWGN for the SISO model. Its sole function is to add noise to overall channel modeling as in the SISO model. The SNR in dB is defined by the user.

5. Space-Time Diversity Combiner

In this block, the received signal is detected after being adjusted by the channel estimation. In the first section, the channel is estimated by dividing the received preamble by the transmitted preamble. The channel's estimations and the received signal with the DC component removed are then provided to the space-time combiner for signal

detection. This block is an embedded MATLAB® code S-function. It contains MATLAB® code that implements the Alamouti scheme at the receiver as described in chapter II. The code is available in the Appendix.

Finally, the amplitude of the detected signal is adjusted by the Gain Compensator. The detected signal is divided by the sum of norm of the channels estimations to obtain the desired compensation. The detected signal is then sent to the Data Carries Extraction block for further processing similar to that of the SISO model.

D. MIMO OFDM MODEL

The MIMO OFDM model is shown in Figure 29. The blocks are similar to the previous cases apart from the MIMO Fading Channel and the Space-Time Diversity Combiner, which are presented next.

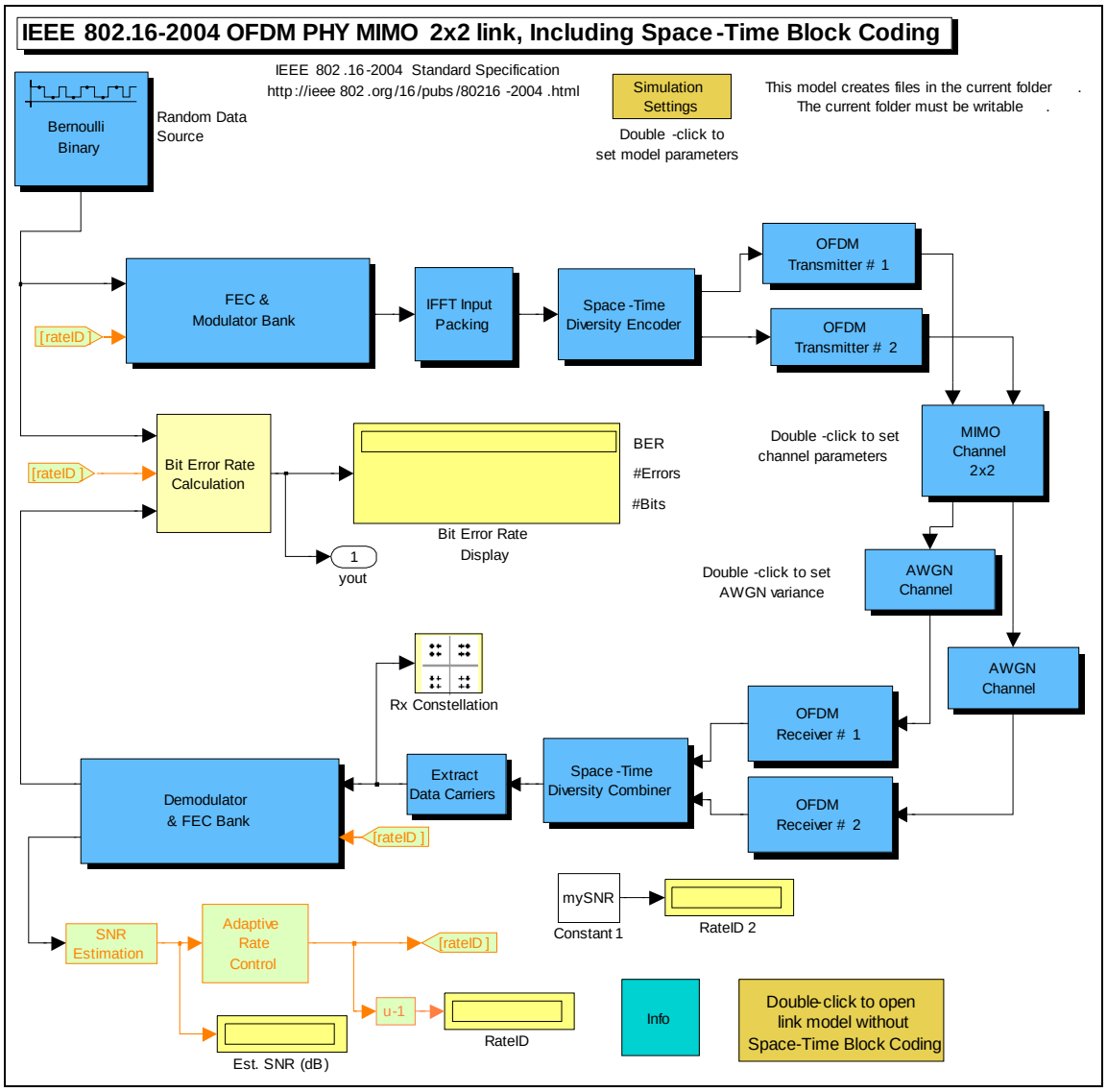

Figure 29. MIMO OFDM Model.

1. MIMO Fading Channel

This block, shown in Figure 30, simulates a MIMO multipath fading channel with two inputs and two outputs. The phase values were selected randomly. Again, correlation parameters simulated by the gain elements were selected to be 0.5 to simulate an intermediate level of correlation between the antenna elements. The Rayleigh Fading elements simulate a multipath fading channel where the delay and gain parameters are defined by the user.

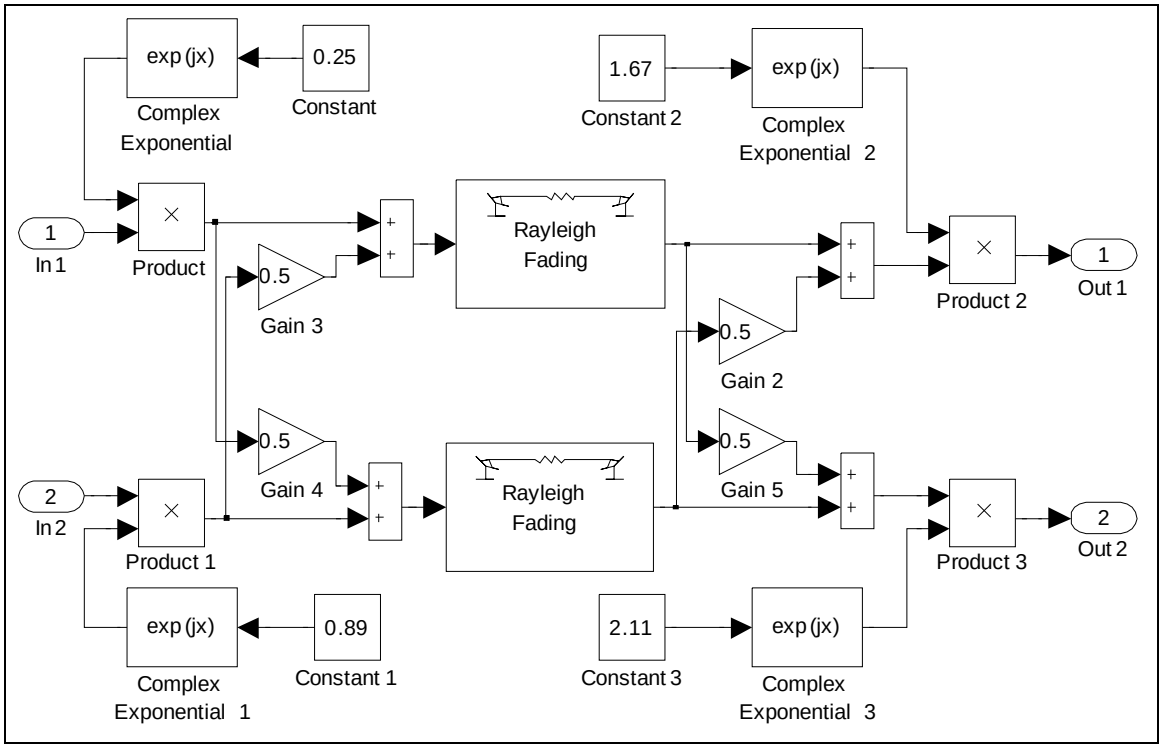

Figure 30. MIMO Fading Channel.

2. Space-Time Diversity Combiner

The Space-Time Diversity Combiner block, shown in Figure 31, as in the MISO model, detects the received signal as compensated by the channel estimation. First, the four possible channels are estimated by dividing the received preamble by the transmitted preamble. The channels' estimations and the received signals with the DC component removed are then provided to the space-time combiner for signal detection. This block is an embedded MATLAB® code S-function. It contains MATLAB® code that implements the Alamouti scheme at the receiver as described in chapter II, for two receiving antennas. The code is available in the Appendix.

Lastly, the detected signal is compensated in gain by the Gain Compensator depicted in Figure 32. The detected signal is divided by the sum of norm of the channels'

estimations to obtain the desired compensation. The detected signal is then sent to the Data Carriers' Extraction block for further processing analogous to that of the SISO and MISO models.

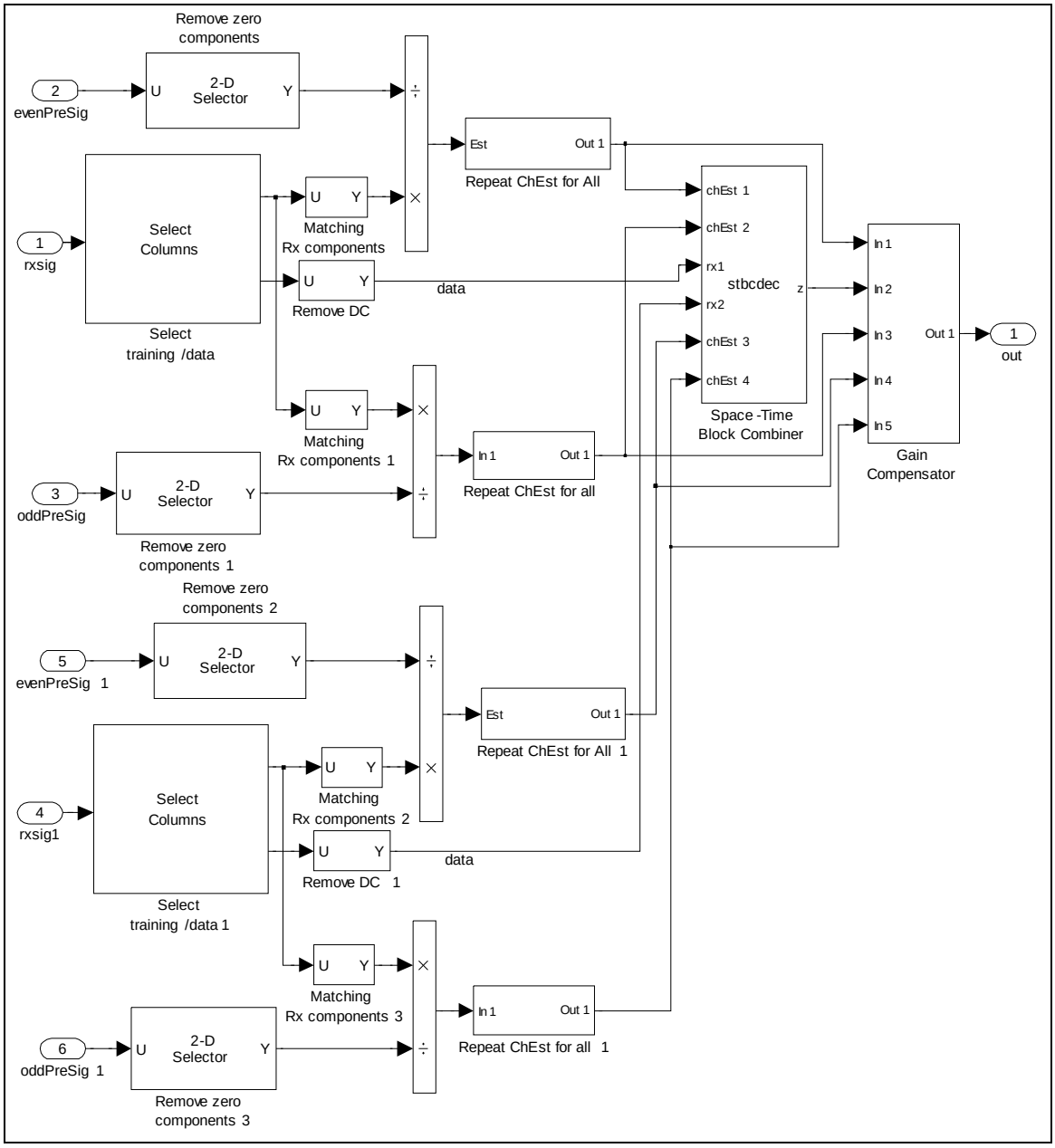

Figure 31. Space-Time Diversity Combiner.

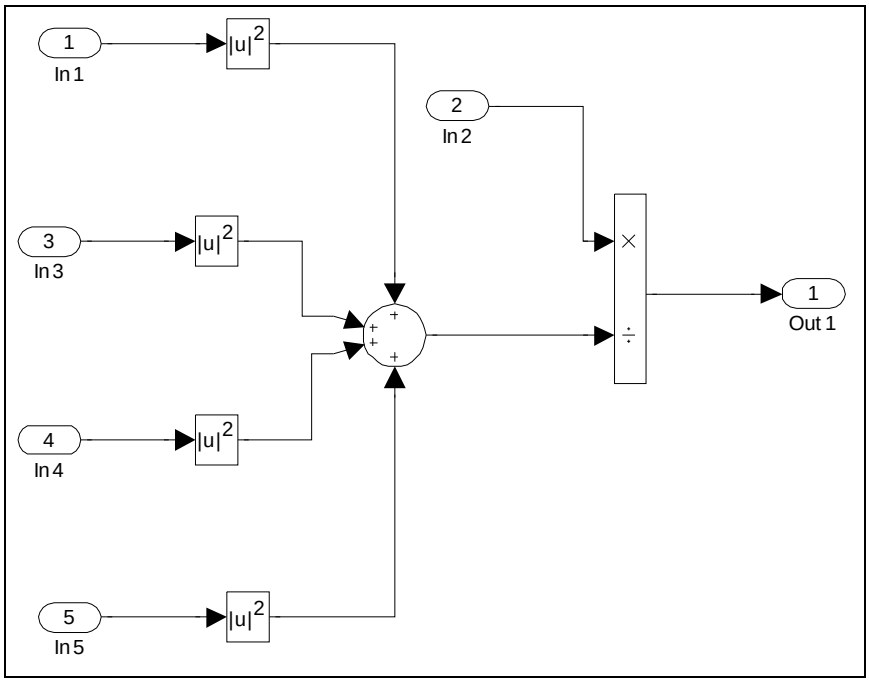

Figure 32. Gain Compensator of the MIMO Space-Time Diversity Combiner.

E. ITU CHANNEL MODELS

For simulation purposes, the multipath channel models chosen for the executed simulations were those specified by the ITU. These channel models provide a variety of situations considered typical. Three user locations are considered: indoor, pedestrian and vehicular. The indoor location user is a fixed subscriber, thus its Doppler spread is null. The pedestrian user has normally a speed up to 3km/h, which will induce a maximum Doppler shift of $f_d = 6.389\text{Hz}$, considering the use of a carrier frequency of $f_c = 2.3\text{GHz}$. The vehicular user is considered to have a speed between 60km/h and 120km/h, which corresponds to Doppler shifts of $f_d = 127.77\text{Hz}$ and $f_d = 255.56\text{Hz}$, respectively, for the same carrier frequency. For each one of these types of user, the ITU specified two profiles of multipath: A and B. Profile A has shorter delay spread when compared to profile B. Profile A replicates rural macro-cellular surroundings, while profile B reproduces an urban macro-cellular environment. For scenarios of micro-cells

with radius less than 500m profile A is also suggested. The values of delay and relative power for each of the users and profiles are presented in tables Table 10, Table 11 and Table 12

Table 10. ITU Multipath Channel Models – Indoor, after [1].

Tap Number	Delay (ns)	Relative Power (dB)	Delay (ns)	Relative Power (dB)
	Channel A		Channel B	
1	0	0	0	0
2	50	-3	100	-3.6
3	110	-10	200	-7.2
4	170	-18	300	-10.8
5	290	-26	500	-18.0
6	310	-32	700	-25.2

Table 11. ITU Multipath Channel Models – Pedestrian, after [1].

Tap Number	Delay (ns)	Relative Power (dB)	Delay (ns)	Relative Power (dB)
	Channel A		Channel B	
1	0	0	0	0
2	110	-9.7	200	-0.9
3	190	-19.2	800	-4.9
4	410	-22.8	1200	-8.0
5			2300	-7.8
6			3700	-23.9

Table 12. ITU Multipath Channel Models – Vehicular, after [1].

Tap Number	Delay (ns)	Relative Power (dB)	Delay (ns)	Relative Power (dB)
	Channel A		Channel B	
1	0	0	0	-2.5
2	310	-1	300	0
3	710	-9	8900	-12.8
4	1090	-10	12900	-10.0
5	1730	-15	17100	-25.2
6	2510	-20	20000	-16.0

F. SUMMARY

In the present chapter we have introduced the SISO, MISO and MIMO OFDM models used in this thesis to obtain the results presented later. A brief presentation on the ITU channel models used in the simulations was also provided. In the next chapter, we will address the results obtained from the several performed simulations.

THIS PAGE INTENTIONALLY LEFT BLANK

IV. SIMULATIONS AND RESULTS

A. INTRODUCTION

In the previous chapter, a description of the several communication systems and multipath channel models used in this thesis were presented. In the present chapter the simulation settings used and the results obtained will be addressed. On the results, first the performance of the communication systems is discussed with respect to BER versus SNR and later the measured system's capacity is presented.

B. SIMULATION SETTINGS

Table 13. Simulation Settings for Systems Benchmarking.

Parameter	Value
Channel bandwidth B	3.5MHz
Number of subcarriers L_{FFT}	256
Carrier frequency f_c	2.3GHz
Ratio of cyclic prefix time to useful symbol time $G = T_g / T_b$	$1/8$
MISO & MIMO fading correlations	$\rho_T = 0.5$ $\rho_R = 0.5$
MISO & MIMO random phases	$\phi_1 = 1.67; \phi_2 = 2.11$ $\phi_3 = 0.25; \phi_4 = 0.89$
Number of data bits transmitted	10^6

The simulation settings were chosen to be those of the IEEE® 802.16-2004, also known as fixed WiMAX. Table 13 presents the significant parameter values of the OFDM systems and also the MISO and MIMO channel factors. Each system was tested under several ITU user-channel profiles presented in the previous chapter. The AWGN

SNR value was varied from 0dB up to 44dB, in 1dB steps, for each modulation scheme presented in Table 9. For each SNR value 10^6 data bits were transmitted to measure BER values as low as 10^{-5}. The curves obtained were considered to be the system's benchmarks under the several user-channel conditions. From these performance curves, after observing the values obtained for each modulation at a BER of 10^{-4}, we defined the SNR threshold vectors for the rate control. These values were used in the second part of the simulations to obtain performance figures of all systems with partial CSI feedback. The simulation settings in this phase are presented in Table 13.

C. PERFORMANCE RESULTS

In this section, the overall performance in terms of measured BER versus the link overall SNR is discussed for several user profiles and channel profiles.

1. AWGN Channel Performance

The systems were first tested with an AWGN channel model. These results provide a benchmark for comparison when the multipath channel effect is added to the simulations. The results obtained for this case are depicted in Figure 33 and Figure 34. The MISO system showed very little improvement when compared to the SISO system. On average, a gain less than $1/2\,\text{dB}$ was achieved. In the particular case of the BPSK signal, the MISO system actually performed worse than the SISO system. However, the MIMO system performed significantly better than both the SISO and MISO systems. On average a gain of 2dB was obtained.

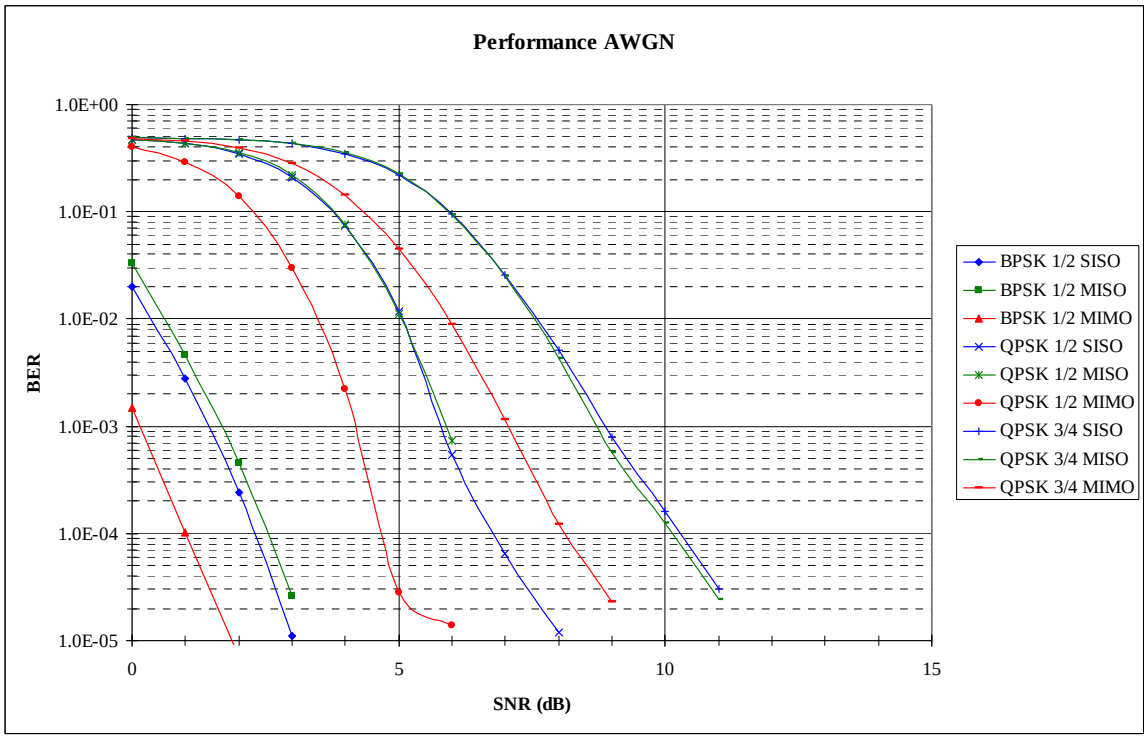

Figure 33. Performance in AWGN Channel for PSK Signals.

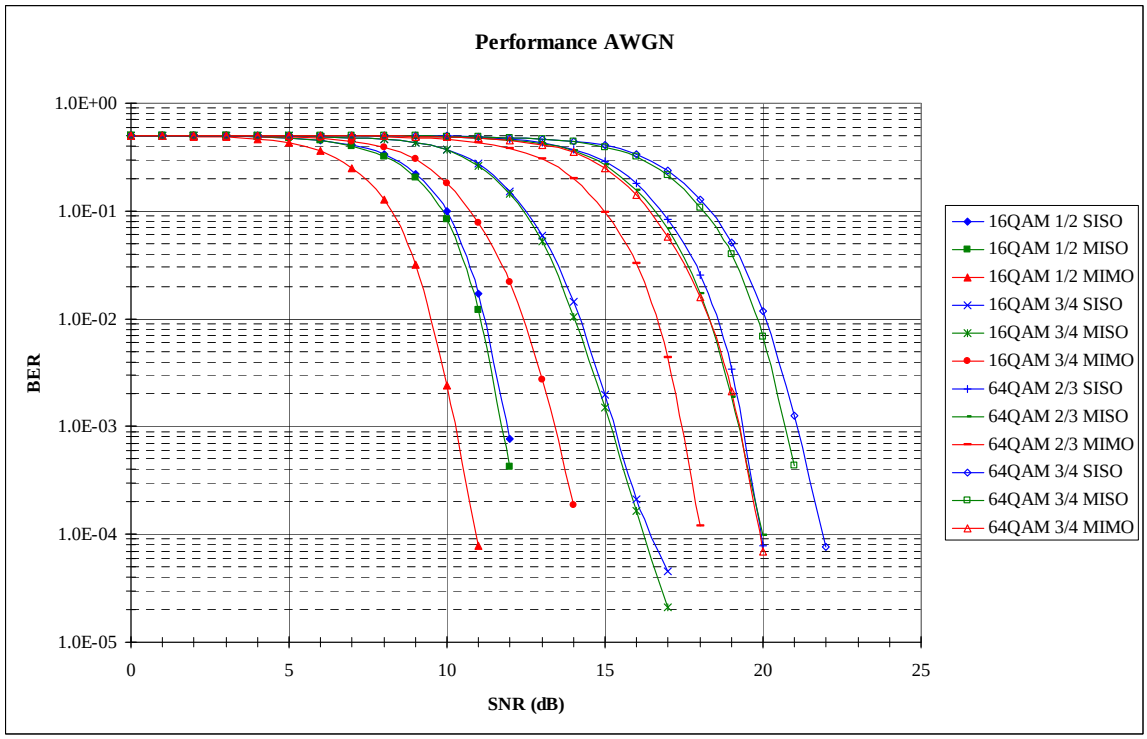

Figure 34. Performance in AWGN Channel for QAM Signals.

2. AWGN plus Multipath Channel Performance

In this general channel scenario, all ITU profiles presented in the previous chapter were simulated. In the next sections the relevant results are discussed.

a. Indoor Channel A

In this scenario, the results obtained were encouraging. With BPSK and QPSK the MISO system performed on average 1dB better than the SISO system, while the MIMO system showed a performance 3dB better than the MISO system. These results are presented in Figure 35. Figure 36 shows the results for the QAM signal families. In this case the MISO system shows a 2dB average performance improvement from the SISO system. Also, the MIMO system has an average performance improvement of 3dB when compared to the MISO system, and a 5dB improvement when compared to the SISO system.

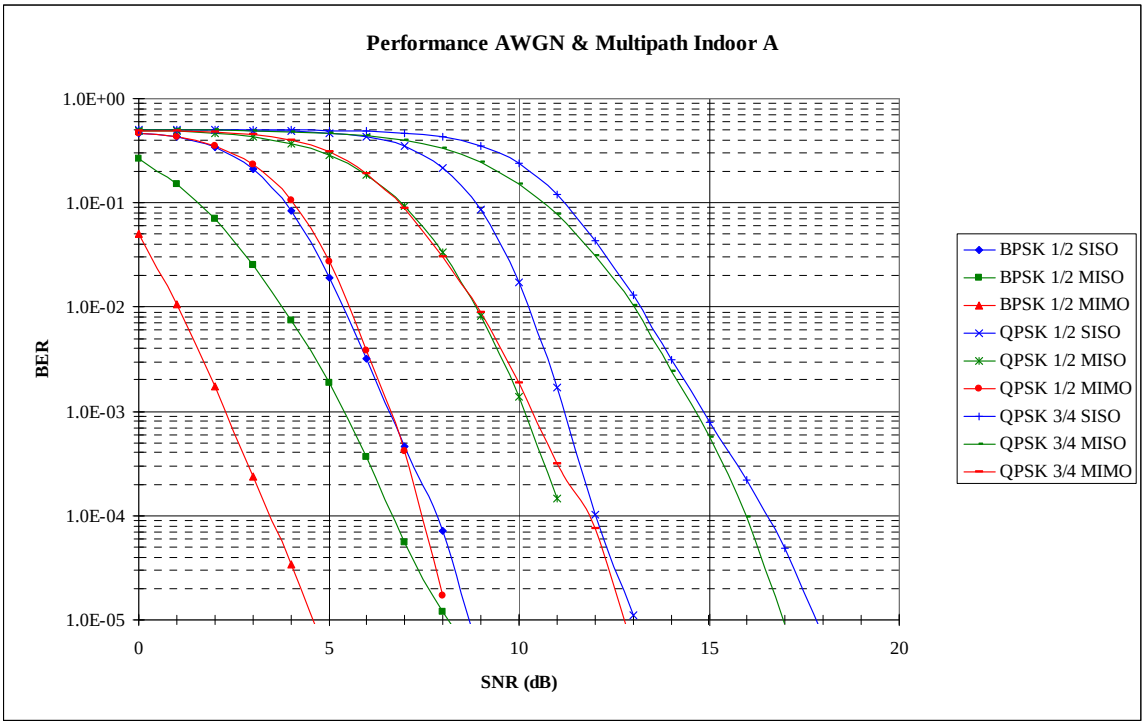

Figure 35. Performance in AWGN plus Multipath Indoor A for PSK Signals.

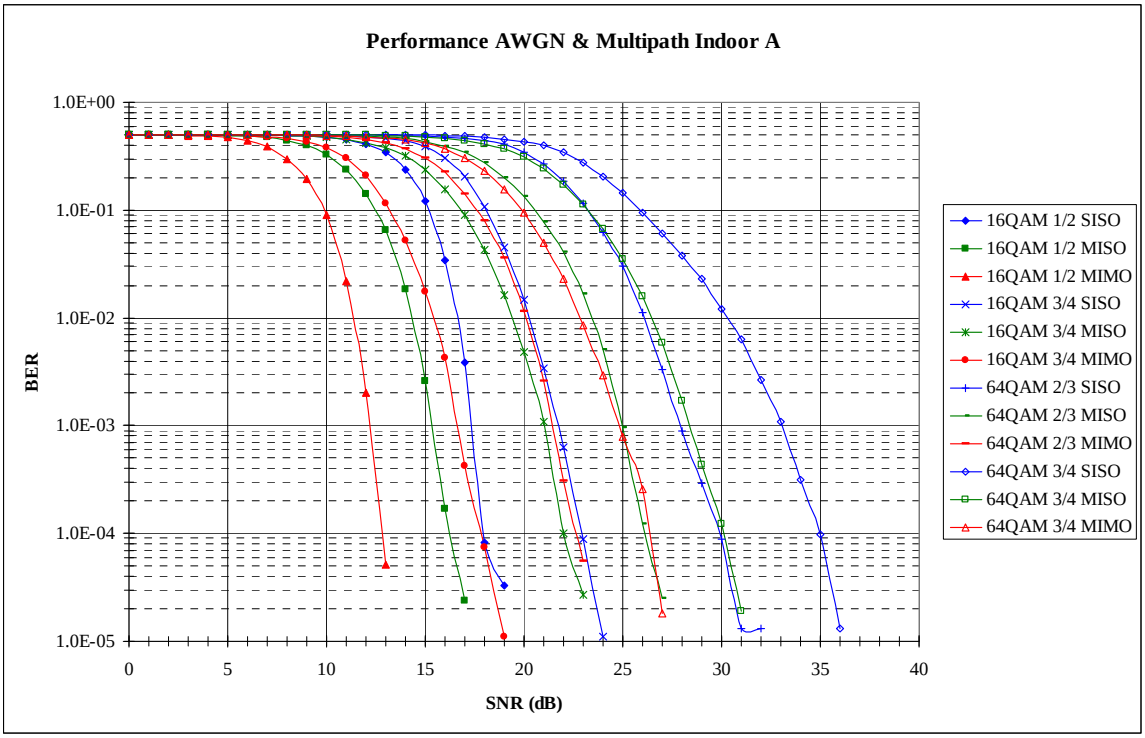

Figure 36. Performance in AWGN & Multipath Indoor A for QAM Signals.

b. Indoor Channel B

In this simulation profile some significant results were obtained. Recall that the profile of channel B has a bigger time delay spread than the profile of channel A, more than twice to be more quantitative. This factor plays a big role in the systems' performances. Observing both Figure 37 and Figure 38, the performance of the SISO system is not satisfactory, in particular for the case of QPSK $r = 3/4$ and QAM signals. Where comparison is possible, a 13dB average improvement was obtained when comparing MISO to SISO system. The MIMO system showed a performance improvement compared to the MISO system that varies between 3dB and 5dB, depending on the type of signal in use. Overall, in this particular user-channel profile, the MIMO system reached a peak performance improvement of 18dB when compared to the SISO system.

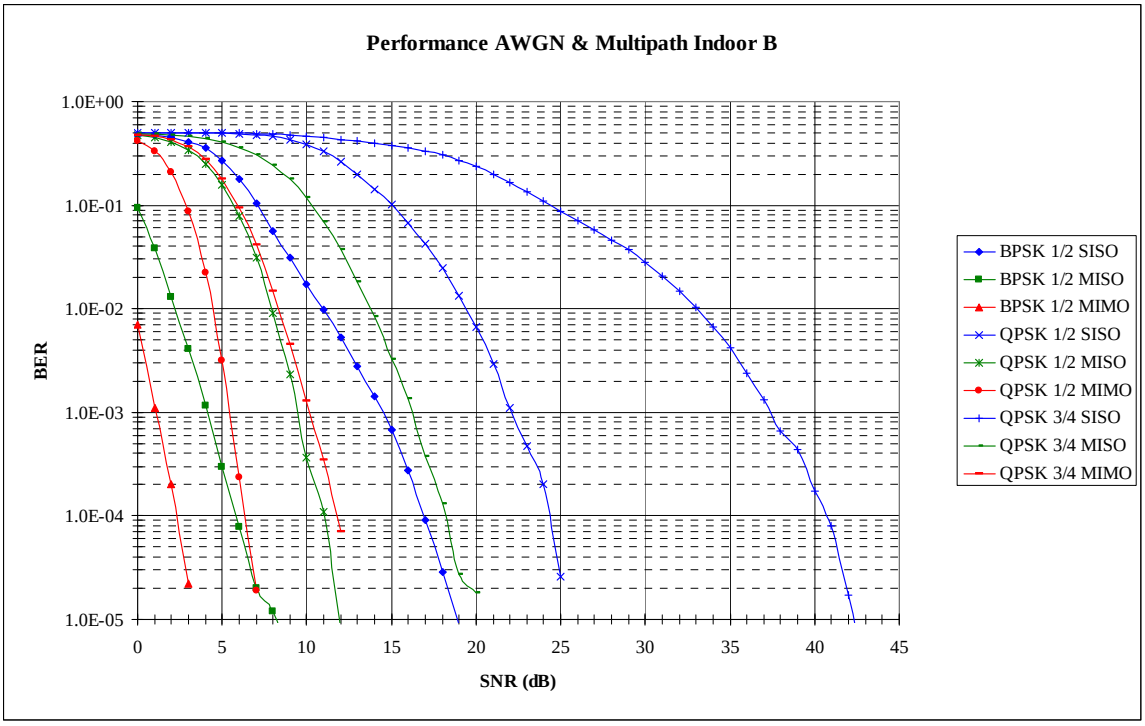

Figure 37. Performance in AWGN & Multipath Indoor B for PSK Signals.

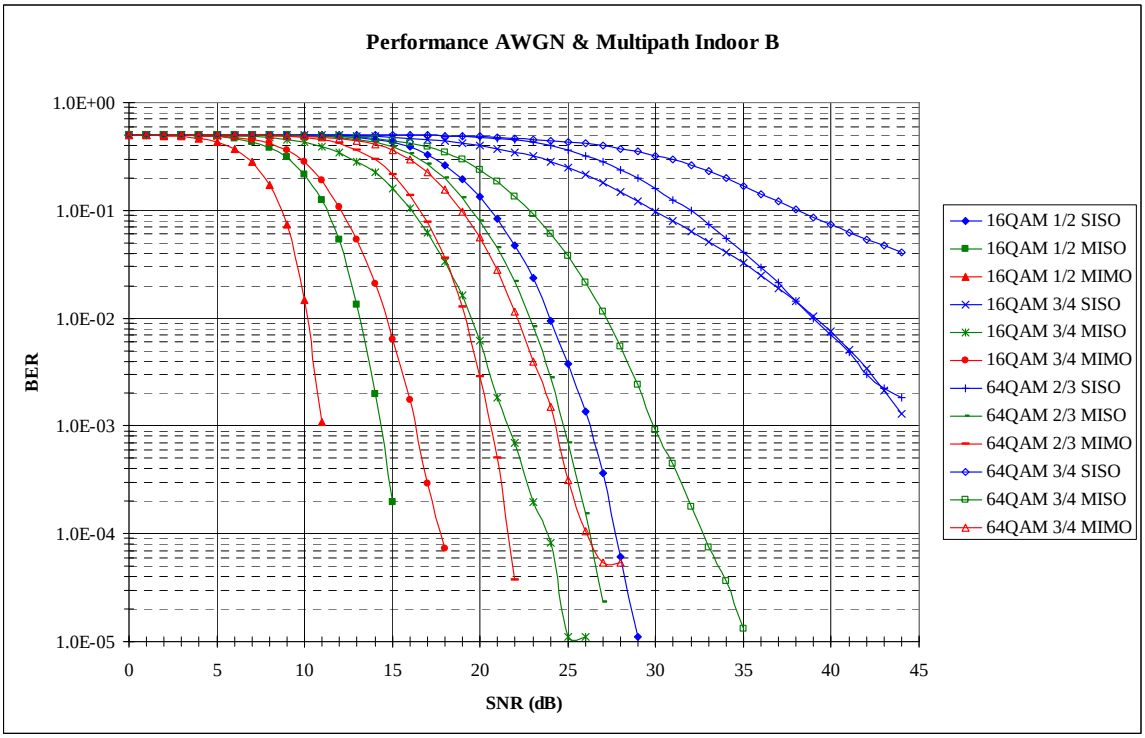

Figure 38. Performance in AWGN & Multipath Indoor B for QAM Signals.

c. Pedestrian Channel A

In the pedestrian profile, two different situations were considered: a moving and a stationary person. In this latter case, the MISO system performed worse than the SISO system for almost every type of signal. A $1/2$ dB to 1dB degradation was measured. On the other hand, the MIMO system performed better than the SISO system on average 2dB to 3dB for all types of signals. These results are depicted in Figure 39 and Figure 40.

For the case of a fast moving pedestrian, the SISO system performance was poor. Some BER curves showed unpredictable behavior, leading to its exclusion of use under this user-channel profile. Where it was possible to compare the MISO system performed better than the SISO system, except for the case of the 16QAM $r = 1/2$ signal. Comparing the MIMO to the MISO system, the measured average improvement of performance was on the order of 5dB.

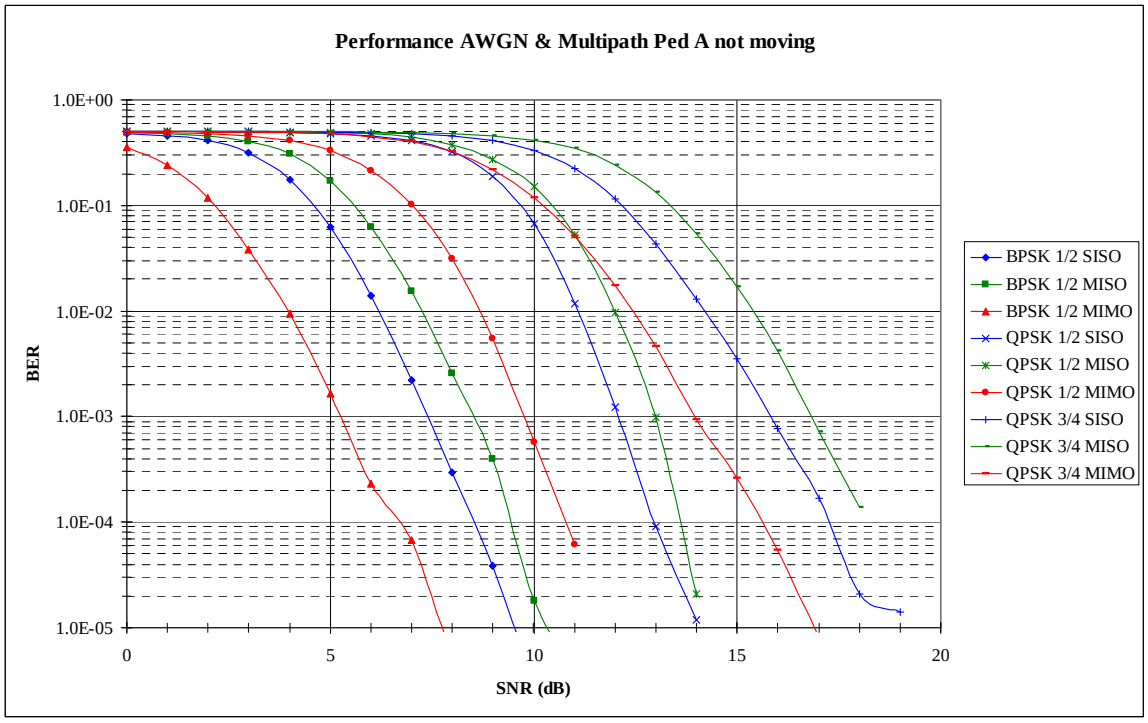

Figure 39. Performance in AWGN & Multipath Stopped Pedestrian A for PSK Signals.

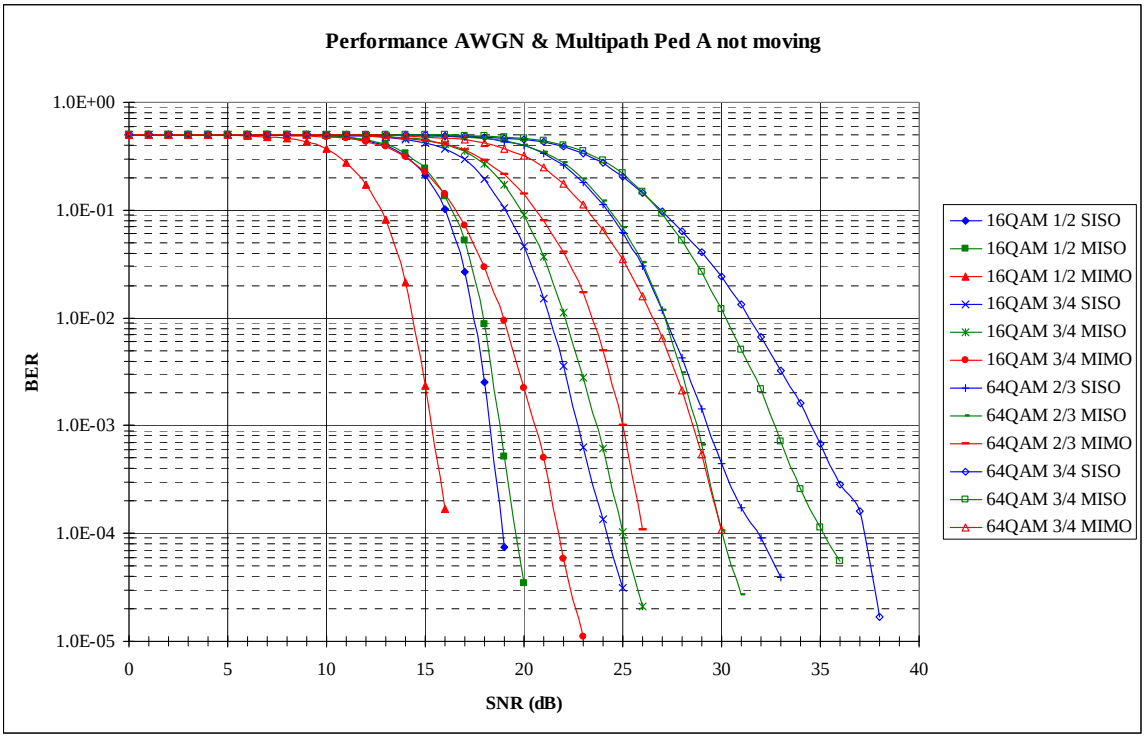

Figure 40. Performance in AWGN & Multipath Stopped Pedestrian A for QAM Signals.

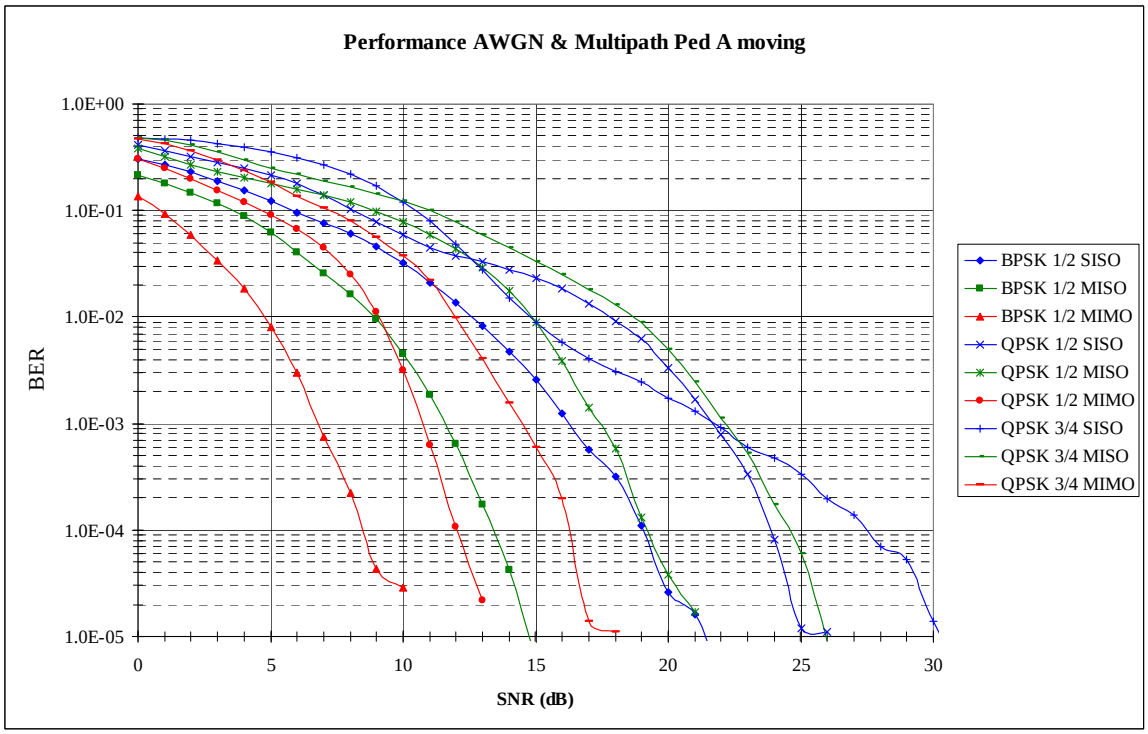

Figure 41. Performance in AWGN & Multipath Active Pedestrian A for PSK Signals.

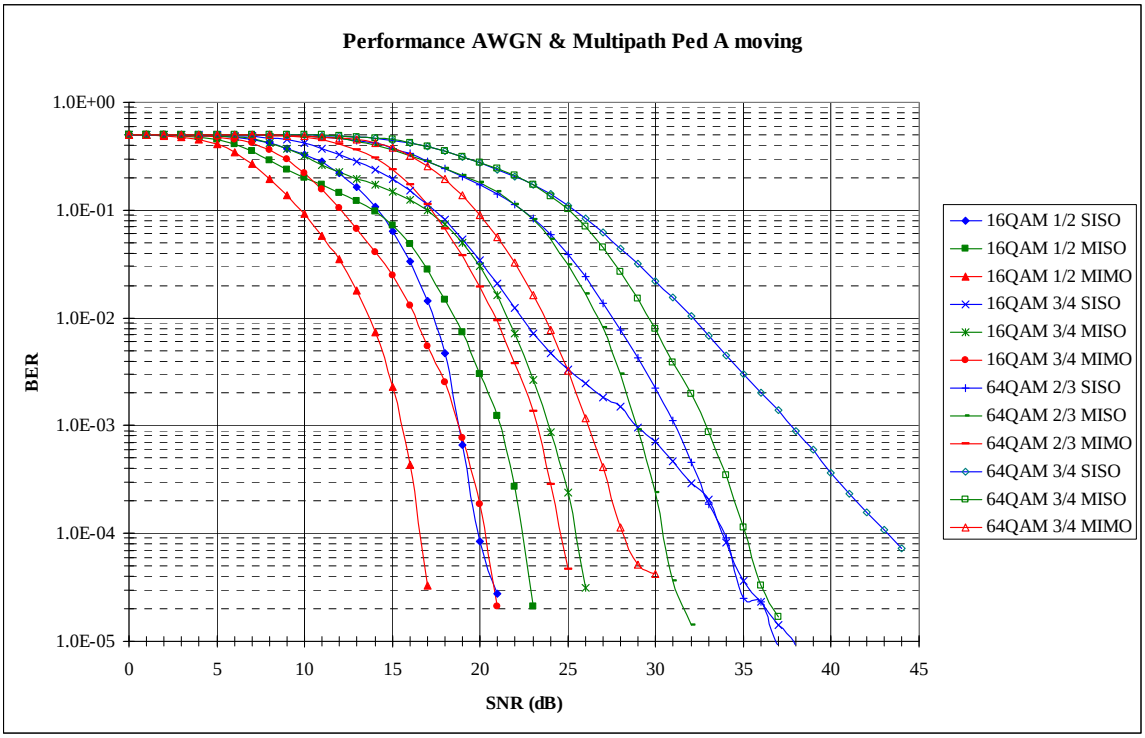

Figure 42. Performance in AWGN & Multipath Active Pedestrian A for QAM Signals.

d. Pedestrian Channel B

Using the same methodology as in the previous section, simulations for both active and stationary pedestrians were carried out. For both cases the SISO system was unable to deal with multipath. Only the BPSK and QPSK $r = 1/2$ signals were able to combat multipath. Because of this fact, no comparison of the SISO system to the other systems will be addressed. Also, in the case of the MISO and MIMO systems, the utilization of 64QAM signal appears to be impossible. As soon as the noise effect on the channel is negligible the multipath effect becomes clear, since the performance curves present horizontal asymptotes. Where comparison was possible, 2dB to 3dB average performance improvement was measured, comparing the MIMO to the MISO system in the stationary pedestrian case. In the active pedestrian situation 3dB to 4dB improvement was achieved.

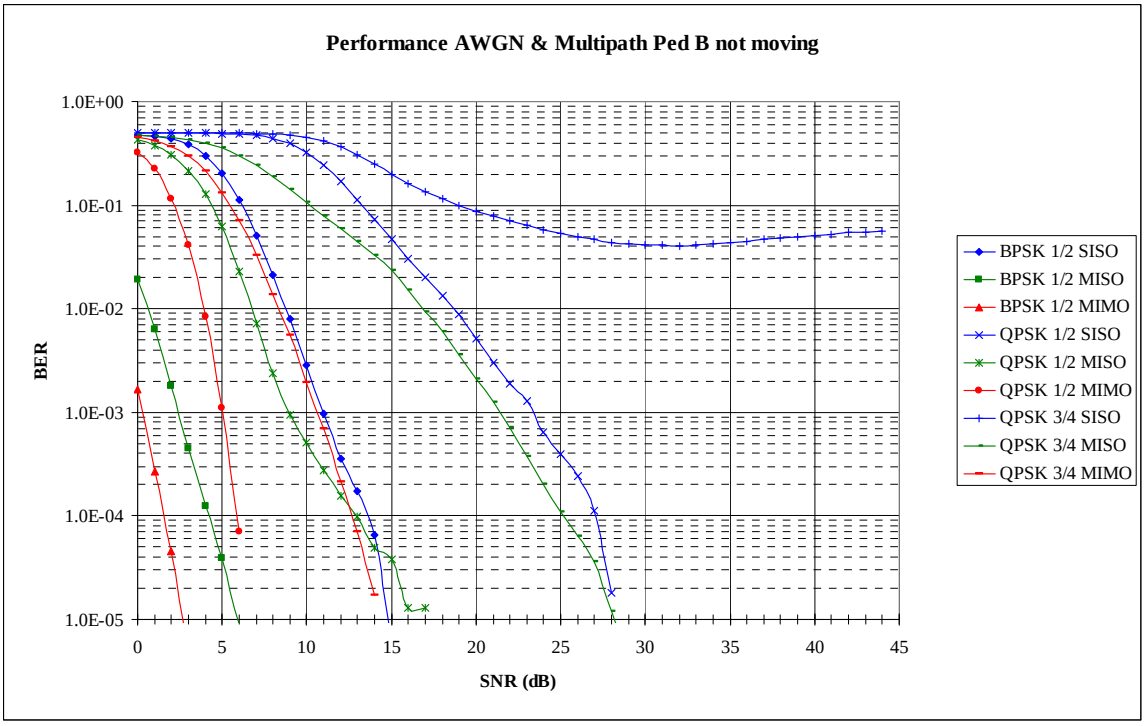

Figure 43. Performance in AWGN & Multipath Stopped Pedestrian B for PSK Signals.

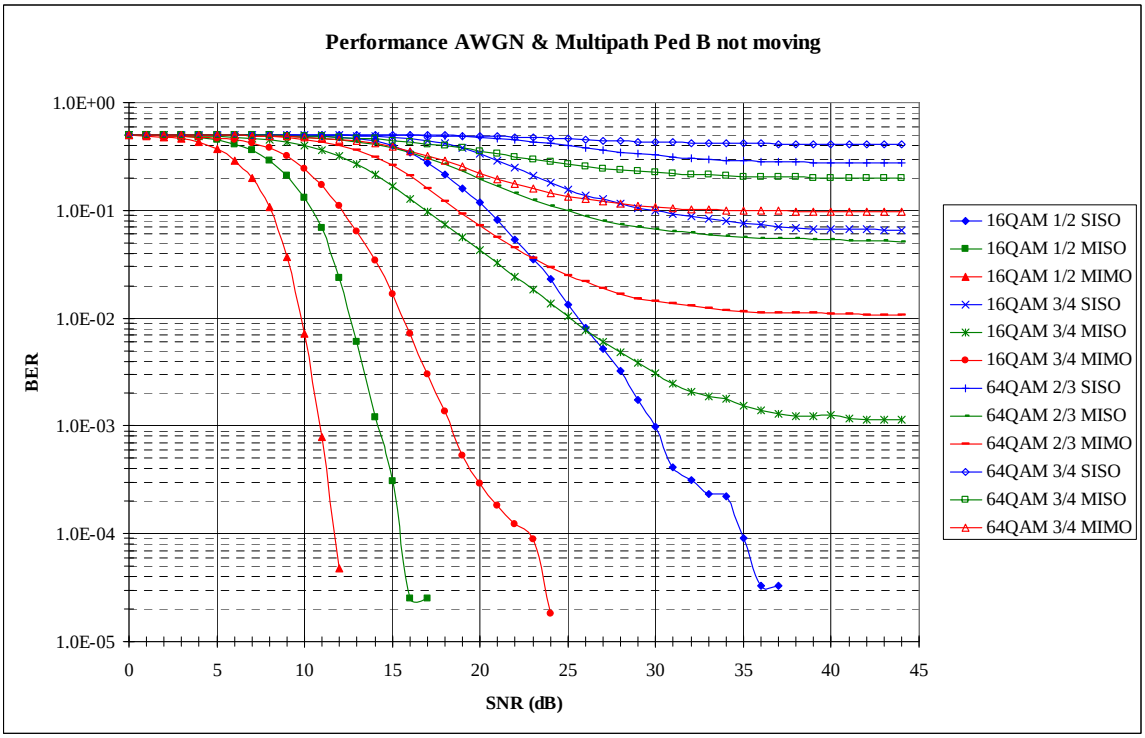

Figure 44. Performance in AWGN & Multipath Stopped Pedestrian B for QAM Signals.

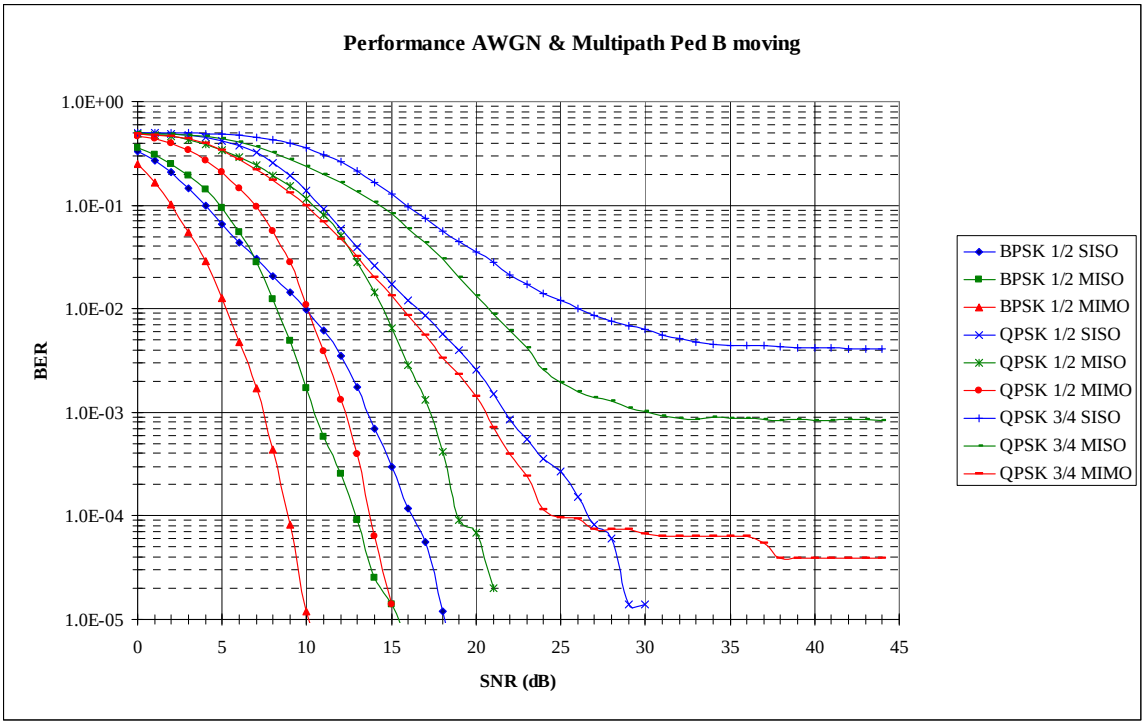

Figure 45. Performance in AWGN & Multipath Active Pedestrian B for PSK Signals.

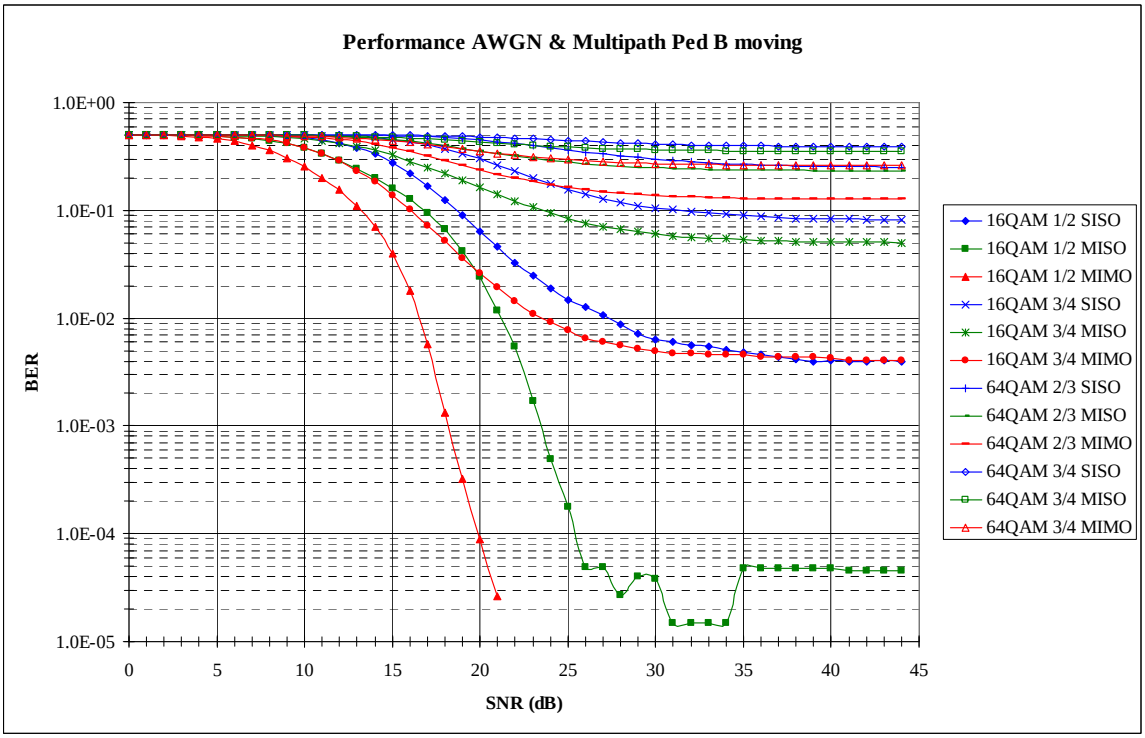

Figure 46. Performance in AWGN & Multipath Active Pedestrian B for QAM Signals.

e. Vehicular Channel A

The IEEE® 802.16-2004 standard was not proposed for communication links under mobility, i.e., vehicular use. However, simulations under these conditions were performed to get a sense of the effects and to eventually reflect on solutions to combat the negative consequences. With this perspective in mind, we will only present two extreme cases under mobility, among all that were simulated. In this section the performance of the link under the user-channel vehicular A profile with 60 km/h is addressed. In the following section the user-channel vehicular B profile with 120 km/h is presented.

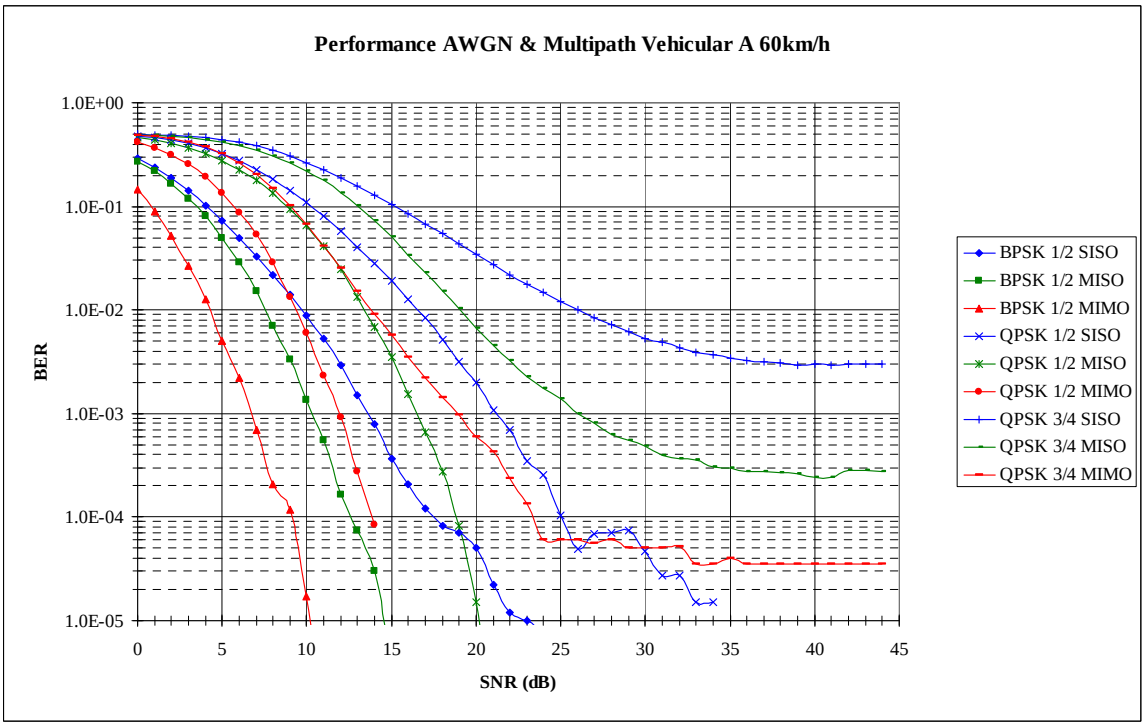

Figure 47. Performance in AWGN & Multipath Vehicular A for PSK Signals.

The results obtained for the user-channel vehicular A profile with 60 km/h are somewhat promising in the MIMO case. The SISO and MISO systems clearly showed overall poor performance. In the cases where the systems could be compared, the MIMO system performed 3dB to 4dB better than the MISO system. For a

BER on the order of 10^{-4}, the MIMO system can be considered a viable solution, since only with the 16QAM $r = 2/3$ and 64QAM cases did it show poor performance.

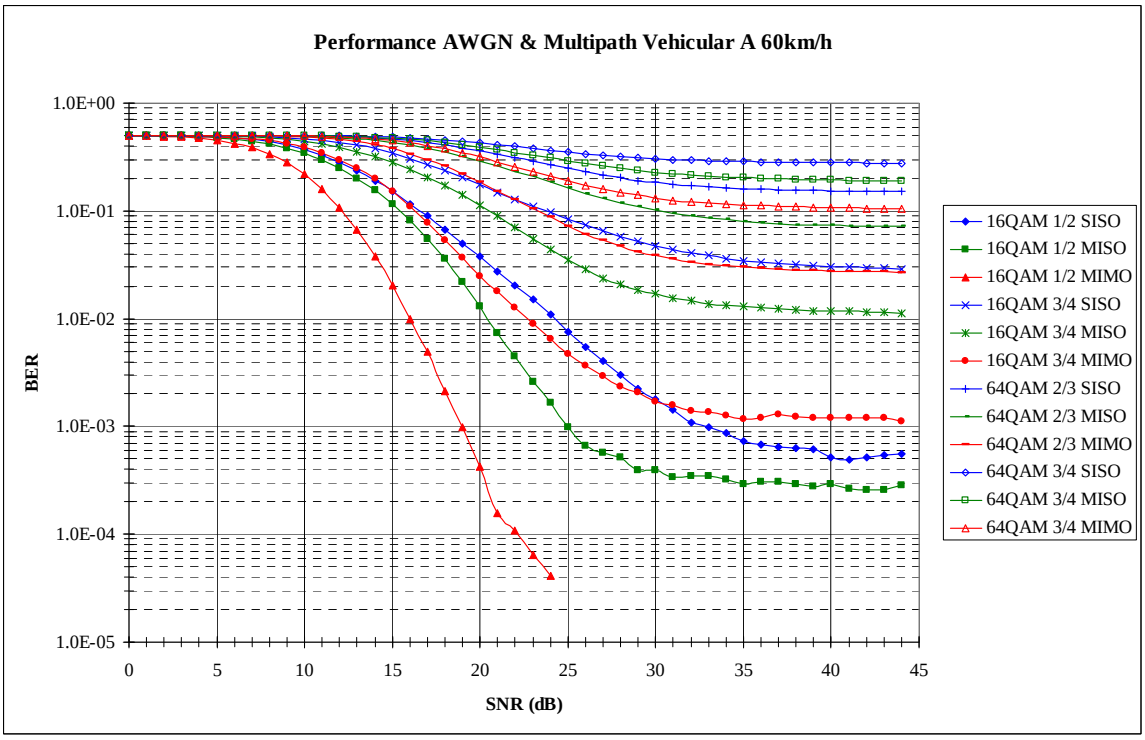

Figure 48. Performance in AWGN & Multipath Vehicular A for QAM Signals.

f. Vehicular Channel B

In this section, we present the results obtained under the user-channel vehicular B profile with speed $120\,\text{km/h}$. It is clear that all systems performed poorly since none of them can combat the multipath and Doppler spread combined effect of this kind of channel. Also visible is the fact that the MIMO outperforms the MISO which outperforms the SISO system. Looking at the point where the noise effect on the channel is negligible (around 25dB SNR), the best achieved BER are 0.006, 0.02 and 0.04 for the MIMO, MISO and SISO systems, respectively, using the BPSK signal. This has tremendous effects on the channel throughput and confirms the fact that the IEEE® 802.16-2004 standard has not been designed for mobile applications.

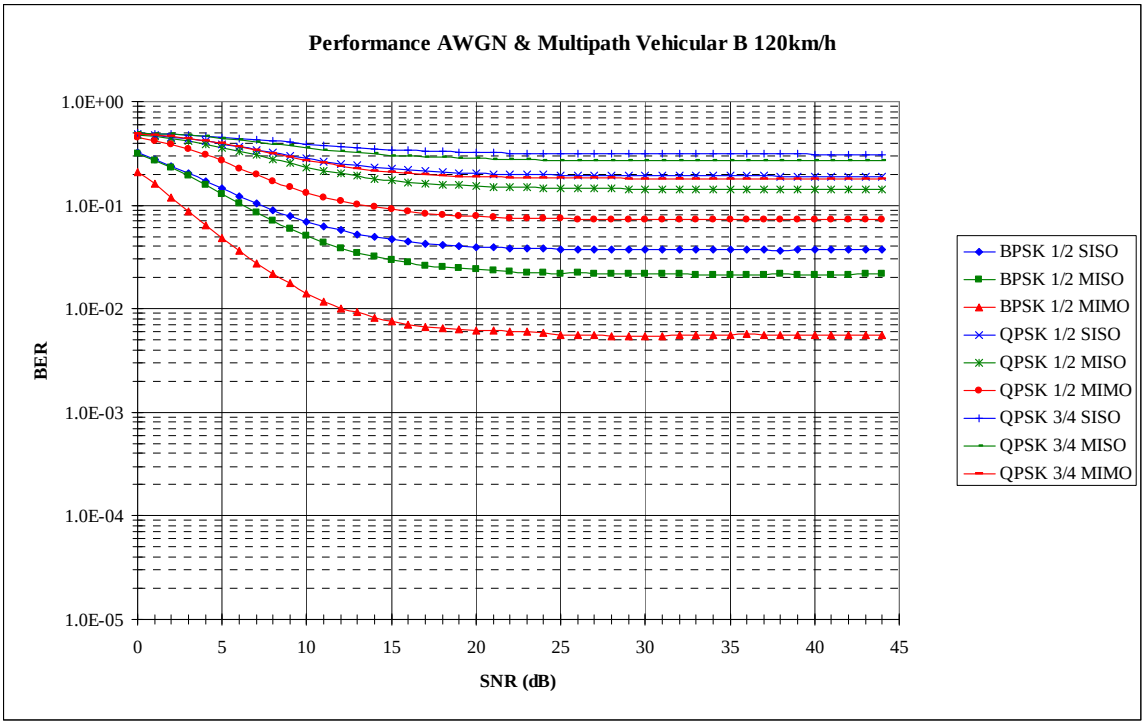

Figure 49. Performance in AWGN & Multipath Vehicular B for PSK Signals.

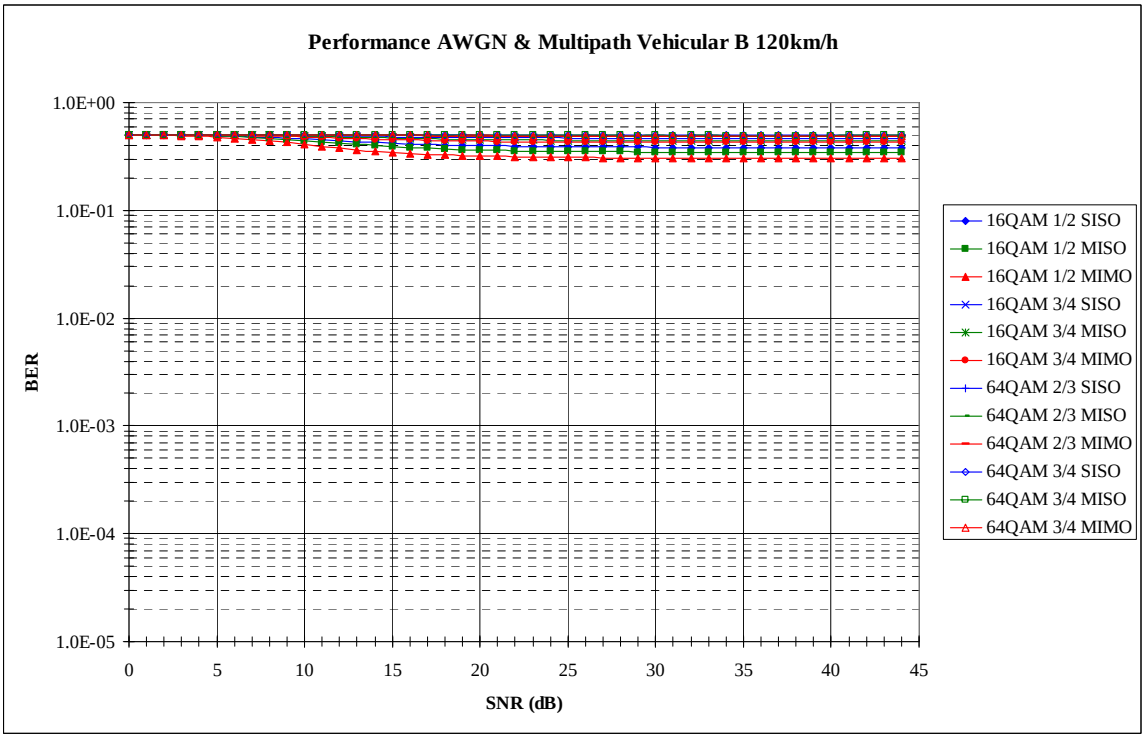

Figure 50. Performance in AWGN & Multipath Vehicular B for QAM Signals.

3. AWGN plus Multipath Channel Performance with Partial CSI Feedback

Table 14. SNR Threshold Vectors for *Auto Rate Control Mode*.

User-Channel Profiles	System	Vector
Indoor A	SISO	$[12.5, 17, 18.5, 23.5, 30.5, 35.5]$
	MISO	$[12, 16.5, 17, 22.5, 26.5, 30.5]$
	MIMO	$[8, 12, 13, 18, 23, 27]$
Indoor B	SISO	$[25, -, 28, -, -, -]$
	MISO	$[11.5, -, 16, 24, 26.5, 33]$
	MIMO	$[9, 12.5, 13, 18, 22, 27]$
Pedestrian A not moving	SISO	$[13.5, 18, 19.5, 25, 33, 38]$
	MISO	$[14, 19, 20, 26, 31, 36]$
	MIMO	$[11, -, 16, 22, 27, 31]$
Pedestrian A moving	SISO	$[-, -, 21, -, 34, 44]$
	MISO	$[14, 19, 20, 26, 31, 36]$
	MIMO	$[11, -, 16, 22, 27, 31]$
Pedestrian B not moving	SISO	$[28, -, 36, -, -, -]$
	MISO	$[14, -, 16, -, -, -]$
	MIMO	$[9, -, 14, 24, -, -]$
Pedestrian B moving	SISO	$[28, -, 36, -, -, -]$
	MISO	$[14, -, 16, -, -, -]$
	MIMO	$[9, -, 14, 24, -, -]$

In this phase of simulations, the systems were set in *auto rate control mode*. That is, using the performance curves obtained in the previous simulations, a set of SNR threshold vectors was defined and its values introduced under each system's settings. These vectors, presented in Table 14, were defined for each of the ITU user-channel profiles and aim for a maximum BER of 10^{-4}. Taking into account the performances obtained in the previous simulations, the SNR threshold vectors were only defined for

indoor and pedestrian user-channel profiles. The simple AWGN channel was ignored since it is not realistic for indoor or pedestrian environments. Some vectors do not present values in some indices, meaning that a particular or several modulations (rate ID) can not be employed. If the missing value was located before an existing value, for simulation purposes it assumes the upper existing value. If there are one or more none existing values in the right side of the vector, for simulation purposes they assume extremely high values, so that the rate control block never selects a rate ID that would induce a BER above the desired value. Simulations for all the systems and user-channel profiles presented in Table 14 were executed to validate the defined vectors. In some few cases, an adjustment was made in some values to obtain the desired BER of 10^{-4}. The vectors presented in Table 14 are the tuned values. Running simulations with the *auto rate control mode* enabled showed effective and as depicted in Figure 51, Figure 52 and Figure 53, the overall system's performance was limited by the BPSK signal, as expected. In Figure 52 and Figure 53 it is also visible the degradation effect caused by the Doppler spread induced by an active pedestrian when compared to a stationary pedestrian.

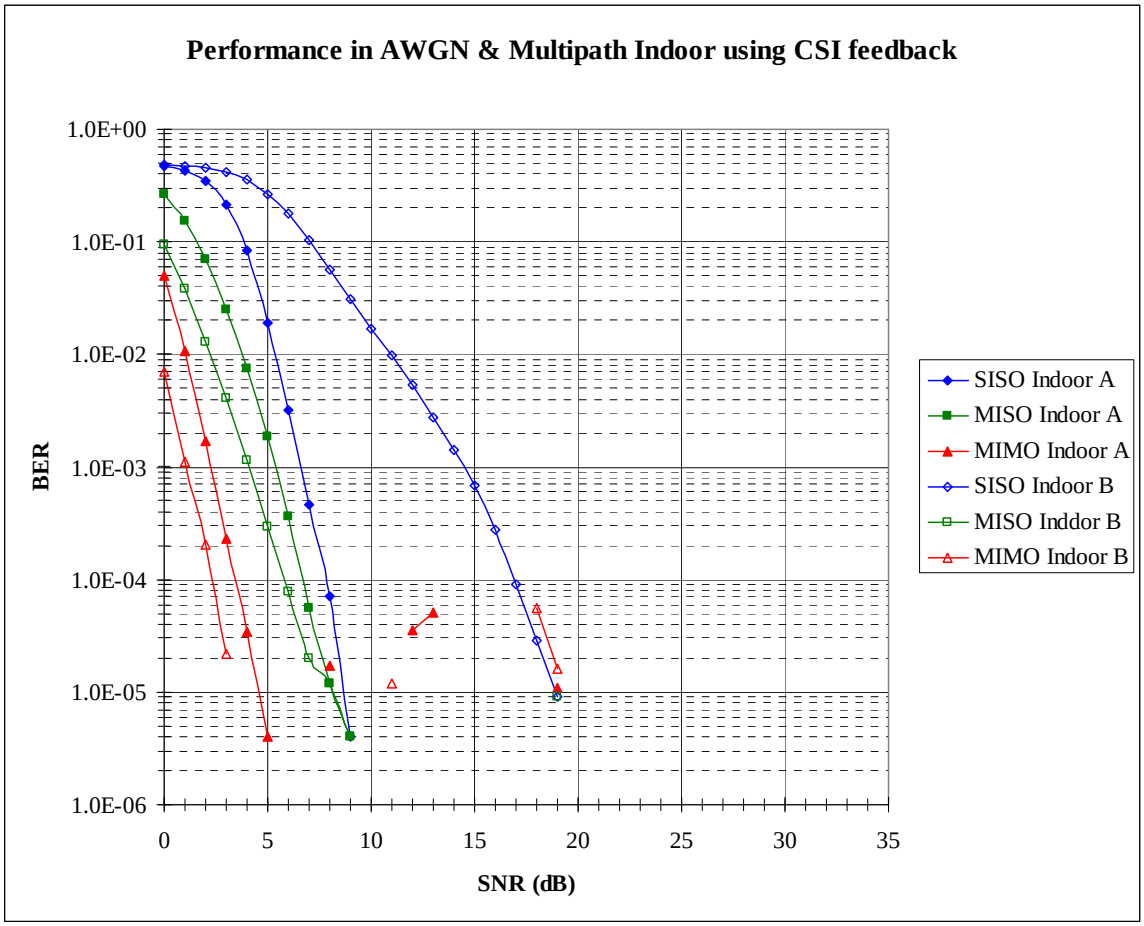

Figure 51. Performance in AWGN & Multipath Indoor using CSI Feedback.

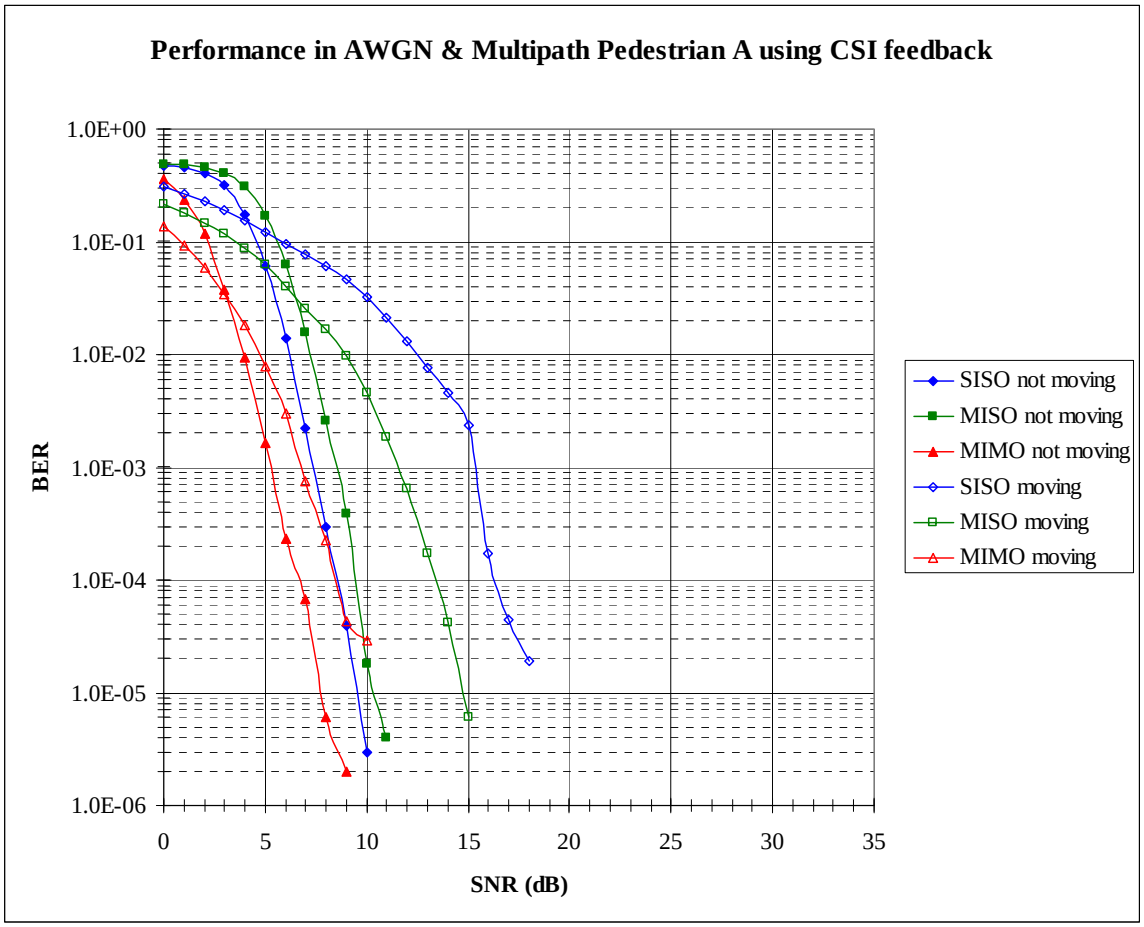

Figure 52. Performance in AWGN & Multipath Pedestrian A using CSI Feedback.

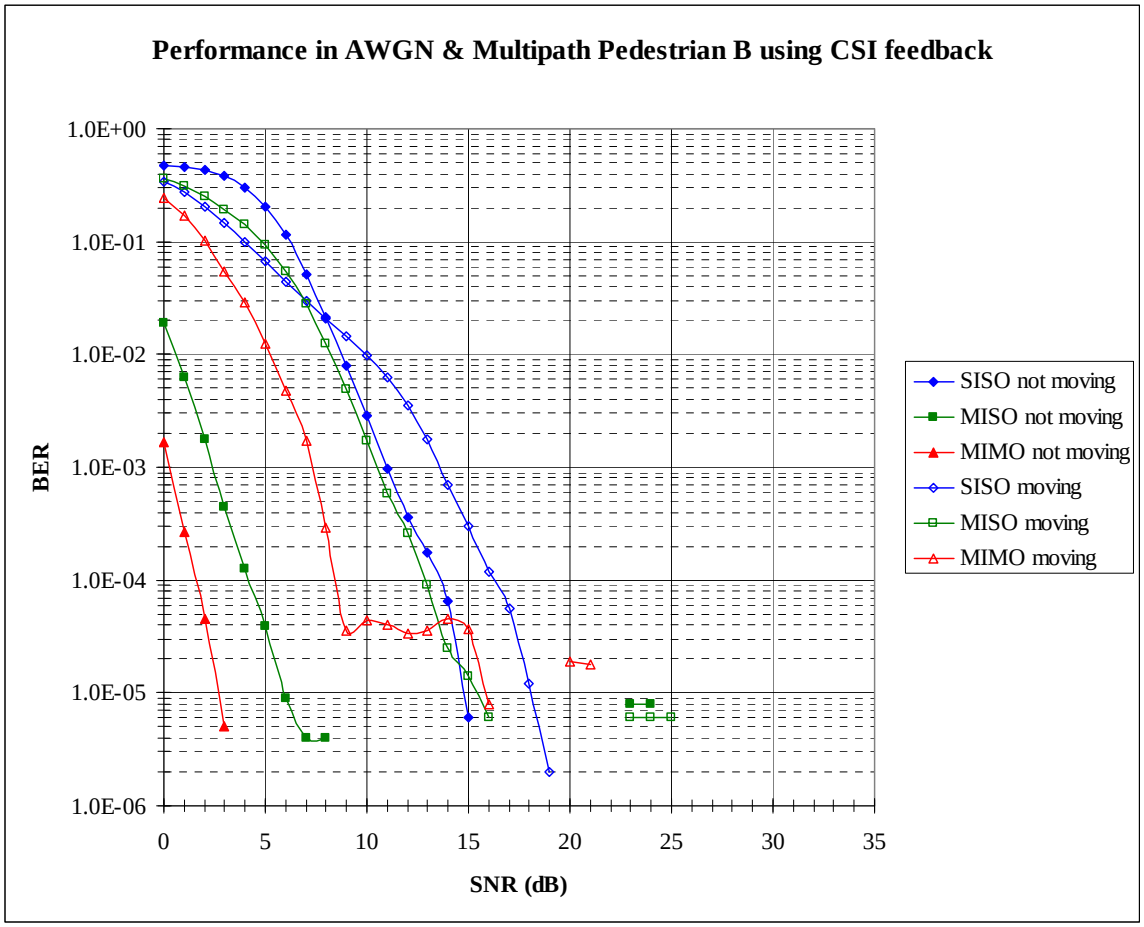

Figure 53. Performance in AWGN & Multipath Pedestrian B using CSI Feedback.

4. AWGN plus Multipath and Shadowing Channel Performance with Partial CSI Feedback

One further step was taken to test the systems' performance under adverse conditions. Simulations on all systems under AWGN plus multipath and shadowing were executed. The simulation settings were those presented in Table 13, plus a shadow standard deviation $\sigma_s = 8\text{dB}$. The results for both indoor user-channel profiles are present in Figure 54. Again, the systems overall performance was limited by the use of BPSK modulation. Also visible is the *auto rate control mode* effect. Notice that errors

were measured beyond the BPSK curve, related to the other modulation schemes in use, but as expected below the established BER threshold of 10^{-4}.

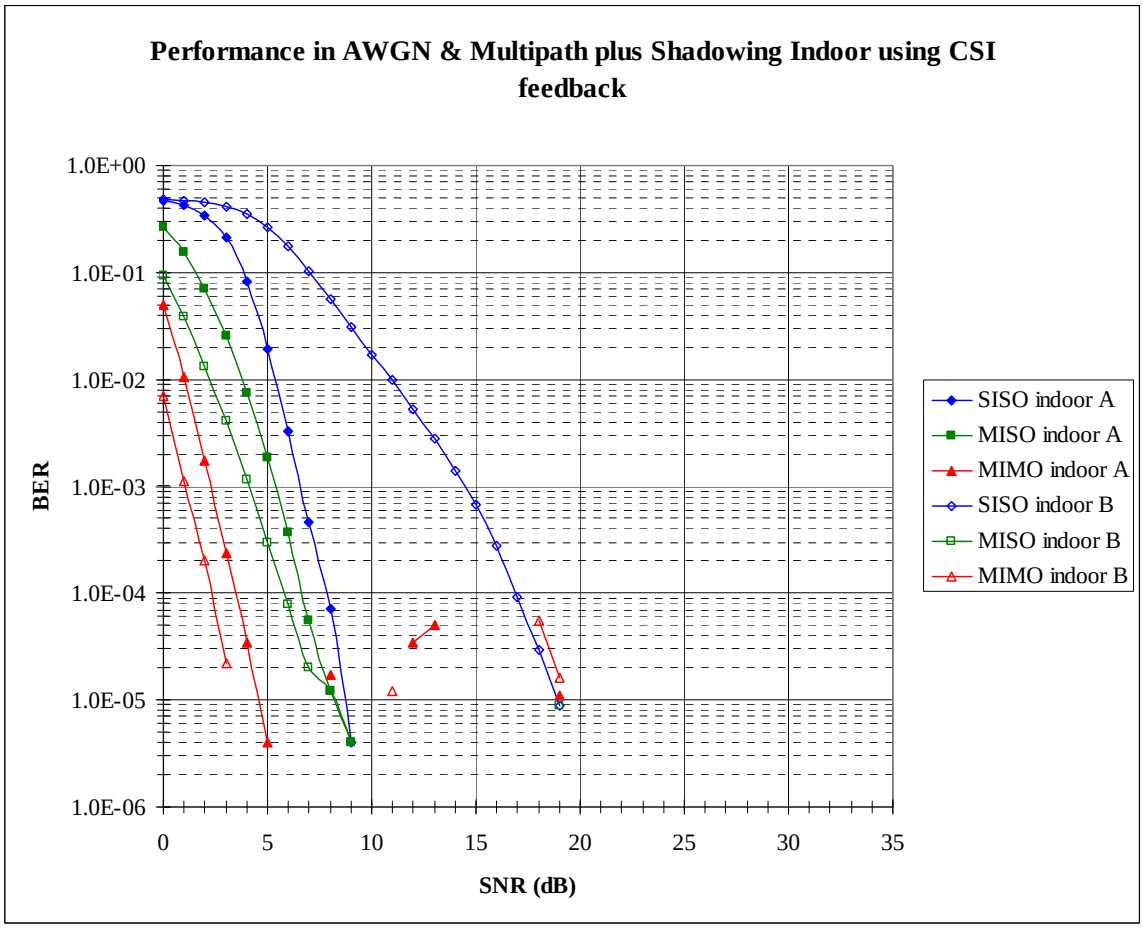

Figure 54. Performance in AWGN & Multipath plus Shadowing Indoor.

5. Achievable Data Rates

The maximum data rates per modulation scheme can be calculated using the parameters presented in Table 13 and the parameter definitions available in [10]. The computed values are presented in Table 15.

Table 15. Maximum Data Rates per Modulation Scheme.

Modulation Scheme	Maximum Channel Data Rate (Mbps)	Maximum Uncoded Data Rate (Mbps)
BPSK $r = 1/2$	2.667	1.333
QPSK $r = 1/2$	5.333	2.667
QPSK $r = 3/4$	5.333	4.000
16QAM $r = 1/2$	10.667	5.333
16QAM $r = 3/4$	10.667	8.000
64QAM $r = 2/3$	16.000	10.667
64QAM $r = 3/4$	16.000	12.000

Table 16. Maximum Data Rates per User-Channel Profile.

User-Channel Profiles	System	Maximum Channel Data Rate (Mbps)	Maximum Uncoded Data Rate (Mbps)
Indoor A	SISO	16.000	12.000
	MISO	16.000	12.000
	MIMO	16.000	12.000
Indoor B	SISO	10.067	5.333
	MISO	16.000	12.000
	MIMO	16.000	12.000
Pedestrian A not moving	SISO	16.000	12.000
	MISO	16.000	12.000
	MIMO	16.000	12.000
Pedestrian A moving	SISO	16.000	12.000
	MISO	16.000	12.000
	MIMO	16.000	12.000
Pedestrian B not moving	SISO	10.067	5.333
	MISO	10.067	5.333
	MIMO	10.067	8.000
Pedestrian B moving	SISO	10.067	5.333
	MISO	10.067	5.333
	MIMO	10.067	8.000

From the values present in Table 15 and the taking into account the highest modulation scheme employed in each user-channel profile, the maximum achievable data rates per system and user-channel profile can be predicted. These values are presented in Table 16. Notice that these values are peak values and only consider a simplex link. If we consider a more realistic situation of systems using time division duplexing (TDD) with a down-link to up-link ratio of one to one $(1:1)$, the values are around half of those presented. Furthermore, the data throughput will be even less because of packet overhead. Nevertheless, it is visible from the values presented that the MIMO system capacity is superior to both the MISO and SISO systems capacities. In adverse situations, like larger delay spread multipath channels and/or presence of Doppler shift, the MIMO system can provide an increase of 50% or more in data rate when compared to the MISO and SISO systems.

D. SUMMARY

In the present chapter, we addressed the significant results obtained during this thesis work. In general, the MISO system outperformed the SISO system and was outperformed by the MIMO system under nearly all user-channel profiles. Furthermore, when the systems were set to use the *auto rate control mode*, based on the overall channel's measured SNR, all adapted to the channel conditions. Cases of AWGN plus multipath and AWGN plus multipath with shadowing were simulated. In all, the systems reacted as expected, changing the rate ID as appropriate. Finally, predicted data rates for each system and user-channel profiles were presented as a measurement for the systems' capacities. In the following chapter, we present a summary of the work performed during this thesis, the main results, conclusions, and suggestions for future work.

V. CONCLUSIONS

The objective of the present thesis was to evaluate the MIMO OFDM performance and to reach its optimal data transmission. This was accomplished by selecting an OFDM standard and evaluating its performance under several user-channel profiles. The IEEE® 802.16-2004 standard was selected since it is a broad standard that permits several settings and implementation options, and also because it is an active area of research where its technical and commercial implementation is ongoing. The results presented in this thesis were obtained by systematic measurements using MathWorks™ SIMULINK® R2008a software package models.

A. SUMMARY OF THE WORK DONE

A comprehensive study of MIMO OFDM material and wireless channel behavior was presented in Chapter II. The principles of OFDM were studied and its modern digital implementation was addressed. On the wireless channels concepts of path loss, fading and shadowing were introduced in order to understand the various effects that produce degradation in the transmitted signal. A broad introduction to MIMO systems was given starting from the basic SISO system, and passing through the intermediate MISO and SIMO systems. Following, the STBC technique known as Alamouti's scheme was discussed.

In total, three models were available by the end of the work. The first one was provided by the MathWorks™, and the remaining two were improved and modified versions. For simulation purposes, each system was complemented with MATLAB® code that enabled each simulation desired settings. In total, each SIMULINK® model has three corresponding MATLAB® control programs. The simulations were performed using the ITU user-channel profiles, since they are the most frequently used power-delay profiles in simulations. The results obtained from the several simulations were presented in performance curves of BER vs. SNR, enabling comparison among the systems.

B. SIGNIFICANT RESULTS AND CONCLUSIONS

Several significant results can be taken from this thesis:

- An increase in the number of antennas used in a wireless communications system enhances its performance and capacity. In this thesis, in most scenarios, the 2x1 MISO system outperformed the SISO system and was outperformed by the 2x2 MIMO system.
- User-channel characteristics under which wireless communications is tested or used have significant impact on the systems overall performance. In our case, using the IEEE® 802.16-2004 standard, it became clear that channels with larger delay spread are a bigger challenge to any system. The MIMO system proved its effectiveness in combating the multipath effect on the channels. The MISO system, under smaller delay spread conditions was also effective, but always less than the MIMO system. The SISO system experienced difficulties in combating the multipath effect in both large and small delay spread conditions.
- Also under the user-channel profile, the Doppler spread plays an important role. In indoor or pedestrian user profiles all systems were able to achieve a certain level of performance, where again the MIMO system was the best followed by the MISO system which was better than the SISO system. In the medium speed vehicular profile, only the MIMO and MISO systems were capable of counteracting the combined multipath and Doppler spread effect. Despite that, both systems were essentially limited to the use of the PSK family of signals. All systems, with the settings used, were incapable of dealing with high speed vehicular user-channel profiles.
- Measuring the overall SNR on a wireless communications link, as described in Chapter III, is a simple technique to obtain CSI. This enables only partial CSI and has limitations when *auto rate control* is desired. In this thesis this scheme proved effective while the noise present in the channel was considerable. When it became negligible and systems were left under the multipath effect alone, it was clear that the systems were restrained from reaching higher performances.

C. SUGGESTIONS FOR FUTURE WORK

After the conclusion of this thesis, several areas for further research and work are indentified:

- Further develop the systems by increasing the number of antennas at either the transmitter or at the receiver, using the Alamouti's scheme a 4x2 MIMO system with stacked STBCs. This system can be implemented using two 2x1 MISO systems with Alamouti's scheme [1]. Eventually, a 4x4 MIMO system with stacked STBCs using two 2x2 MISO systems with Alamouti's scheme may be realizable.
- Implement on the developed systems a more sophisticated CSI feedback that will enable the systems to achieve higher performances. The IEEE® 802.16e-2005 standard, which extends the previous standard to allow usage under mobility, points to two techniques: codebook based feedback and quantized channel feedback [22]. In both cases the standard does not point out how to implement such feature, however two ways of doing so are: maximization of sum capacity and minimization of mean squared error [1].
- In the developed system, we have only focused on the IEEE® 802.16-2004 standard specifications. This led to the use of a specific bandwidth, number of subcarriers (FFT size), and carrier frequency throughout the work. Further work using the IEEE® 802.16e-2005 standard, where different bandwidths, carrier frequencies and number of subcarriers are allowed, might show performances under certain conditions that are not yet understandable.
- The EC department presently has IEEE® 802.16-2004 standard equipment with one base station antenna and two subscribers, each with a single antenna. It is suggested to further invest in this equipment and the execution of field measurements to validate software models, but also to gather information to better tune future systems.

- On a military perspective, it is becoming clearer every day that we will further and further make use of broadband wireless communication systems. In the naval environment, the VHF and UHF bands which naval forces use for tactical communications are stressed and overloaded. Interference is a constant factor when operating in a task force. The solution will be broadband wireless communication systems. A good example is the American Digital Wideband Transmission System (DWTS). This system has high capacity, can be used with or without security features, is LOS, ship-to- ship or ship-to-shore, and operates in the upper UHF band (1350-1850MHz), with data rates up to 2.3 Mbps [23]. Most of the time naval task forces sail under formations or screens to enable optimization of the combined weapon systems. Under such conditions multipath effects, such as those we have studied in this thesis are a reality. The results presented in this work are a good insight to what can happen to tactical naval communications using the DWTS or similar systems. This author has no knowledge of multipath channel models for naval environments. It would be desirable to collect wireless channel measurements that permit the design of models applicable to naval task forces, and from there study its effects on broadband communications to further improve existing and future systems.

APPENDIX S-FUNCTIONS CODE

MISO

Encoder

```
function [ant1, ant2] = stbcenc(u)
% STBCENC Space-Time Block Encoder
%   Outputs the Space-Time block encoded signal per antenna.

N = 2;
ant1 = complex(zeros(size(u)));
ant2 = ant1;

% Alamouti Space-Time Block Encoder, G2, full rate
%   G2 = [s0 s1; -s1* s0*]
for i = 1:size(u,2)/2
    s0 = u(:, 2*i-1); s1 = u(:, 2*i);
    ant1(:, [2*i-1 2*i]) = [s0 -conj(s1)];
    ant2(:, [2*i-1 2*i]) = [s1 conj(s0)];
end
```

Decoder

```
function z = stbcdec(chEst1, rx, chEst2)
% STBCDEC Space-Time Block Combiner
%

N = 2; M = 1;
z = complex(zeros(size(rx)));
z0 = complex(zeros(size(rx,1), M)); z1 = z0;

% Space Time Combiner
for i = 1:size(rx,2)/2
    z0(:, M) = rx(:, 2*i-1).* conj(chEst1(:, 2*i-1)) + ...
               conj(rx(:, 2*i)).* chEst2(:, 2*i);

    z1(:, M) = rx(:, 2*i-1).* conj(chEst2(:, 2*i-1)) - ...
               conj(rx(:, 2*i)).* chEst1(:, 2*i);

    z(:, [2*i-1 2*i]) = [z0 z1];
end
```

MIMO

Encoder

```
function [ant1, ant2] = stbcenc(u)
% STBCENC Space-Time Block Encoder
%   Outputs the Space-Time block encoded signal per antenna.

N = 2;
ant1 = complex(zeros(size(u)));
ant2 = ant1;

% Alamouti Space-Time Block Encoder, G4, full rate
%   G4 = [s0 s1; -s1* s0*;s0 s1;-s1* s0*]
for i = 1:size(u,2)/2
    s0 = u(:, 2*i-1); s1 = u(:, 2*i);
    ant1(:, [2*i-1 2*i]) = [s0 -conj(s1)];
    ant2(:, [2*i-1 2*i]) = [s1 conj(s0)];
end
```

Decoder

```
function z = stbcdec(chEst1, chEst2, rx1, rx2, chEst3, chEst4)
% STBCDEC Space-Time Block Combiner
%

N = 2; M = 1;
z = complex(zeros(size(rx1)));
z0 = complex(zeros(size(rx1,1), M)); z1 = z0;

% Space Time Combiner
for i = 1:size(rx1,2)/2
    z0(:, M) = rx1(:, 2*i-1).* conj(chEst1(:, 2*i-1)) + ...
               conj(rx1(:, 2*i)).* chEst2(:, 2*i) + ...
               rx2(:, 2*i-1).* conj(chEst3(:, 2*i-1)) + ...
               conj(rx2(:, 2*i)).* chEst4(:, 2*i);

    z1(:, M) = rx1(:, 2*i-1).* conj(chEst2(:, 2*i-1)) - ...
               conj(rx1(:, 2*i)).* chEst1(:, 2*i) + ...
               rx2(:, 2*i-1).* conj(chEst4(:, 2*i-1)) - ...
               conj(rx2(:, 2*i)).* chEst3(:, 2*i);

    z(:, [2*i-1 2*i]) = [z0 z1];
end
```

LIST OF REFERENCES

[1] J. G. Andrews, A. Ghosh and R. Muhamed, *Fundamentals to WiMAX – Understanding Broadband Wireless Networking,* Prentice Hall, 2007.

[2] R. van Nee, R. Prasad, *OFDM for Wireless Multimedia Communications,* Artech House, 2000.

[3] A. Paulraj, R. Nabar and D. Gore, *Introduction to Space-Time Wireless Communications,* Cambridge University Press, Cambridge, United Kingdom, 2003.

[4] A. J. Paulraj and T. Kailath, "Increasing capacity in wireless broadcast systems using distributed transmission/directional reception (DTDR)," US Patent 5345599, 4 April 1994, http://www.freepatentsonline.com/5345599.pdf

[5] E. Telatar, "Capacity of Multi-antenna Gaussian Channels," Bell Lab. Tech. Memo., October 1995, http://mars.bell-labs.com/papers/proof/.

[6] G. J. Foschini, "Layered space-time architecture for wireless communication in fading environments when using multiple antennas," Bell Lab. Tech. J., 41-59 1996.

[7] G. J. Foschini and M. Gans, "On the limits of wireless communication in a fading environment when using multiple antennas," *Wireless Personal Commun,* Vol. 6, pp. 311-335, March 1998.

[8] V. Tarohk, N. Seshadri and A.R. Calderbank, "Space-time codes for high data rate wireless communication: performance criterion and code construction," *IEEE Transactions on Information Theory,* Volume 44, Issue 2, pp. 744 - 765, March 1998.

[9] S. M. Alamouti, "A Simple Transmit Diversity Technique for Wireless Communications," *IEEE Journal on Select Areas in Communications,* Vol. 16, No. 8, pp. 1451-1458, October 1998.

[10] Institute of Electrical and Electronics Engineers, 802.16-2004, Air Interface for Fixed Broadband Wireless Access Systems, 1 October 2004.

[11] M. Vu and A. Paulraj "MIMO Wireless Linear Precoding," *IEEE Signal Processing Magazine,* Volume 24, Issue 5, pp. 86-105, September 2007.

[12] R. Zhang, Y.C. Liang, R. Narasimhan, and J.M. Cioffi**, "**Approaching MIMO-OFDM Capacity with Per-Antenna Power and Rate Feedback," *IEEE Journal on Select Areas in Communications,* Volume 25, Issue 7, pp. 1284-1297, September 2007.

[13] A. B. Carlson, *Communication Systems*, Third Edition, McGraw-Hill, 1986.

[14] S. Haykin and M. Moher, *Introduction to Analog and Digital Communications*, Second Edition, Wiley, 2007.

[15] J. G. Proakis and M. Salehi, *Digital Communications*, Fifth Edition, McGraw-Hill, 2008.

[16] B. Sklar, *Digital Communications – Fundamentals and Applications*, Second Edition, Prentice Hall, 2001.

[17] T. S Rappaport, *Wireless Communications – Principles and Practice*, Second Edition, Prentice Hall, 2002.

[18] R. Cristi, Notes on IEEE802.16 and WiMax, Naval Postgraduate School, Monterey, CA, 2008 (unpublished).

[19] A. Goldsmith, *Wireless Communications*, Cambridge University Press, 2005.

[20] D. Gesbert, M. Shafi, D. Shiu, P.J. Smith and A. Naguib, "From Theory to Practice: An Overview of MIMO Space-Time Coded Wireless Systems," *IEEE Journal on Select Areas in Communications*, Vol. 21, No. 3, pp. 281-302, April 2003.

[21] J.J. Breur, A.B. Smolders, W.M.C. Dolmans and H.J. Visser, "Bluetooth Radio Module with Embedded Antenna Diversity," retrieved from http://www.brabantbreedband.nl/PDF/Publications/EMC03_Dolmans.pdf

[22] Institute of Electrical and Electronics Engineers, 802.16e-2005, Air Interface for Fixed and Mobile Broadband Wireless Access Systems, 28 February 2006.

[23] Joint Requirements Oversight Council (JROC), "Joint Tactical Radio System (JTRS) Operational Requirement Document," version 3.2, 09 April 2003, http://www.eng.auburn.edu/users/hamilton/security/SDR/JROC_Approved_ORD_v3.2_09Apr03.pdf

INITIAL DISTRIBUTION LIST

1. Defense Technical Information Center
   Ft. Belvoir, Virginia

2. Dudley Knox Library
   Naval Postgraduate School
   Monterey, California

3. Chairman, Code EC
   Department of Electrical and Computer Engineering
   Naval Postgraduate School
   Monterey, California

4. Professor Roberto Cristi, Code EC/Cx
   Department of Electrical and Computer Engineering
   Naval Postgraduate School
   Monterey, California

5. Assistant Professor Frank Kragh, Code EC/Kh
   Department of Electrical and Computer Engineering
   Naval Postgraduate School
   Monterey, California

6. Luís Miguel Mendes Simões
   Barreiro, Portugal